DOT/FAA/CT-03-90-C-00044

FAA Technical Center
Atlantic City Airport
N.J. 08405

Biodynamics Response for the Evaluation of Aircraft Crash Safety

Dr. Hamid M. Lankarani

National Institute for Aviation Research
Wichita State University
Wichita, KS 67260-0093

September 1993

Final Report

This document is available to the public through the National Technical Information Service, Springfield, Virginia 22161

NATIONAL INSTITUTE FOR AVIATION RESEARCH

FINAL REPORT - FAA SAFETY RESEARCH

SUBTASK D-1: BIODYNAMIC RESPONSES FOR EVALUATION OF AIRCRAFT CRASH SAFETY

Principal Investigator: Hamid M. Lankarani

ABSTRACT

A comprehensive study of the capabilities of the program SOM-LA/TA (Seat Occupant Model - Light Aircraft/Transport Aircraft) has been performed and deficiencies of its occupant models have been identified. For the prediction of occupant head injuries, formulations and mechanisms of head injury have been evaluated. Head-Injury-Criteria (HIC) from analysis codes and experiments have been computed and compared. Feasibility and detailed designs of a simple non-sled HIC-measuring test mechanism have been accomplished and issues regarding the construction of test facility has been discussed.

Major improvements of the code SOM-LA/TA and its corresponding occupant model were achieved. These include the development of a more accurate nonlinear contact force model for the head impact of an occupant seated behind the interior walls, adjustment of the stiffness and damping parameters of the occupant model, creation of an envelope for the occupant, and development of two detailed non-linear finite element models of the lumbar spine for the Hybrid II dummy and for the 50th percentile male human respectively. These new developments have been incorporated into the code SOM-LA/TA and have shown to provide closer match to the experimental results than the original version of SOM-LA/TA. In order to add graphical output capability to SOM-LA/TA, post-processor has also been generated both on a micro-computer and on a IBM RISC/6000 workstation. To overcome the difficulties associated with the data analysis of each impact sled test by the optical methods, an automatic target tracking system has been developed so that the accuracy of the photometric results is enhanced and a great deal of time is saved. The improved code SOM-LA/TA will be a powerful tool for studying the post-crash dynamic behavior of the aircraft occupants and to assess the occupant survivability and performances of seat/occupant/restraint system in various crash environments. Finally recommendations are made regarding further improvements in the biodynamic models of the occupant. [1]

This report was prepared by the Wichita State University under Contract Number DTFA03-90-00044, modification 003, with the Federal Aviation Administration Technical Center. The work monitored by Mr. Anthony Wilson and Mr. William Nissley Jr.

TABLE OF CONTENTS

CONTENTS page

ABSTRACT i

LIST OF FIGURES iv
LIST OF TABLES vi

EXECUTIVE SUMMARY 1

1. INTRODUCTION 3

2. ASSESSMENT OF THE CODE SOM-LA/TA 7

2.1 Multibody Dynamic Modeling of Occupants 7
2.2 Results from Earlier Assessments 10
2.3 Comparison with Code MADYMO 10
2.4 Comparison with Experiments at NIAR 12

3. HEAD INJURY CRITERIA AND EVALUATION 14

3.1 Measures of Head Injury 14
3.2 Numerical computation of HIC 15
3.3 Design of Non-sled Setup to Measure HIC 19

4. IMPACT DYNAMICS OF AIRCRAFT OCCUPANTS SEATED BEHIND INTERIOR WALLS 25

4.1 Non-Linear Contact Force Model 25
4.2 Parametric Study of the Contact Force Model 27
4.3 Selection of Padding Material Absorbing Head Impacts Onto Aircraft Interior Walls 31

5. TWO-DIMENSIONAL OCCUPANT WITH A FINITE ELEMENT MODEL OF LUMBAR SPINE 34

5.1 Formulations of 2-D Occupant Model 34
5.2 Quasi-static Analysis with Finite Element Model of Lumbar Spine 38
5.3 Programming of Nonlinear Finite Element with Model of Lumbar Spine . . 48
5.4 Numerical Simulation and Comparison to Experimental Results 49

CONTENTS

6. COMPUTER ANIMATION AND VISUALIZATION 62

6.1 PC Version Graphics Post-Processing Software 62
6.2 Workstation Version of Graphics Post-Processing Software 65

7. EXPERIMENTAL TESTING AND PHOTOMETRIC PROCEDURES 73

7.1 Impact Dynamics Sled Testing Facilities and Procedures 73
7.2 Target Automatic Tracking Photometric Procedures 75

8. CONCLUSIONS AND RECOMMENDATIONS 87

8.1 Conclusions 87
8.2 Recommendations 89

9. REFERENCES 90

LISTING OF FIGURES

Figure 1. Twelve-segment (general three-dimensional) occupant model 8
Figure 2. Eleven-segment (plane-motion) occupant model 8
Figure 3. External force acting on occupant model. 9
Figure 4. Dummy pelvis resultant acceleration versus time. 13
Figure 5. Dummy head resultant acceleration versus time. 13
Figure 6. Original data from Wayne State University including all points super-imposed with first published Wayne State University tolerance curve. 17
Figure 7. Acceleration pulse. 17
Figure 8. Modified skull-brain-neck model. 18
Figure 9. Acceleration of the head from the head-neck model. 18
Figure 10. Drop tower setup. 22
Figure 11. Pneumatic driven impact method. 23
Figure 12. Pendulum impact method. 24
Figure 13. Sled test set up for occupant head impact with aircraft bulkhead. 26
Figure 14. Reconstruction of head strike impact. 26
Figure 15. Head-injury-criteria and maximum deformation with variations of coefficient A 28
Figure 16. Components of impact forces and maximum acceleration with variations of coefficient A. 28
Figure 17. Head-injury-criteria and maximum deformation with variations of coefficient B 29
Figure 18. Components of impact forces and maximum acceleration with variations of coefficient B. 29
Figure 19. Head-injury-criteria and maximum deformation with variations of coefficient C_0. 30
Figure 20. Variation of Allowable stiffness with impact velocity for a HIC of 1000. . 33
Figure 21. Variation of HIC with stiffness at different impact velocities. 33
Figure 22. Flexible body connecting two rigid bodies. 42
Figure 23. Finite element model of Hybrid II lumbar spine. 44
Figure 24. Relationships between global and local coordinate systems. 44
Figure 25. Finite element model of male human lumbar spine. 47
Figure 26. Detailed program flowchart of non-linear finite element lumbar spine model. 52
Figure 27. Configuration of testing setup with energy absorbing seat. 54
Figure 28. Input pulse for energy absorbing seat test. 54
Figure 29. Lumbar spine axial loads in case 1. 55
Figure 30. Deformation configuration of lumbar spine in case 1. 55
Figure 31. Lumbar spine bending moment in case 1. 56
Figure 32. Comparison of Dynamic Response Index in case 1. 56
Figure 33. Comparison of Severity Index in case 1. 57
Figure 34. Deformation configuration of lumbar spine in case 2. 57

Figure 35. Comparison of lumbar axial deformations between male human and Hybrid II dummy 58
Figure 36. Carriage setup with 60^0 pitch. 58
Figure 37. Deceleration pulse of dynamic sled test in case 3. 59
Figure 38. Lumbar spine axial loads in case 3. 59
Figure 39. Comparison of head resultant acceleration in case 3. 60
Figure 40. Comparison of chest pelvis and head resultant acceleration in case 3. 60
Figure 41. Shear force acting on the lumbar spine in case 3. 61
Figure 42. Flowchart of PC version animation system. 63
Figure 43. Simulation results of dummy. 66
Figure 44. Flowchart of workstation version animation program. 67
Figure 45. Configuration of dials. 69
Figure 46. Interaction menu on the screen. 69
Figure 47. Wire-frame representation of dummy model. 72
Figure 48. Animation of solid dummy model. 72
Figure 49. Impact Test Sled at NIAR. 74
Figure 50. Standard 50th percentile (Hybrid II) dummy. 74
Figure 51. Un-filtered head strike path. 80
Figure 52. Head strike path smoothed by filtering technique. 80
Figure 53. Smoothed head velocity in X direction. 81
Figure 54. Smoothed head acceleration in X direction. 81
Figure 55. Target configuration on dummy head. 83
Figure 56. Head strike path obtained manually. 85
Figure 57. Head strike path obtained automatically. 85
Figure 58. Head acceleration in X direction obtained by manual tracking. 86
Figure 59. Head acceleration in X direction obtained by automatic tracking. 86

LISTING OF TABLES

1. Results comparison of SOM-LA/TA and MADYMO. 12
2. Comparison of HIC values of SOM-LA/TA, MADYMO and sled test. 12
3. Comparison of results from the two programs. 19
4. Properties of 1 inch thick padding materials for an impact velocity of 10 mph. . . 32
5. Geometrical and physical properties of lumbar spine. 46
6. Limits and representative values of ranges of rotation of lumbar spine. 48

EXECUTIVE SUMMARY

The development of faster computers has provided a powerful and practical alternative to approach problems of aircraft structural crashworthiness and post-dynamic behavior of the occupants. This effective and versatile method provides rigorous analytical techniques which can be used to evaluate the performances of occupants and seat structures. Program SOM-LA/TA (Seat Occupant Model-Light Aircraft/ Transport Aircraft), developed under the sponsorship of Federal Aviation Administration provides such capabilities [1-4]. It incorporates both a two- and a three-dimensional occupant model and a finite element model of the seat structure. The goal of this study was to assemble a powerful analytical tool for evaluation of aircraft crash safety using new developments in the code SOM-LA/TA.

A comprehensive study of the capabilities of the program SOM-LA/TA was first performed and deficiencies of its occupant models were identified. It was observed that the analytical results from SOM-LA/TA matched the experimental results in terms of segment positions and velocities. The acceleration have the same order of magnitude but do not match, which is most likely due to compliance characteristics data in the occupant models. It is well known that SOM-LA/TA has difficulties in accurate prediction of lumbar loads. This was demonstrated in a number of tests for which largest differences between the analysis and experimental results were observed in the lumbar loads, especially for the tests that had a pitch configuration. This suggested that improvements in the lumbar spine model are necessary. It was also observed that the parameters in the SOM-LA/TA occupant model tend to be a bit stiffer than the actual values corresponding to the Hybrid II ATD and an average size male occupant.

In the first stage of this study, major improvements of the code were achieved. These includes adjustment of stiffness and damping parameters in the occupant model, creation of an envelope for the occupant, development of a more accurate nonlinear contact force model for the head impact of an occupant seated behind interior walls, and finally development of nonlinear finite element models of the lumbar spine. For better prediction of the lumbar loads, two finite element models of lumbar spine were created for the Hybrid II (part 572) ATD and for a 50th percentile male human. Detailed information of kinematic, geometric, inertial and material properties of the lumbar spine were used in the model construction. A quasi-static methodology for the dynamic analysis of the multibody model of the occupant with the nonlinear finite element model of the lumbar spine was developed. Comparison of the isolated lumbar spine models showed that the spine of ATD is much stiffer than that of the human. The new methodology and the two spine models were then incorporated in the program SOM-LA/TA. A number of test cases were considered, and the results from the experiments at CAMI and NIAR, the old SOM-LA/TA code and the modified SOM-LA/TA code were compared. It was observed that with the new modifications, a better prediction of lumbar loads were obtained for all the test cases considered. In order to add graphical output capability to SOM-LA/TA, post-processors were developed both on a micro-computer and on an IBM RISC/6000 workstation. The improved code SOM-LA/TA will be a powerful tool to study the post-crash dynamic behavior of the aircraft occupants and to assess the occupant survivability and performances of

1. INTRODUCTION

The progressive increase in number of aircraft and congested air traffic conditions have led to an increasing number of collisions and, consequently, to a large increase in the potential for human injury and fatality. Public concern about safety and demand for better protection against injury from crash has become increasingly vocal in the recent years. Due to the importance of the problem, the studies of crashworthiness, structural impact analysis, and post-crash dynamic behavior of the aircraft occupants is necessary in order to determine the mechanisms that cause injuries. Furthermore, in order to achieve safe designs of seats and restraint systems that meet the FAA regulatory standards, the characteristics of the human body motion must be known. Different restraint systems, such as lap belts and shoulder harness, allow different types of body motion. Prediction of the human body motion, seated over an energy-absorbing seat and equipped with a specific restraint system, yields important information on the performance of the seat and the restraint system.

Quantitative values such as displacements and forces cannot be obtained from field observations of a crash scene. Clinical experiments with animal subjects have been conducted as early as 1941 [5-7]. Studies on human cadavers [8] as well as pathological studies of injured human subjects [9,10] were first used to establish the criteria and critical levels of dynamic loads [11-13]. These studies were not only preliminary, but more importantly raised ethical questions concerning the use of human and animal subjects.

Experimental impact sled testing is a technique to determine the structural impact responses, to evaluate the performance of seat/occupant responses, and to examine the effectiveness of the safety system in reducing the potential for serious injuries. The post-collision biodynamic responses of occupants are determined to examine the possibility of injuries or fatalities in a certain crash environment. Experiments with instrumented anthropomorphic dummies have also been conducted for the purpose of determining the dynamic response of the human body segments. Many improvements have been made in the biofidelity of dummies during the past three decades such as the well-known Sophisticated-Sam [14], Eurosid [15], and Hybrid III [16] dummies. These studies, although necessary, are limited due to still-existing deficiencies in physical accuracy of the dummies. Furthermore, only a limited type of crash tests can be conducted in relation to the wide range of real-world crashes.

The development of faster computers provides a powerful and practical alternative to approach problems of structural crashworthiness and post-dynamic behavior of the occupants. Mathematical modeling and simulations utilize the principles of multibody dynamics, continuum mechanics and finite element methods along with the numerical techniques. The methods, if combined properly, provide rigorous analytical techniques which can be used to evaluate the performances of occupants and seat structures. If a model can be shown to be reliable and valid, as compared to known experimental data and pathological correlations, it is an effective and versatile method for investigating the response of the modeled system to a wide variety of input conditions. Computer models are less costly and less time-consuming, and have the potential

of yielding substantial results. Moreover, they are capable of re-constructing many different crash scenarios, which may be neither possible nor feasible in a laboratory setup.

Several studies of occupant models have been performed in the area of computer simulation of body crash dynamics. In 1963, McHenry [17] proposed the first of such models which contained eight masses and eleven degrees-of-freedom. The model was later revised by Segal [18], and named ROS (Revised Occupant Simulation). The MODROS model by Danforth et. al [19] represents further modifications on the introduction of spike loads and simple contact surfaces. These models were all developed at Cornell Aeronautical Laboratory, and were thus referred to as CAL models. The two-dimensional gross-motion simulator of the University of Michigan is known as HSRI (Highway Safety Research Institute) [20]. Between 1972 and 1974, three versions of MVMA-2D (Motor Vehicle Manufactures Association) model were developed for simulating an occupant in frontal or rear impacts [21]. The model was described by using ten segments and nine masses connected by eight hinged joints. Torques generated in the joints were of elastic, viscous damping, coulomb frictional types and a nonlinear energy dissipating type for the joint stop. The occupant interaction with vehicle interior surfaces was detected by contact ellipses. Several experimental validations have been made by sled tests using both cadavers and Hybrid II dummy [21-23]. Simulation results compared well with the experimental results. In 1972, Glancy and Larson proposed the SIMULA model as an eight-mass joined structure, with masses concentrated at the joints [24]. Modifications to SIMULA were performed by Twiggs and Karnes in 1974, and the results were named PROMETHEUS [25]. The prescribed models and most of the ones developed later were all two-dimensional models, and could not be used for the analysis of many impact configurations such as side impact or vehicle rollover.

The earliest known three-dimensional occupant model was proposed by Robbins in 1970, named HSRI-3D (Highway Safety Research Institute) model, it contained only three-mass segments [26]. In 1974 Robbins et. al introduced a three-dimensional six-mass HSRI model [27]. In this model, a minimum number of degrees-of-freedom were selected consistent with a realistic and economical description of the biodynamic problem. The arms of the occupant were neglected based on their small mass and small effects on general body dynamic responses. Force interactions between the crash victim and his environment were modeled by impingement of ellipsoids attached to segments into planar surfaces, which are attached to the moving vehicle or inertial reference frame. Bartz developed the CAL-3D occupant simulation model or CVS (Crash Victim Simulator) model [28]. This lumped-mass model included fifteen rigid-body segments with forty degrees-of-freedom. A contact model was developed to generate the external forces acting on the occupant. Further modifications of CAL-3D by Fleck et. al [29,30] resulted in a model consisting of an arbitrary number of segments to describe an occupant. In addition, the concept of null joints was introduced to simulate disjointed sets of segments interacting against one another. Huston et. al [31] analyzed a more easily constructed 3D model, UCIN, by using a Newtonian formulation of the nonlinear dynamics equations of motion. The simple 3D ATB (Articulated Total Body) model has been used by the US Air Force for human injury prediction in a crash environment [32]. The MADYMO crash victim simulation program, consisting of a two-dimensional and a three-dimensional model, has been extensively

used during the last few years for the analysis of automobile crashes [33]. There are no limitations on the number of rigid bodies for the human surrogate. Two types of joints are used to connect the rigid body segments, hinged joints in the two-dimensional model and ball-and-socket joints in the three-dimensional model. Joint torques are described in tabular forms as opposed to polynomial form. There are three standard force interaction models: acceleration forces, ellipsoids with planes in both the two- and the three-dimensional models, and ellipsoids with ellipsoids in three-dimensional models. The contact forces can be of the nonlinear spring, viscous damping or frictional forces. Some validations have been reported by Wismans et. al [33] and Wijk et. al [34]. The model predictions are within or close to the range of experimental results. Lankarani and Ma [35] proposed a multiple segment model of the human body and a computer environment to simulate the post crash behavior of a vehicle pilot/passenger in specific types of collision situations, including static equilibrium analysis, frontal crash, and aircraft seat ejection. The human body is modeled as a collection of rigid elements interconnected by an array of kinematic joints constraining the relative motion of the elements. These elements include the upper body combined with head and neck, thighs and lower legs. A more complex occupant model, an improvement of previous model, was later proposed by Ma and Lankarani [36]. This model includes head-neck, upper body, upperarms, forearms, thighs and lower legs. Non-linear rotational springs and dampers are incorporated at the joints mimicking the anatomical characteristics and limits. An interface between the seat and occupant, and representation of the seat belts are constructed. To perform a dynamic analysis, a three-dimensional code was developed that generates and numerically solves the governing differential equations of motion in a systematic fashion. Graphical images of the model are obtained by running through a developed post-processing program. Program SOM-LA/TA incorporates both a two- and a three-dimensional occupant model and a finite element model of the seat structure. In the 3-D model, the occupant is represented by 12 rigid bodies with rotational springs and dampers at the joints. While the 2-D occupant model is represented by eleven rigid segments. For 2-D model, there is a nonlinear force-deformation model of lumbar spine to predict the lumbar loads.

As shown in a large number of existing models cited earlier, the concept of occupant modeling is usually based on a number of rigid bodies connected by various force and moment producing joints. In all, the linkage systems are all tree or open-loop structures. The equations of motion for multibody systems are formulated using either a Lagrangian or a Newtonian approach. The shapes of occupant segments are described by ellipses and/or hyperellipses in two-dimensional models and ellipsoids and/or hyperellipsoids in three-dimensional models. The interaction forces between body segments and their surroundings are calculated by using the amount and the rate of penetration of the ellipses or ellipsoids into a plane.

In view of the large number of variables involved, the assessment of the performance of these models is difficult. Generally, it has been observed that the models make good displacement correlations with experimental data, but do not match the acceleration responses well. Most of the gross motion simulators have not been formulated to be general-purpose. They have been basically developed for specific crash situations, and can not handle all configurations. Furthermore, most of existing computer models have been primarily developed

for automotive applications. They lack generality as well as flexibility for model updating. In addition, most of these simulators do not have capabilities to predict responses of seat structures. An important measure of safety, and a requirement for aircraft seat certification, is the amount of load transferred to the occupant spine. The gross motion simulators described earlier do not have the capability of predicting lumbar loads and moments accurately.

2. ASSESSMENT OF THE CODE SOM-LA/TA

2.1 Multibody Dynamic Modeling of Occupants

A multibody system is defined as a collection of bodies in which the bodies can move relative to one another. The interconnection between pairs of bodies is through either the kinematic joints or the force elements. The kinematic joints between two bodies, such as spherical, revolute and transnational joints, constrain the relative motion between two bodies. The force elements such as springs, dampers, and actuators, exert forces on pairs of bodies. In addition to the force elements, some additional forces and/or moments may be applied individually on the bodies. The study of time history of motion of system components without consideration of forces and inertia effects on the motion is referred to as a kinematic analysis. On the other hand, dynamic analysis is the study of the time-history of the system motion under the action of forces. Study of motion and force relationships is the main interest of the dynamic analysis.

SOM-LA/TA (Seat Occupant Model-Light Aircraft/Transport Aircraft) is a code developed under the sponsorship of Federal Aviation Administration by Professor D. H. Laananen [1-4]. The multi-segment (multibody) occupant models used in SOM-LA/TA have been developed based on the concepts of rigid multibody dynamics. The occupant models consist of a various number of segments connected with hinge and ball-and-socket joints. Rotations at the joints are resisted by torsional spring-dampers whose characteristics are represented by parameters such as stiffness and damping coefficients. These parameters are typically estimated from experimental results. The models are utilized to predict displacements, accelerations, joint torques and some injury measures.

Both two- and three-dimensional SOM-LA/TA occupant models are available. In the 3-D model, the occupant is represented by 12 rigid bodies with rotational springs and dampers at the joints (Figure 1). Described body segments represent the head, neck, upper torso, lower torso, upper arms, forearms, thighs, and lower legs. Each of the torso joints possesses three rotational degrees of freedom. The elbows, the knees, and the head/neck joints are hinge-type connections. Rotations at the body joints are resisted by torsional springs and dampers whose characteristics depend on the user selection of human or dummy occupant. The 2-D occupant model is represented by 11 rigid segments (Figure 2). External loads are applied to the body segments by the seat cushion, the floor, and by the restraint systems (Figure 3). The surfaces of the body segments are represented by ellipsoids, spheres, and cylinders. Based on these surfaces, the external forces exerted on the occupant by the seat cushion and the restraint system and also the internal forces between penetrating segments can be evaluated, and the impact between the occupant and the aircraft interior can be predicted.

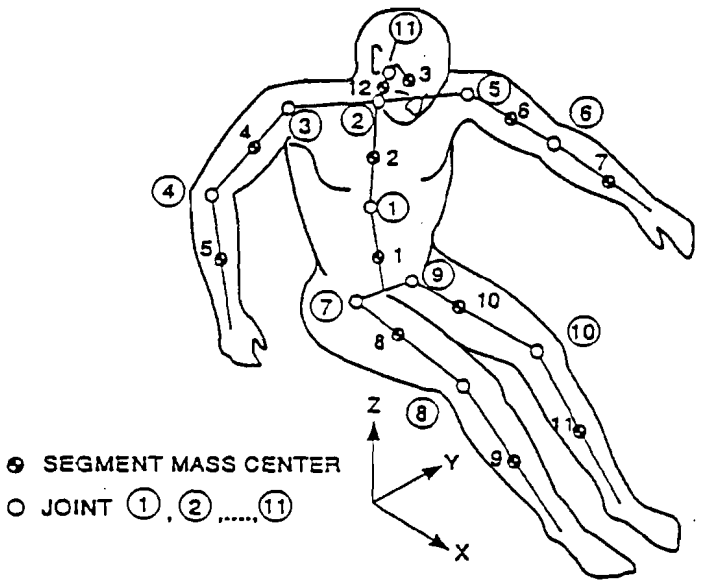

Figure 1. Twelve-segment (general three-dimensional) occupant model.

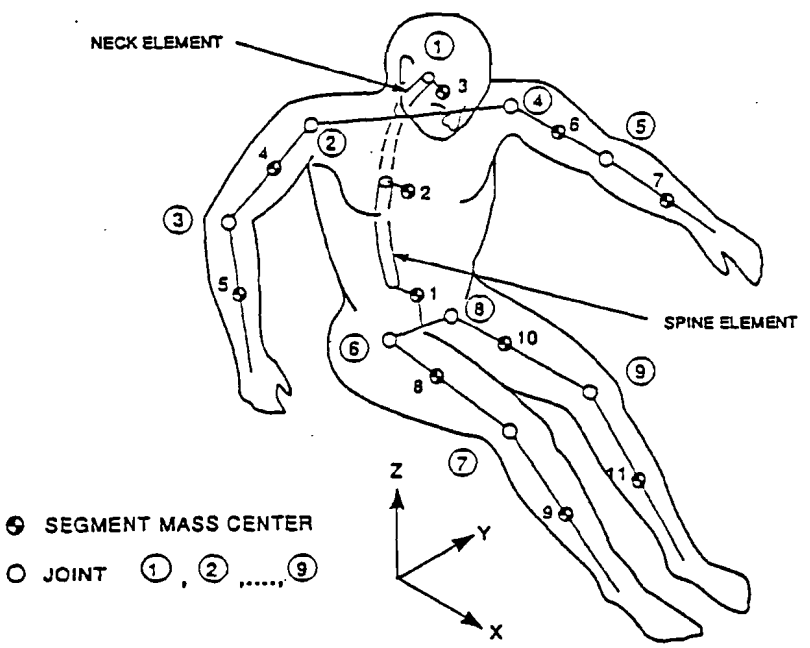

Figure 2. Eleven-segment (plane-motion) occupant model.

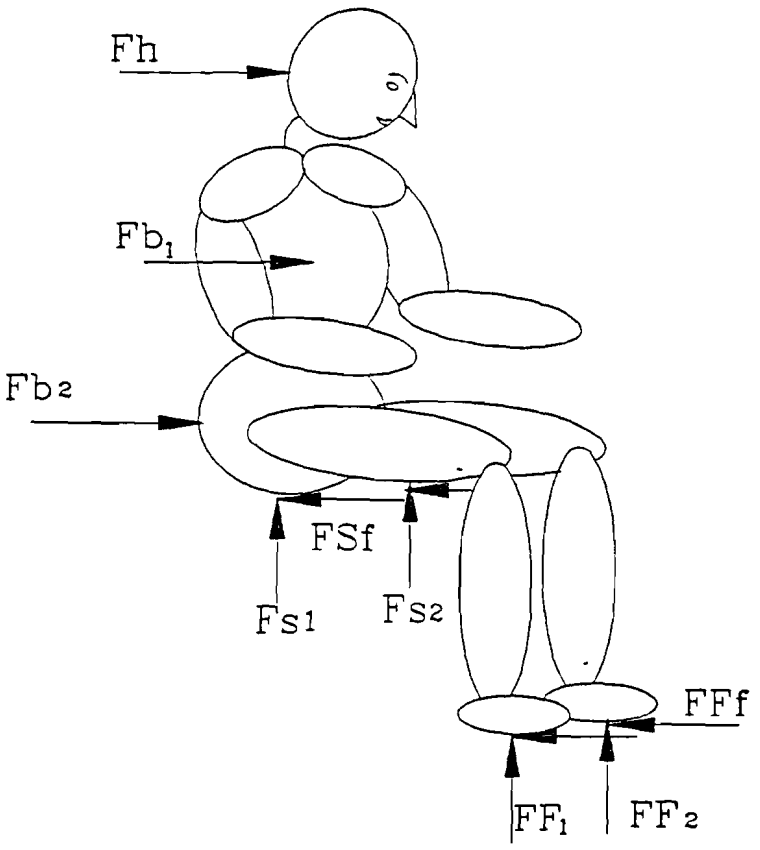

Figure 3. External force acting on occupant model .

2.2 Results from Earlier Assessments

Some experimental studies, including deceleration sled tests with forward-facing and pitch configurations were performed at CAMI (Civil Aeromedical Institute) to validate the SOM-LA/TA model [1]. The final report for the first phase of this project included descriptions of different test cases including a simple seat, an energy-absorbing seat, and a general aviation seats models [59]. These cases are briefly described next.

Test 1: Low deceleration forward-facing simple seat test

A 50th percentile Hybrid II ATD was used as the occupant in this test. The input pulse used was a trapezoidal pulse with a peak value of 6 G, digitized from the CAMI test results and the impact velocity was 44 ft/sec. The results from this simulation were compared with the older version of SOM-LA and also with the experimental dynamic sled results obtained at CAMI. The results of both the versions, SOM-LA/TA and SOM-LA, were similar in segment positions, segments accelerations etc [59]. However, some differences were observed, which could be due to differences in values of stiffness and damping characteristics, used in the models.

Test 2: Energy-absorbing seat test for the Sikorsky UH-60A Black Hawk Helicopter

Analytical study of an energy absorbing seat for the Sikorsky UH-60A Black Hawk helicopter was performed. The input pulse applied was a triangular pulse with a peak value of 44 G and a span of 0.06 seconds. The impact velocity was 44 ft/sec and the occupant selected was a 50th-percentile Hybrid II ATD. The results showed that the energy absorber loads used in SOM-LA/TA were much higher than those used in the older version and CAMI tests results [59]. Also the lumbar loads and moments were higher than the test results.

Test 3: General aviation seat test

Analysis was also carried out for a general aviation seat, with a 3-dimensional occupant model. The input pulse used had a trapezoidal shape with a peak of 12 G and a span of 0.17 seconds. Though the program terminated, when the ultimate strength of the seat legs were exceeded some results were obtained. The results showed that the head resultant accelerations and right lap belt forces were very close to the older version and to the CAMI test results [59]. However, since the 3-dimensional version of SOM-LA/TA does not have the capability to predict lumbar, the lumbar loads were not obtained.

The above test results showed that the occupant model, the interactions with the seat and the parameters of SOM-LA/TA are more stiffer than the older version SOM-LA. The lumbar loads predicted by SOM-LA/TA were much higher than the experimental values. Therefore, the lumbar spine of the occupant models have to be modified. Prediction of lumbar loads for the 3-dimensional models are also necessary. In this case, the program SOM-LA/TA is not capable of predicting vertebral pelvic loads, pelvic moments, femur loads. furthermore, there

is no envelope to study the effects of impact between the occupant and the cockpit interior. Chapter 4 presents the details on the development of an envelope and the adjustment of stiffness parameters to study the occupant interactions with seat and interior walls. The lumbar spine models of a two-dimensional 50th percentile Hybrid II dummy and an adult human male are also developed and further validations are performed. The lumbar details and test descriptions are discussed in chapter 5.

2.3 Comparison with Code MADYMO

In order to assess capabilities of code SOM-LA/TA, the crash victim simulation package MADYMO was acquired and successfully installed in the IBM RISC/6000 workstation. This discrete-parameter and multibody model is currently being used extensively by the auto industries for the prediction of impact responses of vehicle occupants and restraints (including airbags). It has provisions for both 2-D and 3-D occupant biodynamic simulations. A database, which provides details about different types of dummies is also available. The 2-D database has details about 50th percentile standard part 572 dummy, 50th percentile hybrid III dummy, three year old child dummy, and nine month old child dummy. The 3-D database has details about 50th percentile standard part 572 dummy, 50th percentile (sitting) hybrid III dummy, advanced 50th percentile (sitting) hybrid III dummy, European side impact dummy and three year old child dummy. In an effort to improve the constructed models, SOM-LA/TA models were compared to those of MADYMO. MADYMO also offers a set of force models for belts, air bags and contact of bodies with each other or with their surroundings. User defined subroutines can be added to the program for special modeling purposes.

Before using MADYMO to assess the capability of SOM-LA/TA, a simulation was performed with a 50th percentile dummy seated on a decelerated sled and restrained by an automatic belt system was performed in order to verify the installation of MADYMO. The sled had an initial velocity and was decelerated due to impact. The event was simulated in MADYMO by considering the sled stationary and by prescribing an acceleration field on the dummy. The maximum acceleration field applied was 15.4 G. In MADYMO, the interactions between the dummy and the sled are represented by plane-ellipse force interactions. The interaction between dummy parts is represented by an ellipse-ellipse force interaction. Automatic belt system is represented by a standard MADYMO belt model. The kinematic data is stored every 10 ms. The injury parameters HIC for the head resultant acceleration and 3 ms for the chest resultant acceleration are generated as well. The results include the linear accelerations near the center of gravity of pelvis, chest and head. The obtained results for this particular test matched the ones given in the application manual of MADYMO. The output kinematic data were then used to simulate the motion of the dummy. Efforts are being made to collect the data for the 5th and 95th percentile adult occupants.

A comparison between SOM-LA/TA and MADYMO occupant models seated on a Sikorsky UH-60A Black Hawk helicopter seat model was performed. A rigid seat model and a standard 50th percentile (part 572) dummy were used. The dummy was restrained with a lap

belt. Since both SOM-LA/TA and MADYMO have standard data bases for standard 50th percentile Hybrid II dummy, these data bases were used to input the details of the dummy (example: masses, moments of inertia, location of center of gravity etc.). The characteristics of the seat belt, the seat cushion, and seat back cushion properties were described by force-deflection relationships. The acceleration pulse applied has a peak value of 6 G. The simulation was conducted for 180 ms seconds in both cases. Some results are compared in Table 1. Figure 4 gives the comparison of resultant accelerations of head. As observed the resultant accelerations of the head are very similar from the two codes. The injury criteria for the head (HIC), evaluated from both codes are very close. Further comparison of the two codes will be conducted in the next phase of the project.

Table 1. Comparison of results from SOM-LA/TA and MADYMO.

	HIC	Head Peak Resultant Acceleration, (G's)
		a_{max}
SOM-LA/TA	95.6	21.9
MADYMO	99.1	26.5

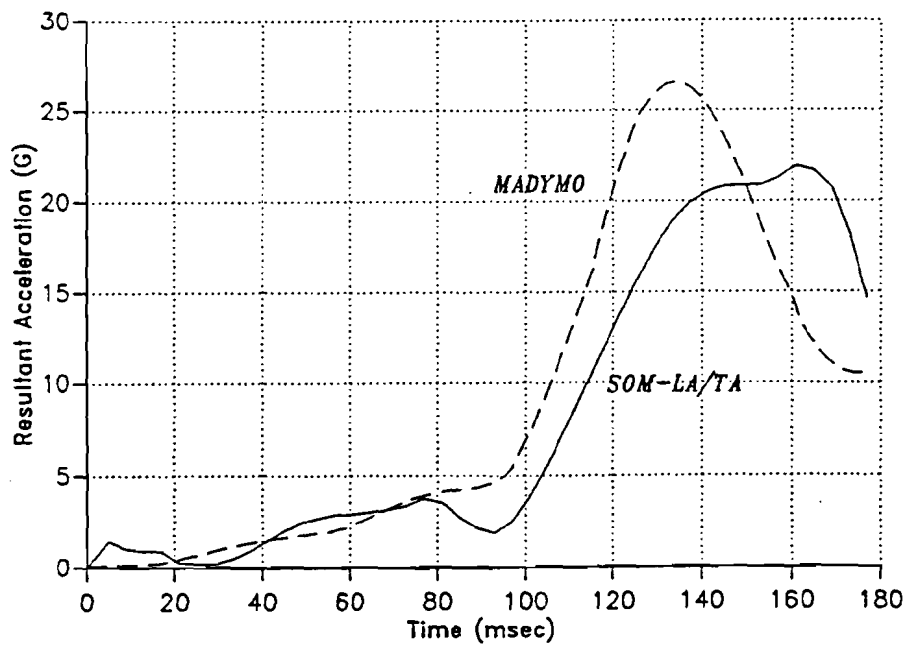

Figure 4. Comparison of SOM-LA/TA and MADYMO head resultant acceleration for the Helicopter seat.

2.4 Comparisons with Experiments at NIAR

Some experimental studies, including deceleration sled tests with forward-facing and pitch configurations were also performed at the Impact Dynamic Laboratory of National Institute for Aviation Research (NIAR) to validate the SOM-LA/TA model. A general aviation rigid seat with a pitch of 60° from the plane of the sled was used in the test. The deceleration pulse corresponds to Federal Aviation Regulations Part 23_Test_1 for a passenger, with a 15 G triangular pulse of 120 ms duration. The dummy was restrained using a lap belt to the rigid seat. The simulation was performed on SOM-LA/TA and MADYMO and the results were compared. As an example, Figure 5 shows the resultant head acceleration of a Hybrid II dummy versus time. As observed, the results from code SOM-LA/TA, MADYMO and experiment are similar. The HIC values are shown in Table 2, suggests a close match between MADYMO and tests. More validation tests will be performed and the results will be compared as more modifications are being performed on SOM-LA/TA.

Table 2. Comparison of HIC values of SOM-LA/TA, MADYMO and sled test.

	SOM-LA/TA	MADYMO	Sled Test
HIC	118.2	76.9	59

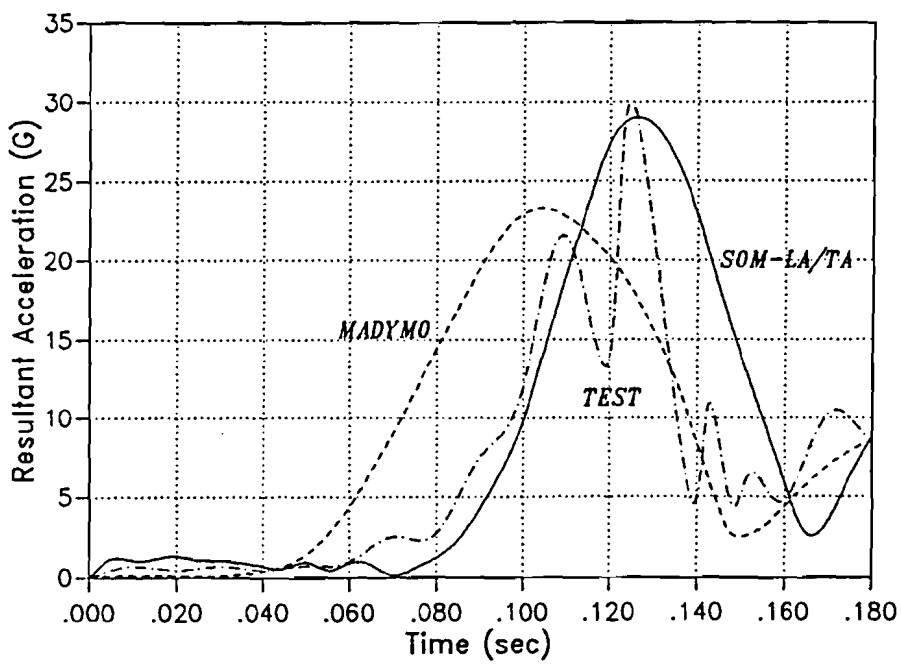

Figure 5. Hybrid II ATD head resultant acceleration versus time for a GA rigid seat under Part 23_Test_1 Passenger.

3. HEAD INJURY CRITERIA AND EVALUATION

Head Injury Criteria is an indicator used to predict head injuries. The study and development of Head Injury Criteria will assist in understanding mechanisms of head injury. This knowledge, intern, can be applied to improve design standards to reduce injuries in aircraft crash situations. In this study, an effort has been made to provide some details of the type of head injuries, the mechanisms associated with head injuries, the historical development of various head injury criteria and their measures, some comparisons of the head injury criteria and computational aspects of Head Injury Criteria.

3.1 Measures of Head Injury

It is well recognized that a head impact produces both translational and rotational motion as well as deformation of the skull with resultant brain injury from both absolute motion of the brain and its relative displacement with respect to the skull. At present, there are several physical parameters used in the evaluation of head injury, including translational and/or rotational acceleration levels of head impact, impact force, velocity and kinetic energy, impulse and impact duration, etc. These measures have been widely used for analyzing animal, human cadaver, and dummy experimental data to determine tolerable and survival thresholds for head impact in translation or rotation. Other parameters such as skull displacement and stresses, brain pressures and strains, as well as neck stretch/strain are usually related to analytical and experimental head model studies.

Wayne state tolerance curve (WSTC)

Skull fracture indicates that either a maximum load or energy input has led to failure [37]. Unfortunately when one considers other mechanisms of injury, particularly closed skull brain injury from impacts to the head, the shape, frequency content and duration of the pulse become significant. One of these earliest methods to quantify the effects of pulse duration was known as the Wayne State Head Injury Tolerance Curve. Figure 6 shows a composite of data points and one version of the WSTC. The injury assessment is based on the average acceleration and pulse duration. In spite of many interpretive and other difficulties associated with this curve, it has been the principle source of head injury tolerance information used by the automotive safety community.

There are also some limitations of WSTC. As the construction of WSTC was based on the acceleration time histories measured from longitudinal impact tests on the forehead, this curve is valid for longitudinal head impacts only. The measured longitudinal acceleration time history approximates the longitudinal rigid body acceleration of a specimen's head where the duration of a slow rise impulse is longer than 5 ms. The longitudinal head acceleration at very short duration impacts may differ markedly from the rigid body acceleration of specimen's head because severe skull vibration is excited by short duration pulse. If one wishes to establish an assessment for internal head injury hazard on the basis of the WSTC, one should recognize those limitations.

Severity index

The WSTC shown in Figure 6 is difficult to apply to complex acceleration-time pulse because of uncertainties in determining the effective acceleration and time [38]. A determined effort has been made to represent the WSTC in analytic form. Severity Index (SI) was derived by Gadd [39] from WSTC. The SI is defined by

$$SI = \int_0^T a^{2.5}(t)\, dt \tag{1}$$

where a(t) is the acceleration of head mass center in g's and T is the duration of the impact time in seconds. A SI value of 1000 based on a moderate or serious injury is generally accepted as the head injury survival threshold. The advantage of using SI is that it can be easily evaluated.

Head injury criteria

Head-Injury-Criteria (HIC) is generally accepted as an indicator of the likelihood of severe head injury and is determined from

$$HIC = \left\{ (t_2 - t_1)\left[\frac{1}{(t_2 - t_1)}\int_{t_1}^{t_2} a(t)dt\right]^{2.5} \right\}_{max} \tag{2}$$

where t_1 and t_2 are the initial and final integration time, respectively, and a(t) is the resultant acceleration (g) verses time (s) curve for the head strike. The HIC is a method for defining an acceptable limit; i.e., the maximum value of the HIC should not exceed 1000. It is a part of the Federal Motor Vehicle Safety Standards (FMVSS) and FAA Regulations. Although HIC is an acceptable parameter for the determination of head injuries, more research needs to done for a fuller understanding of the mechanism of injury to the head and to determine the new injury thresholds to predict the injury precisely. Program SOM-LA/TA computes the HIC by a moving-window integration of the data and a specific choice of data sampling.

3.2 Numerical Computation of HIC

The HIC is calculated from the head CG resultant acceleration - time profile of time duration t. Since the maximum HIC of 1000 is specified in FMVSS and FAA Regulations, a reliable and accurate method for HIC computation is needed. There are two computing program have been investigated. A code developed by Mentzer called HICOP has been debugged and used to evaluate the HIC at NIAR crash tests. The program listing is included in Appendix I. The other program called HIC has also been developed using direct computation for computing HIC at the Wichita State University. The associated program listing is provided in Appendix II.

Numerical determination of HIC number by evaluating Equation (2) for all iterative combinations of t_1 and t_2 in the maximizing process is extremely time consuming. Computation

algorithms are, therefore, needed to render a more practical and efficient evaluation of the HIC value. In the matter of fact, HIC is based on the data obtained from three mutually perpendicular accelerometers. The magnitude of the resultant acceleration vector obtained from the three accelerometers is function of time. Then, beginning at or just prior to the time of initial head contact (t_1), the average value of the resultant acceleration is found for each increment of time (t_2-t_1). This calculation will use all data points provided by the minimum 8000 samples for second digital sampling rate for integration. However, the maximizing time intervals need be no more precise than 1 ms. The average values are then raised to the 2.5 power and multiplied by the corresponding increment of time (t_2-t_1). This procedure is repeated, increasing t_1 by 1 ms for each repetition. The maximum value of the set of computations that is obtained by this process is the HIC. The procedure may be simplified by noting that the maximum value will only occur in the intervals where the resultant magnitude of acceleration at t_1 is equal to the resultant magnitude of acceleration at t_2, and when the average resultant acceleration is equal to the 5/3 times the acceleration at t_1 or t_2. However, in direct computational approach, it requires a combination of N*(N-1)/2 computations for a given discrete sample of N points. Although it is time consuming, an evaluation of HIC yields an almost "exact" value. Both the programs have been run for a simple acceleration pulse in g's as shown in Figure 7. HIC values from both programs were similar.

To further verify these programs, another run was made using results from a dynamic multibody model of head-neck to extension whiplash [40]. This multibody model, shown in Figure 8, consists of the head and the seven vertebrae (C1 through C7) attached to an upper thoracic region (T1) combined with the torso as a rigid base. The joints between the vertebrae allow rotations. The effects of muscles, intervertebral discs, cartilage and ligaments, cerebrospinal fluids and other tissues are depicted by nonlinear rotational spring dampers. Kinematic information on head and neck elements including the range of rotation in the flexion and extension directions are all taken into consideration. Another modification is construction of a brain model, based on the principles of hydrodynamics (squeeze effects). The basic model, representing the skull-brain interaction, studies the effects of two spherical bodies with fluid between them. For such a model, the pressure p and corresponding reaction force f developed inside are calculated using

$$p = \frac{3\mu_v V}{(c/R)^3 R\epsilon}\left[\frac{1}{1 - \epsilon\cos(\theta)^2} - 1\right] \tag{3}$$

$$f = \frac{6\pi\mu_v VR}{(c/R)^3}\left[\frac{1}{\epsilon^3}\ln(1 - \epsilon) + \frac{1}{1 - \epsilon} - \frac{1}{2\epsilon}\right] \tag{4}$$

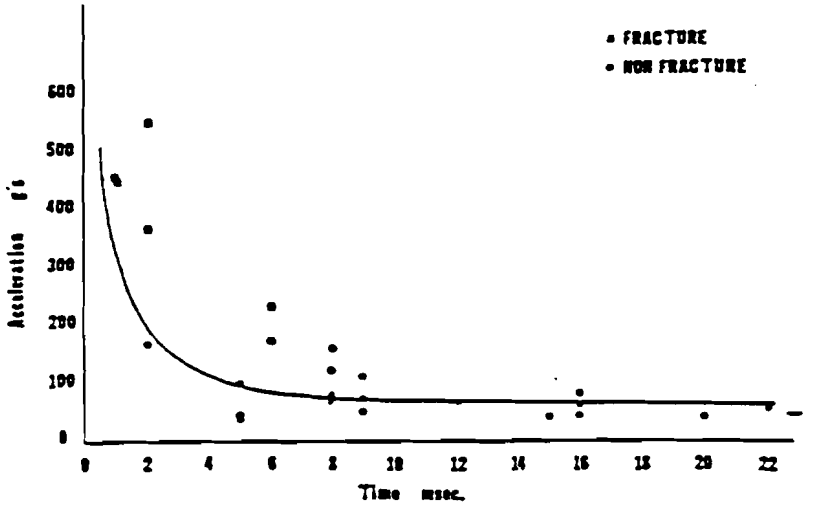

Figure 6. Original data from Wayne State University including all points super-imposed with first published Wayne State University tolerance curve.

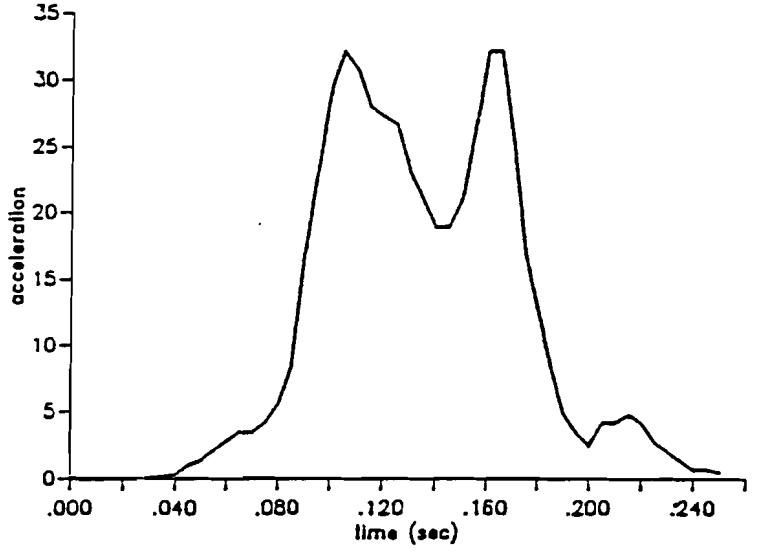

Figure 7. Acceleration pulse.

HIC from HICOP program = 278.78 t1 = 95.0 msec, t2 = 180.0 msec, CPU time = 4.75 msec.

HIC from direct computational approach = 278.78 t1 = 90.0 msec, t2 = 175.0 msec, CPU time = 142.67 msec.

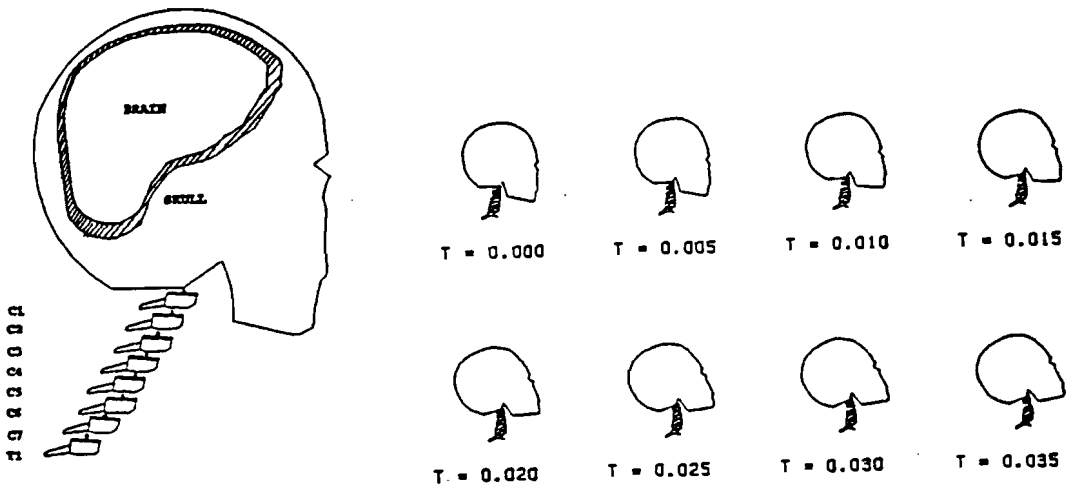

Figure 8. Modified skull-brain-neck model.

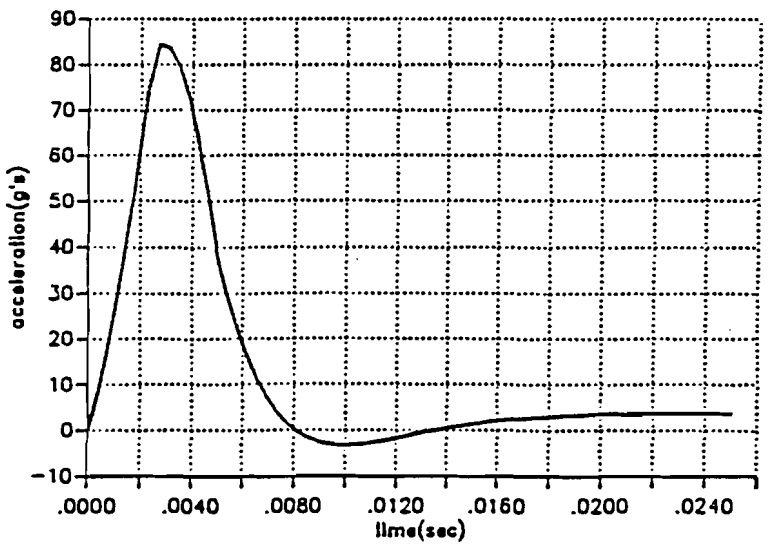

Figure 9. Acceleration of the head from the head-neck model.

where μ_v is the viscosity of the fluid; V the velocity of the inner spherical body; R the radius of the inner spherical body; ε the eccentricity ratio; c the radial clearance, and θ the angular coordinate measured from the maximum film thickness.

A triangular forcing function of 890 lb with a period of 5 ms was applied in the sagittal-plane, anteriorly at the base of T1. With this force as an input, the response of the model was determined for a duration of 25 ms. An output acceleration in the x-direction, shown in Figure 9, is used as an input to evaluate the HIC from the programs. The results are shown in Table 3. Direct computation of HIC is time consuming as evident by the CPU time of approximately 18.67 ms, compared to the CPU time of 4.16 ms obtained by the program code HICOP.

Table 3. Comparison of results from the two programs.

Method	t_1 ms	t_2 ms	t_2-t_1 ms	HIC	CPU ms
HICOP	1.87	5.22	3.36	128	4.16
HIC	1.55	5.03	3.48	132	18.52

3.3 Design of Non-sled Setup to Measure HIC

Impact sled testing is the most important experimental approach to evaluate the performances of safety devices and occupant injuries. However, this method is found to be more complex, time consuming and expensive. To solve this problem, the feasibility analysis of non-sled method has been performed to evaluate the Head Injury Criteria. This task is performed in order to isolate the motion of head from dynamic coupling of the rest of the body, and to determine whether it is possible to produce similar response of the isolated head from both sled and a non-sled tests. Procedures will then be developed for testing different materials and selection of suitable ones for the aircraft bulkhead and interior walls. Three methods of non-sled-test setup have primarily been designed in a simpler, more reliable and cost-effective way [56]. In addition, these methods are more versatile and can deliver more accurate results. These include Drop Tower Method, Pneumatic Driven Impact Method and Pendulum Impact Method.

Drop tower method

A drop tower is a flexible and proven two guide wire propelled system. This system is now in use as a quality control research and development tool in more than 28 laboratories to evaluate the head injuries. Such system with structural modification is designed to determine the Head Injury Criteria in aircraft crash safety.

The drop tower comprises of a dummy head assembly, the holding assembly, wire rope guided system and an impact absorber (Figure 10). This drop tower is designed to function at height level of 50 feet from the ground. Since there are many factors which affect the impact

response of the head with another surface, such as weight and mass distribution, shape, skull stiffness and skin thickness. Taking the above factors into account, a 50th percentile crash test dummy (Hybrid III model) is selected as a head model. The dummy head is fixed on to the position variation fixture which, in turn, is connected to the holding assembly. The whole assembly is lifted up by means of a wire rope system and dropped from the predetermined height levels. An accelerometer is mounted inside dummy's head. The impact absorber on its top surface has a force transducer which is covered by 1/4" thick cushion layer. The pulleys used here are double groove pulleys which facilitates the attachment of second wire rope to the cross bar plates. So when the rope test is to be performed at free gravity fall, the second wire rope is wound tight which in turn causes the compression of the spring which will release the whole drop tower assembly to fall down at gravity force. After the impact the various dynamic variables like acceleration and force are calibrated with the help of the respective measuring devices. From the time history of head acceleration, the HIC value can be evaluated.

Pneumatic driven impact method

This system mainly comprises of a double acting impact cylinder as shown in Figure 11. The cylinder is operated pneumatically with a supply of high pressure air of up to 10 bar. The head and neck assembly is fastened to the piston rod by means of the holding assembly. The air pressure is regulated by means of solenoid valves which facilitates in obtaining a wide range of dynamic variables. Within the dummy head accelerometers are mounted and the acceleration can be calibrated using acceleration transducers. The impact force can be obtained from the force transducer which is fixed on the impact absorber. By controlling air pressure the speed of the piston rod can be varied.

Pendulum impact method

The pendulum fixture essentially comprises of a hollow M.S. pipe, a dummy head-neck holding assembly, wedge fixture, base plate assembly, impact absorthod, a free-flight pendulum

along with the head-neck fixture is made to strike a impact absorber from specific location. Like a sled test, a free-flight pendulum does not simulate the punch of impact. Depending on its shape and size, the pendulum may or may not simulate the possible topography of a typical impacting surface. Because of its simplicity, the pendulum impact is commonly used to calibrate test dummies.

Before the actual operation the various points of location from where the pendulum is going to be released is predetermined according to the required impact velocity and energy. The actual value of the impact velocity and acceleration can be calibrated by fixing up a velocity transducer and acceleration transducer on to the dummy head assembly. The actual impact force can be obtained by calibrating the force transducer which will be fixed on to the impact absorbing stand. Strain gauges are to be fixed on to the dummy head through which deformation of dummy's head can be evaluated during the crash.

Although the main objective in developing these non-sled test rigs was to isolate the articulation of the head from the inertia of the rest of the body, it also enables us to evaluate the HIC while choosing the optimum padding material for bulk heads and interior walls of the aircraft. Of these three devices it has been decided to fabricate the Pendulum impact device since it reduces the complexity of an occupants impact to its simplest level.

Efforts are being made to make these devices in such a way, that it will enable us to do both the dummy calibration as well as the evaluation of HIC and optimum padding material. Fabrication cost has also been evaluated and the total cost for each of the test set-up are listed in Table 4. With the existing facilities in the Impact Dynamics Laboratory at NIAR, the pendulum will be hinged at 20 feet above the deceleration zone and it will be allowed to strike the stationary dummy head which will be fixed over impact sled. By this process, the problems associated with the electric's can be eliminated. Efforts are also being made to fabricate the pendulum in such a way, that the over all length of the pendulum can be varied in order to accommodate the various types of test procedures while generating the crash pulse. Further evaluation, analysis and testing of the head-strike-test rigs will be performed in the next phase of the project.

Table 4. Comparison of fabrication cost for the test setups.

	Impact Sled	Drop Tower Method	Pneumatic Method	Pendulum Method
Total Cost	$ 100,000	$ 7575	$ 11420	$ 6595
Attainable Velocity	80 ft/sec	56 ft/sec	40 ft/sec	44 ft/sec

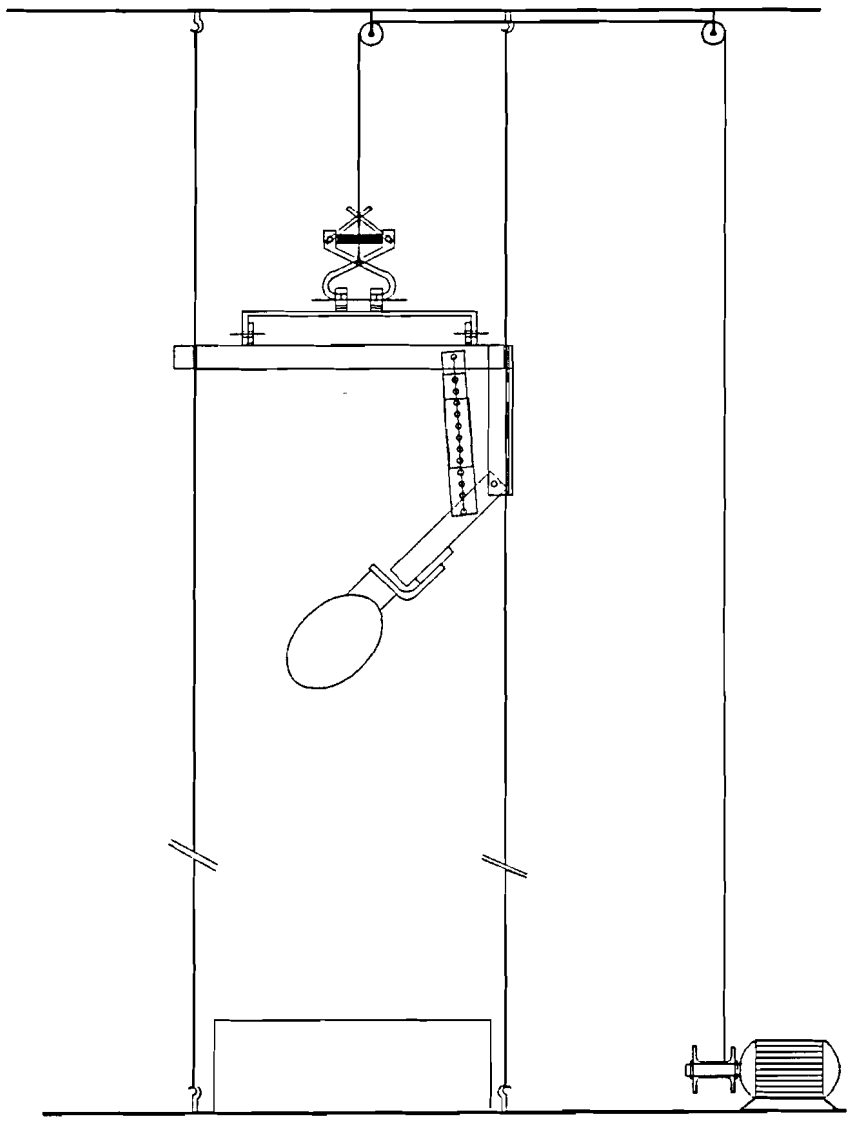

Figure 10. Drop tower setup.

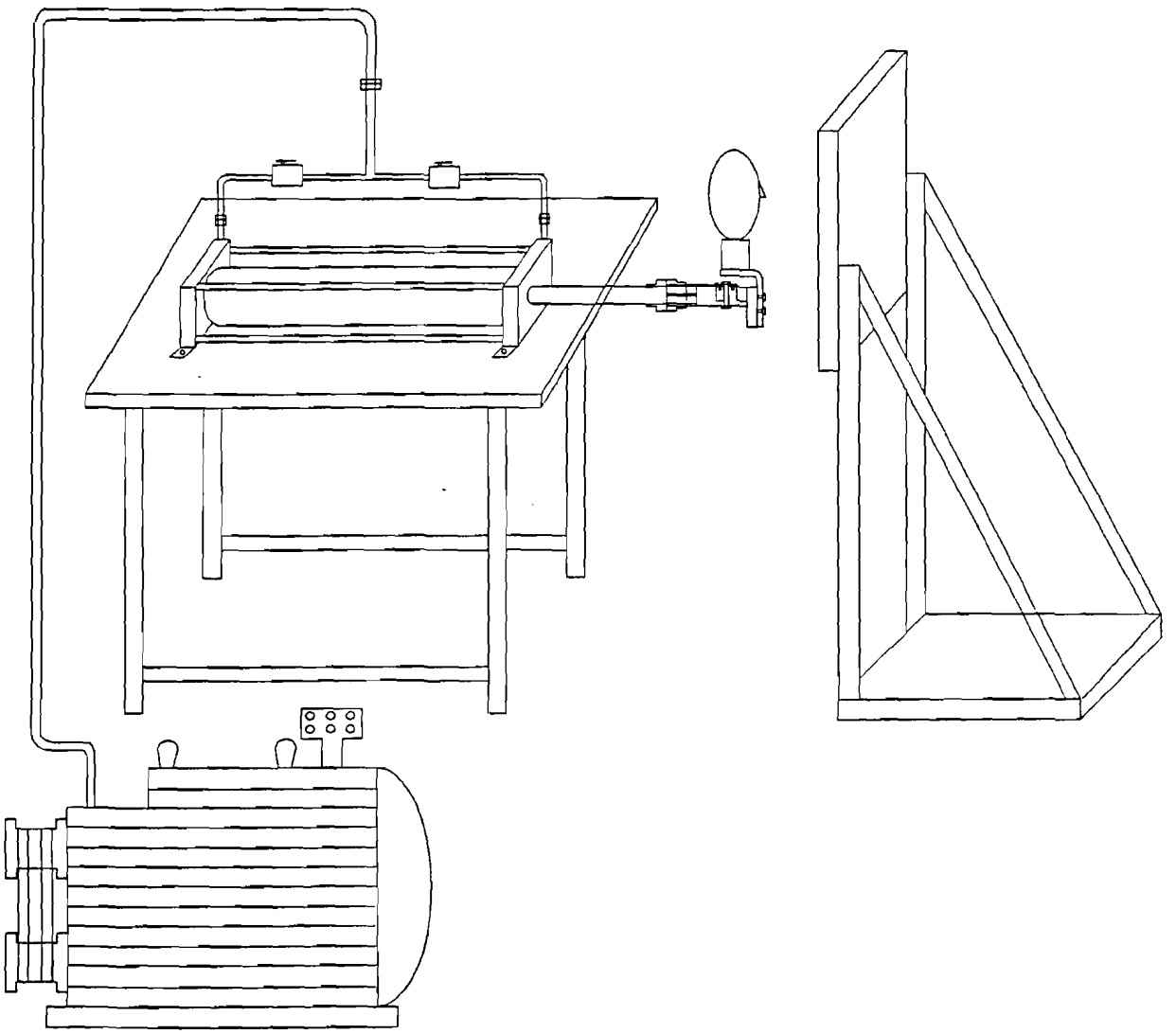

Figure 11. Pneumatic driven impact method.

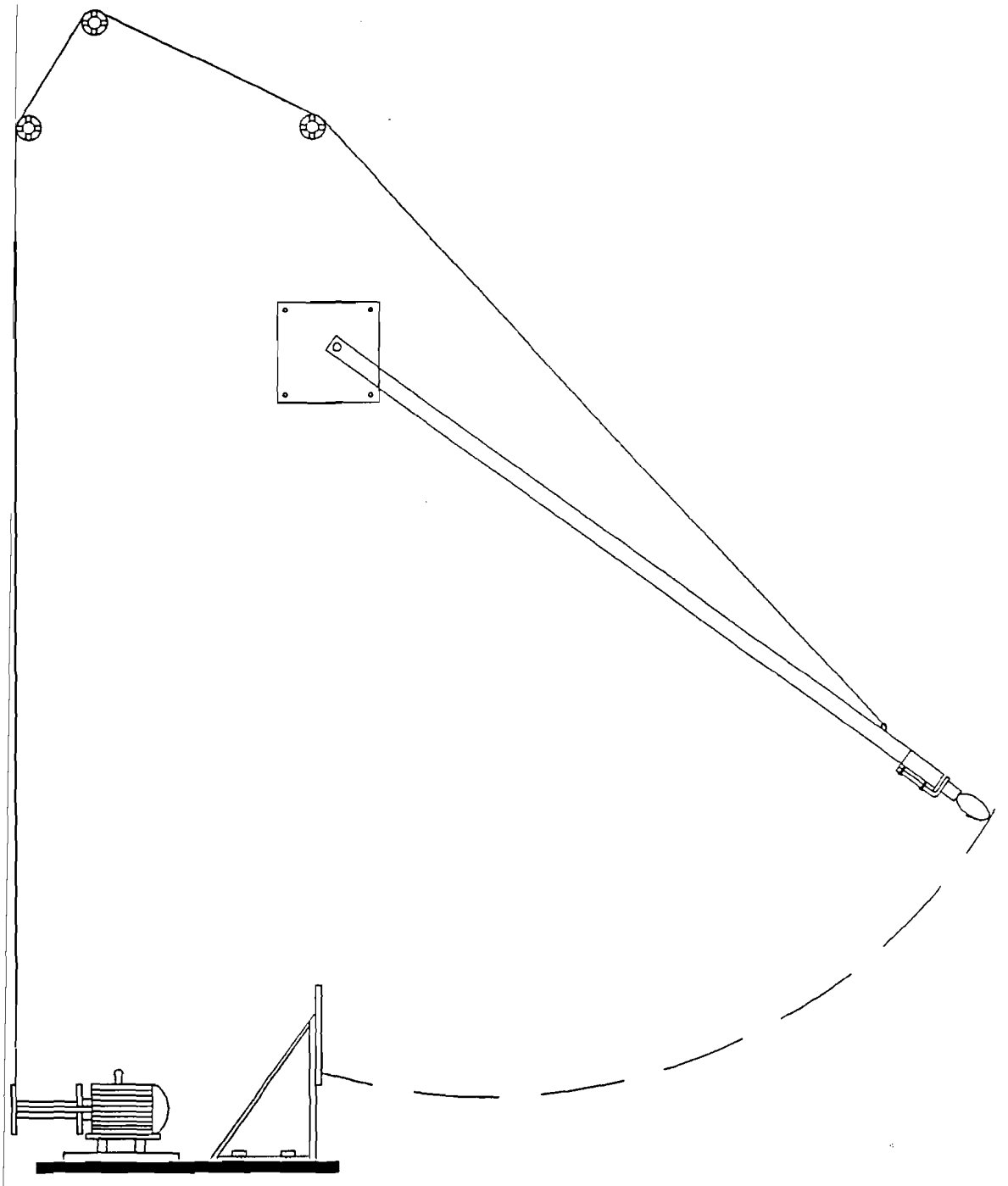

Figure 12. Pendulum impact method.

4. IMPACT DYNAMICS OF AIRCRAFT OCCUPANTS SEATED BEHIND INTERIOR WALLS

4.1 Non-Linear Contact Force Model

To assess our capabilities in predicting HIC during a head impact with the bulkheads of the aircraft, several analytical simulations were performed and the results were compared with that of a dynamic test carried out at CAMI [57]. The protocol in the experiment was developed to measure the head path and velocity from an anthropomorphic test dummy (ATD) restrained in a passenger seat. A mockup of a vertical wall in front of the seat was included in the fixtures. The distance between the seat end and the bulkhead was 35 inches. The test setup is shown in Figure 13. The input pulse was of a triangular shape with a maximum value of 16.9 g and a span of 160 ms. The velocity of the sled at the time of impact was 44 ft/s. A rigid seat was selected in order to eliminate the effects of the seat response on the occupant performance. Cushions were included on the top of the seat pan and seat back surfaces. The seat pan remained fixed in the aircraft floor and the seat back was permitted to rotate forward about a transverse hinge axis at the base of the back if pushed from behind. A standard 50th percentile dummy was then chosen as the occupant.

Series of analytical studies were then performed to match the results from the CAMI test. Figure 14 shows the head strike impact from simulation at different frames. In order to assess the compliance characteristics and displacement requirement of the aircraft bulkheads that minimize injuries as a result of a head contact, an envelope for the occupant and seat was generated, and a more accurate contact force model was also developed. To match the experimental results, a nonlinear, viscoelastic-type contact force model was used such that the contact force **F** was calculated from the deformation (indentation) δ and deformation rate $\dot{\delta}$ according to

$$F = A(e^{B\delta} - 1) + C\dot{\delta} \tag{5}$$

for which A and B are the stiffness coefficients, and C is a damping coefficient. Other models including linear viscoelastic, Hertzian with damping, and Hertzian with permanent indentation were also considered. However, the contact force model of equation (3) correlated best with the experimental static tests done on different padding materials. For different materials, based on the static tests, coefficients A and B are evaluated from experimental correlations. For the damping force, the damping ratio is taken to be constant for all the deformation modes of interest. This reduces the Raleigh formulation of the damping coefficient to

$$C = 2k\alpha \tag{6}$$

where k is the gradient of the contact force-deflection curve; i.e., $k = ABe^{B\delta}$. Variable α is a representative constant for the system, and is evaluated as

$$\alpha = \frac{C_0}{2K_0} = \frac{C_0}{2AB} \tag{7}$$

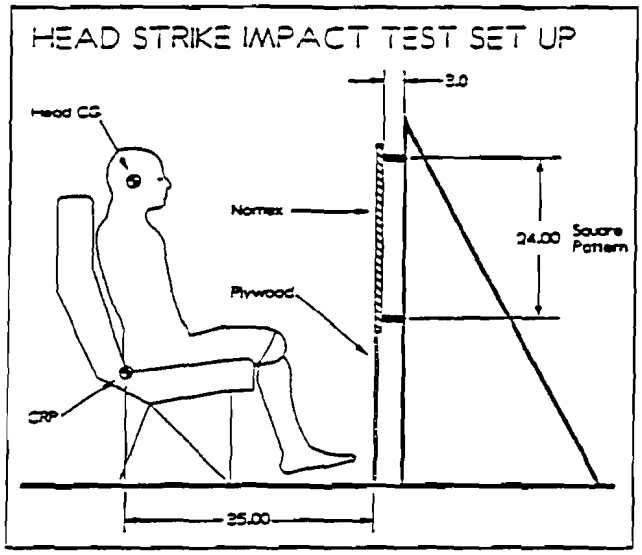

Figure 13. Sled test setup for occupant head impact with aircraft bulkhead.

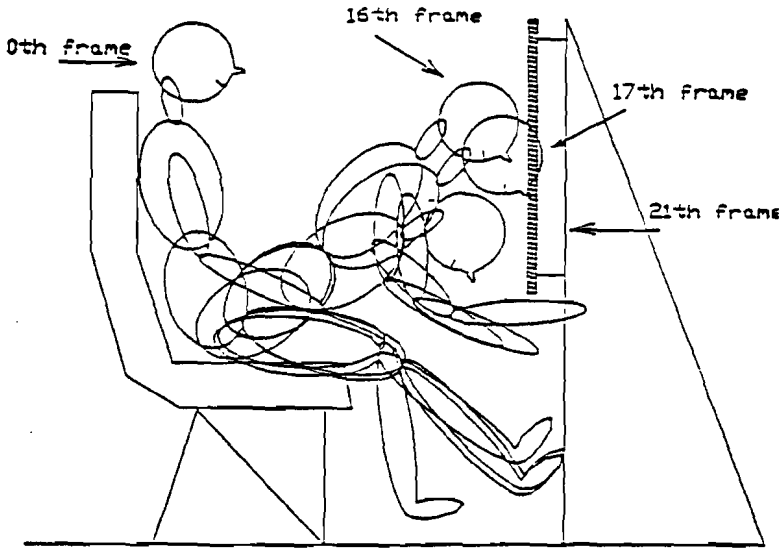

Figure 14. Reconstruction of head strike impact.

where C_0 and k_0 are respectively the damping and gradient of stiffness coefficients for zero deflection condition.

4.2 Parametric Study of the Contact Force Model

The contact force model was then used to determine the occupant response as a result of head contact with any envelope. The coefficients were varied in order to observe how the changes in these coefficients affect the HIC and maximum deformation of the front panel. A particular choice of the coefficients as

$$A = 720 \text{ lb}, \quad B = 0.71 \text{ in}^{-1}, \quad \text{and} \quad C_O = 1.0 \text{ lb-sec-in}^{-1} \tag{8}$$

was obtained, which matched the experimental results from CAMI presented earlier. Three sets of parametric studies of the coefficients in the contact force model were then performed in order to obtain a correlation between the HIC and the coefficients in the contact force model. In the first set, coefficient A representing a static component of the bulkhead material behavior was varied, while coefficient's B and C_O were taken as constants. As it is shown in the Figure 15, the HIC increases almost linearly with increasing coefficient A, and at the same time maximum deformation of the front panel decreases. Also, by increasing the stiffness coefficient A, the maximum spring force, maximum damping force and maximum acceleration of the head increases (Figure 16). Maximum spring force is more sensitive than the maximum damping force to the variations of coefficients A. The second set of simulations was variation of coefficient B holding A and C_O constants. As shown in Figure 17, the HIC increases dramatically with increasing gradient-related coefficient B. The figure also shows that the maximum deformation diminishes quickly at the same time. It can be seen that both the maximum spring and damping forces increase quite proportionally with the increase in coefficient B (Figure 18). The last set of simulations was performed by varying coefficient C_O, keeping A and B constants. It is interesting to observe that for given values of coefficients A and B, there is a value C_O that minimizes the HIC (Figure 19). The figure suggests that in order to keep the head injuries to an occupant seated behind an interior wall of an aircraft, the damping coefficient for zero-deflection must be around 0.5 lb-sec-in^{-1}. The figure also points out that the material for the bulkhead must have around 2¼ inches maximum displacement requirement. This is an important conclusion since it outlines the development of simple procedures for determination of the most suitable material for the aircraft interior walls. One method would be dropping of a weight (approximately equal to the weight of a human head) from a certain distance onto the bulkhead, and recording the maximum deformation of the bulkhead. Pendulum type setup has been used for many years for dummy calibration. A force-flight pendulum along with head assembly is made to strike an impact absorber from a pre-determined height. Again the maximum deformations of the bulkhead are recorded, and compared with the allowable 2¼ inches.

It should be noted that in this parametric study, only one parameter at a time was varied while holding the other two constants. What needs to be done next is to optimize parameter's

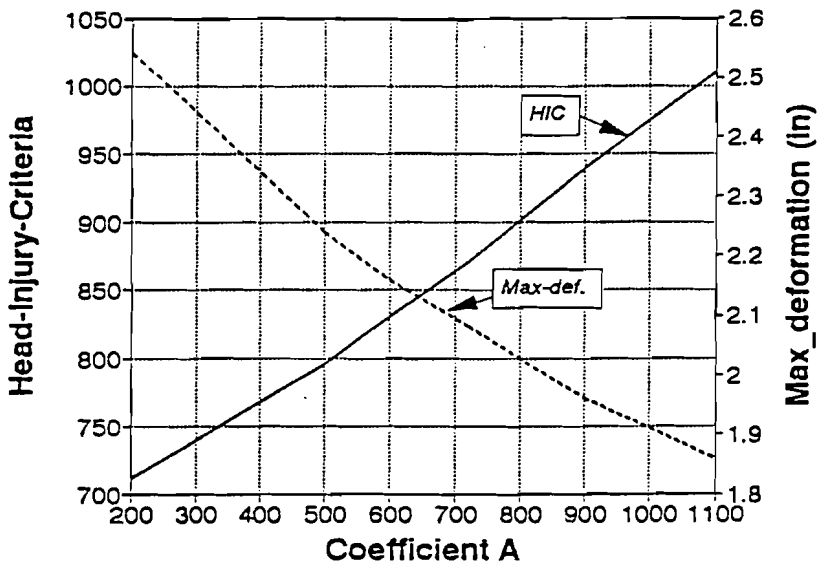

Figure 15. Head-injury-criteria and maximum deformation with variations of coefficient A.

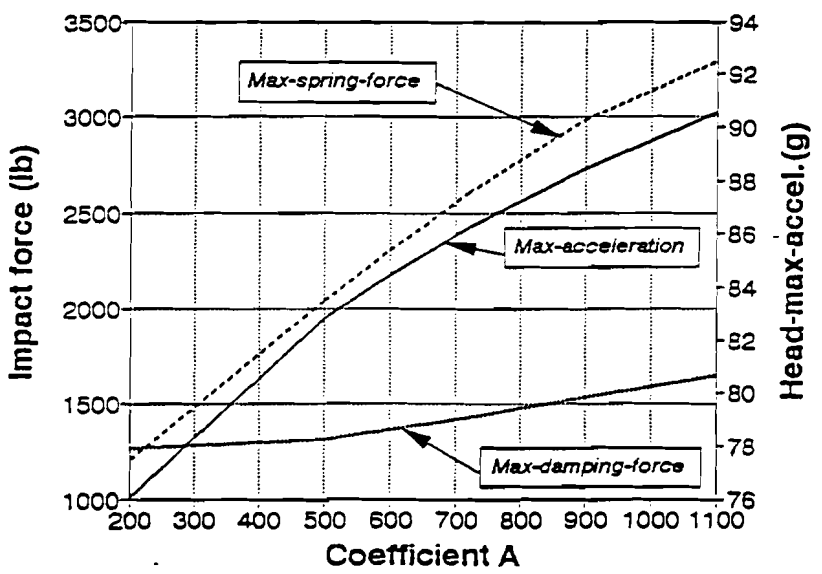

Figure 16. Components of impact forces and maximum acceleration with variations of coefficient A.

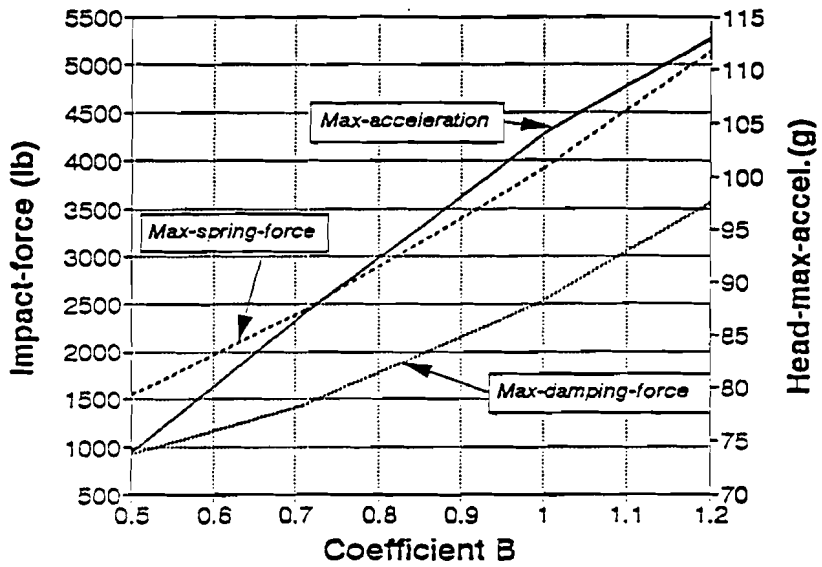

Figure 17. Components of impact forces and maximum acceleration with variations of coefficient B.

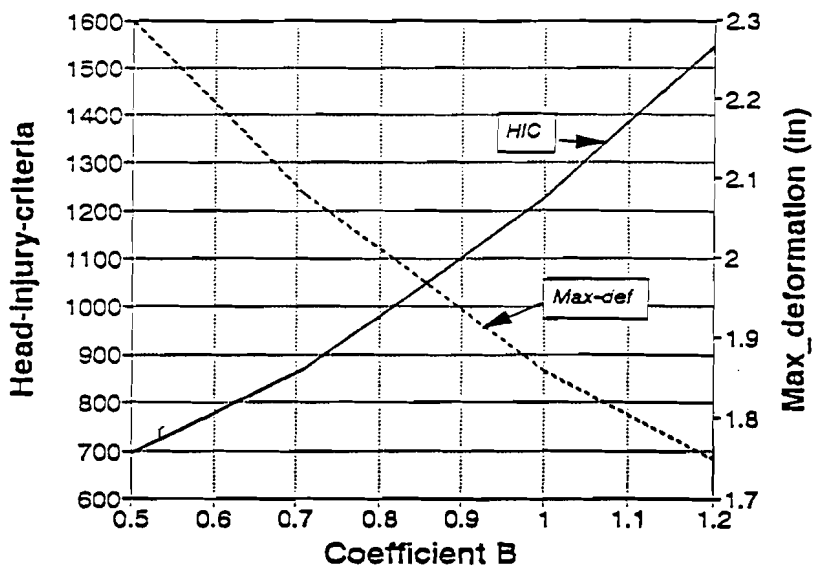

Figure 18. Head-injury-criteria and maximum deformation with variations of coefficient B.

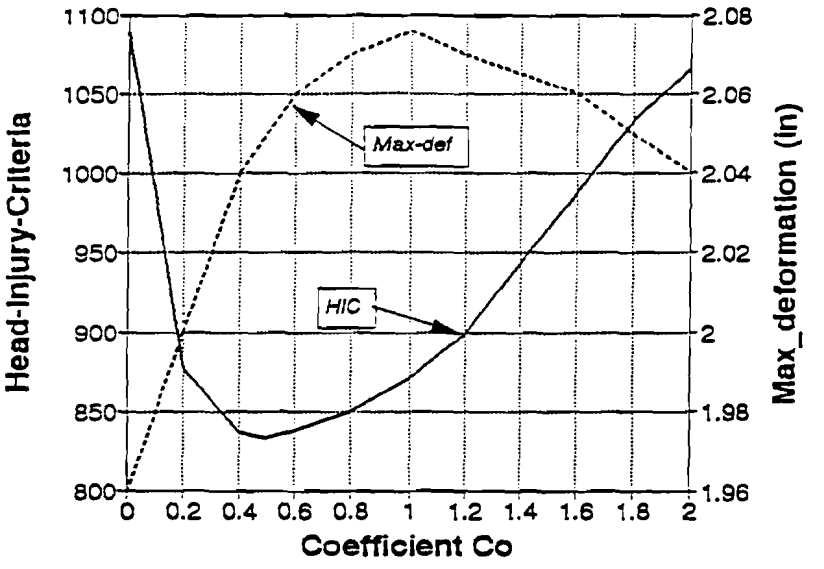

Figure 19. Head-injury-criteria and maximum deformation with variations of coefficient C_0.

A, B, C_o that minimize maximum acceleration of the head or to minimize HIC such that the bulkhead deformation is kept below 2¼ inches. This will result in a contact force model that has optimum stiffness and damping properties. A comparison of these analytical results with static force-deflection results of the different padding materials would point out to the selection of the most suitable material.

The preceding relationships point out some guidelines for selection of material required for keeping HIC within tolerable level. These relationships were obtained under certain conditions such as head acceleration pulse shape, sled initial velocity, restraint system as well as the row pitch (distance between seat reference point and bulkhead), and need to be further investigated and generalized. From the analytical results, it can be observed that there are several ways to keep the HIC below a limit of 1000. For given impact conditions, such as impact pulse shape and velocity, the material of bulkhead can be selected from values of coefficients A, B, and C_0 in order to minimize the HIC.

4.3 Selection of Padding Material Absorbing Head Impacts onto Aircraft Interior Walls

An analytical method for the selection of padding material to absorb head impacts onto aircraft interior walls or bulkhead has been carried out. The selective procedures for impact onto the padding materials at different impact velocities of the head have been developed with the following assumptions:

a) The impact is totally plastic, i.e. coefficient of restitution is zero.
b) The padding material properties are independent of rate sensitivity during crushing.
c) There is no stiffening effect on the padding material and the stiffness remains same through out the process.
d) The material exhibits linear force-deformation relationship.
e) The head impact occurs and maintains a single direction.

Thus, the contact force between the head and padding material is given by

$$F = m\,\ddot{x} = -k\,x \tag{9}$$

with the initial conditions $x(0) = 0$ and $\dot{x}(0) = v$. where F is the contact force, m is mass of the head, k is the stiffness of the padding material, x is the deformation and v is the impact velocity. The above equation was solved numerically for acceleration, and HIC was then evaluated from the HIC evaluation equation (2). Equating the kinetic energy of the head to the strain energy transferred to the padding material, the maximum deformation of the padding material can be determined from the expression

$$\delta_{max} = \sqrt{\frac{m}{k}}\;v \tag{10}$$

For a given velocity, the stiffness which results in a HIC of 1000 was found out by trial and error. The results are shown in Figure 20. From this chart, the value of maximum allowable stiffness for a specified impact velocity can be determined. To keep the HIC less than 1000, the stiffness of the material selected should be less than the maximum allowable stiffness. The maximum deformation obtained from equation (8) should also be less than the thickness of the material. The following example illustrates the selection of padding material for an impact velocity of 10 mph (14.7 ft/s).

It might be noticed that, for an impact velocity of 14.7 ft/s, the maximum allowable stiffness is approximately 6200 lb/in. Experiments on an ATD dummy impact on to different padding materials has been performed [58]. Table 4 shows some of the experimental results and properties of 1-inch thick padding materials for a head impact velocity of 10 mph. It can be observed that all the materials listed have stiffness less than 6200 lb/in. However Dytherm 4.2 and Ethafoam 900 are not suitable since they will result in maximum deformation larger than the material thickness. Dytherm 8.0 with stiffness of 3072 lb/in and maximum crush of 0.60 in. is the most suitable padding material at an impact velocity of 10 mph. Since its stiffness is less than the allowable maximum stiffness, HIC will be less than 1000. In addition, because the material thickness is more than the deformation, it will not get bottomed out.

Table 5. Properties of 1 inch thick padding materials for an impact velocity of 10 mph [58].

Padding material	Stiffness (lb/in)	Displacement(in)
Dytherm 4.2	1005	1.10
Dytherm 6.0	1761	0.85
Dytherm 8.0	3072	0.60
Ethafoam 600	650	1.27
Ethafoam 900	847	1.08

Figure 21 shows the variation of HIC with stiffness at various impact velocities. From this plot, the value of HIC for any given combination of stiffness and velocity can be found out. For example, a stiffness of 1000 lb/in at an impact velocity of 20 ft/s, results in a HIC of approximately 250. Further work is needed to consider materials with non-linear stiffness properties, stiffening effect, rate sensitivity, and also to include rotation of the head and articulation of total body.

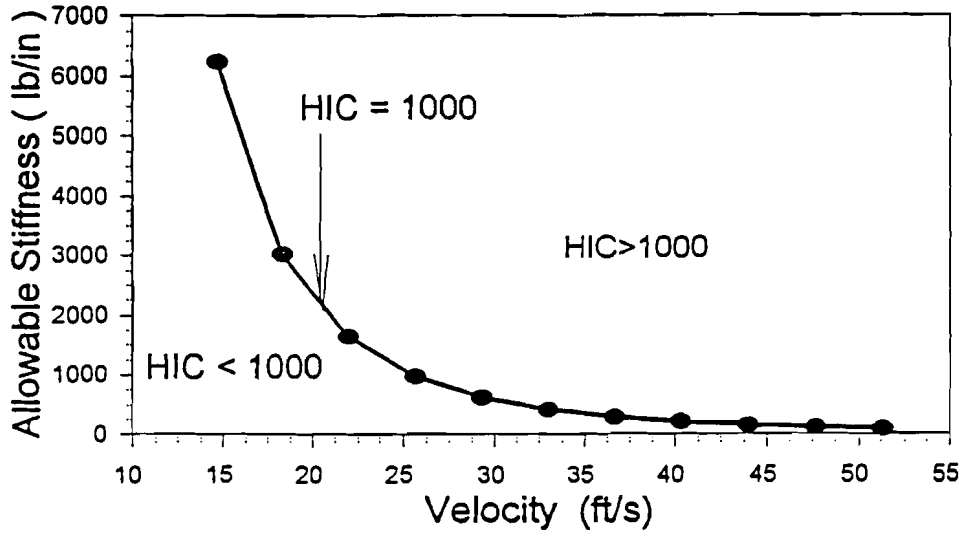

Figure 20. Variation of allowable stiffness with impact velocity for a HIC of 1000.

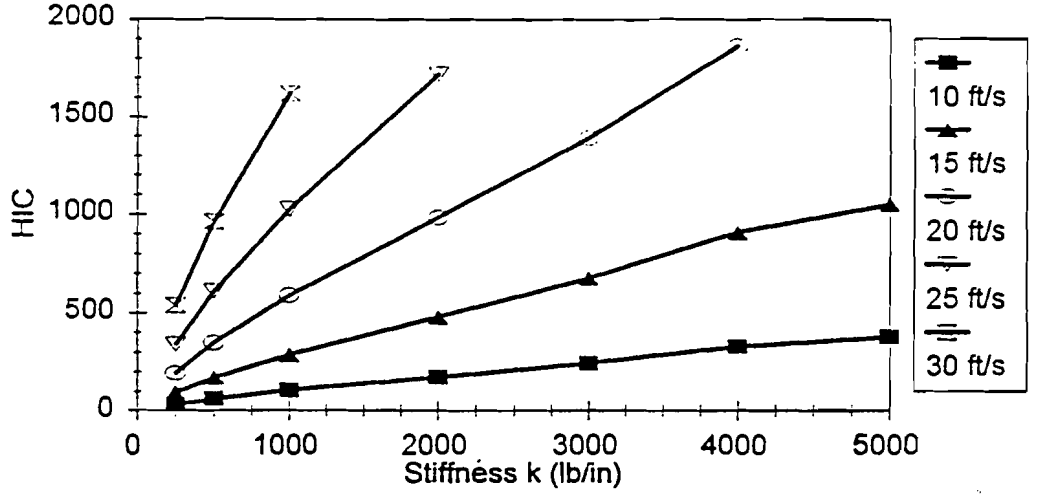

Figure 21. Variation of HIC with stiffness at different impact velocities.

5. DEVELOPMENT OF 2-D OCCUPANT WITH A FINITE ELEMENT MODEL OF LUMBAR SPINE

Although it is important to predict the dynamic behavior of the body segments, attention should be also focused on characterizing its more critical parts, which repeatedly sustain serious injury or significantly affect the overall dynamic behavior of the body during the collision. The spinal column is the main structural and kinematic member of the human torso. Spinal injuries occur frequently during aircraft emergency landing, pilot ejection from a disabled airplane, and vehicle collisions, etc. Numerous studies and considerable research efforts have been devoted toward the spinal modeling and injury prevention. Due to the complexity of the problem, evaluation of possible spinal injury has been strongly dependent on dynamic experiments on the anthropomorphic dummies. This fact is evident in the Federal Aviation Regulations [29] set by Federal Aviation Administration, which suggests that the pelvic loads measured on the spinal base of a modified part 573 (49 CFR 572) anthropomorphic dummy can be used in assessing the probability of a spinal injury.

A good measure of injury experienced by occupant in an aircraft accident is the amount of vertical loads transferred to the occupant spine. Not many studies have been performed to include a detailed model of a spine in the entire occupant model. Program SOM-LA/TA provides some approximation of the lumbar loads by a crude curvature approximation. It is the intent of this research to construct such as a detailed spine models for the 2-D occupant using the quasi-static approach and the finite element methods.

5.1 Formulations of 2-D Occupant Model

The 2-D occupant model is based on the rigid multi-body dynamics, consisting of eleven segments connected with eight hinge joints and eleven degrees-of-freedom. Rotations at the joints are resisted by torsional spring-dampers whose characteristics are represented by parameters such as stiffness and damping coefficients. These parameters are typically estimated from experimental results.

Matrix form of equation of motion

For 2-D occupant model, the dynamic formulations and equations of motion are assembled in terms of a set of independent or generalized coordinates. A set of Lagrange's equations of motion, in terms of the generalized coordinates is formulated according to

$$\frac{d}{dt}\left(\frac{\partial L}{\partial \dot{q}_i}\right) - \frac{\partial L}{\partial q_i} = Q_i \tag{11}$$

where Q_i represents those generalized forces not derivable from a potential function; L is Lagrangian function, which is the difference between the kinetic energy and the potential energy of the system. That is

$$L(q,\dot{q}) = T(q,\dot{q}) - V(q) \tag{12}$$

Applied the Lagrange's equations of motion to the dynamic system of interest results in an alternate form as

$$M(q)\ddot{q} = F_T(\dot{q},q) + F_V(q) + F_R(\dot{q},q) + F_E(\dot{q},q) \tag{13}$$

where, $\mathbf{M(q)}$ is the mass and inertial matrix, $\mathbf{F_T(\dot{q},q)}$ is a force vector due to the system kinetic energy; $\mathbf{F_V(q)}$ is a force vector due to the system potential energy; $\mathbf{F_R(\dot{q},q)}$ is a force vector due to the joint resistance of the system; and $\mathbf{F_E(\dot{q},q)}$ is a force vector due to the generalized external forces. Since the force formulations of three-dimensional occupant model are available in the User's Menu, the detailed force formulations of two-dimensional occupant model are discussed next.

Forces due to kinematic and potential energy

The 2-D occupant model consists of eleven segments. The system kinetic energy contains both translational and rotational parts

$$T = \frac{1}{2}\sum_{i=1}^{n} m_i\,(\dot{X}_i^2+\dot{Z}_i^2)+\frac{1}{2}\sum_{i=1}^{n} I_{\eta i}\,\omega_{\eta i}^2 \tag{14}$$

where m_i is the mass of segment i and $I_{\eta i}$ is mass moment of inertia of segment i with respect to the local coordinate axis η_i. The absolute velocities of the eleven mass segments required for the translational kinematic energy must be written as functions of the generalized coordinates and generalized velocities in order to use matrix form equations of motion (13). Generally, the angular velocity components can not be used directly in Lagrange's equations because they do not correspond to the time derivatives of any set of coordinates that specify the position of segment. However, for the two-dimensional system, since the angular velocity components about local axes ξ and ζ are zero, i.e. $\dot{\phi}_i = \dot{\theta}_i = 0$, then

$$\dot{\psi}_i = \omega_{\eta i} \tag{15}$$

Therefore, the system kinematic energy is

$$T = \frac{1}{2}\sum_{i=1}^{11} m_i\,[\dot{X}_i^2+\dot{Z}_i^2]+\frac{1}{2}\sum_{i=1}^{11} I_{\eta i}\,\dot{\psi}_{\eta i}^2 \tag{16}$$

The force vector $\mathbf{F_T}$ is derived from the system kinematic energy by using Lagrange's equations

$$\frac{d}{dt}\left(\frac{\partial T}{\partial \dot{q}_i}\right) - \frac{\partial T}{\partial q_i} = \sum_{j=1}^{11} M_{ij}\,\ddot{q}_j - F_{T_i} \qquad (j=1,11) \tag{17}$$

The system potential energy is gravitational potential, that is

$$V = \sum_{i=1}^{11} m_i\, g\, (Z_i - Z_{i0}) \tag{18}$$

where g is the gravity acceleration and Z_{i0} is an arbitrary datum. The force vector $\mathbf{F}_V$ is derived from the system potential energy,

$$F_V(q) = -\frac{\partial V}{\partial q_i} \qquad (i=1,11) \tag{19}$$

External forces acting on the occupant

The external forces acting on the occupant segments can be characterized as either contact forces or restraint forces. The contact forces applied to occupant are those forces exerted by the cushions and floor. Each of the forces acts normal to the surface applying the force. Friction forces are also applied by the seat bottom cushion and the floor. They are applied in a direction opposite to the tangential component of relative velocity between the occupant segment and the appropriate cushion of floor surface. Unlike the contact forces, resistance forces do not act at any fixed points on the occupant. The force acting points vary with the geometry of restraint system.

For a 2-D occupant model, assuming the resultant external force $\mathbf{F}_{Ei}$ acts on the segment i undergoing a virtual displacement δr_i. The virtual work on the system done by the external force is

$$\delta w = \sum_{i=1}^{11} (F_{xi}\delta X_{Ei} + F_{Zi}\delta Z_{Ei}) \tag{20}$$

where F_{Xi} and F_{Zi} are the components of external forces acting on segment 'i', δX_{Ei} and δZ_{Ei} the components of virtual displacement of segment 'i'. Writing the virtual displacement components in terms of the generalized coordinates, then

$$\delta X_{Ei} = \sum_{j=1}^{11} \frac{\partial X_{Ei}}{\partial q_j}\delta q_j \tag{21}$$

$$\delta Z_{Ei} = \sum_{j=1}^{11} \frac{\partial Z_{Ei}}{\partial q_j} \delta q_j \tag{22}$$

Therefore, the virtual work is

$$\delta w = \sum_{j=1}^{11} F_{Ej} \delta q_j \tag{23}$$

where, the external force F_{Ej} is

$$F_i = \sum_{j=1}^{8} (F_{Xi} \frac{\partial X_{Ei}}{\partial q_j} + F_{Zi} \frac{\partial Z_{Ei}}{\partial q_j}) \tag{24}$$

Occupant joint resisting torques

There are eight joints in the two dimensional occupant model. Each joint model contains a nonlinear torsional spring and a viscous torsional damper. For the human joint, the resistance consists of up to three terms. The primary resisting force during normal joint rotation is viscous damping term with constant coefficient. The resisting torque is applied at the limit of the joint range of motion. An additional term used to mimic the muscle tone is the moment which drops to zero after a small angular displacement from the initial position, provided that the crash deceleration is sufficient to overcome it. For the dummy joint, the resisting torque M_i is constant throughout the normal range of joint motion and increases rapidly along a third order curve to a higher value at the limiting displacement. The dummy joints torque M_{Di} will be given so that the joints just support a 1-G load in the seated position.

At each joint i, a torque T_i and a torsional damper with coefficient C_i act to resist motion of the joint. Then the virtual work done on the system as each joint i undergoes a virtual displacement $\delta\beta_i$ is

$$\delta w = -\sum_{i=1}^{8} (T_i + C_i \dot{\beta}_i) \, \delta\beta_i \tag{25}$$

where β_i is angular displacement of joint i from its reference position. Since β_i is a function of the generalized coordinate q_i, the virtual displacement $\delta\beta_i$ can be expressed in terms of corresponding virtual displacement of the q_i,

Substituting into equation (25) gives

$$\delta w = \sum_{j=1}^{11} F_R(\dot{q},q)\ \delta q_j \tag{26}$$

where $F_R(\dot{q},q)$is force vector due to the joint resistance of the system

$$F_R(\dot{q},q) = -\sum_{i=1}^{8} (T_i + C_i\dot{\beta}_i)\ \frac{\partial \beta_i}{\partial q_j} \quad (j=1,11) \tag{27}$$

Contact force models

All contact forces are calculated by determining the penetration of a contact surface on the occupant into a surface with known force-deflection characteristics. To each normal contact force a damping term is applied, which is proportional to the deflection rate. It has been assumed in SOM-LA/TA that the damping ratio is constant for all deformation modes of interest.

Different types of restraint systems can also be modeled. They are lap belt, only attached to either the airframe or seat, diagonal shoulder belt over the right or left shoulder attached to either the airframe or seat, double shoulder belt, and double shoulder belt and lap belt tiedown strap. These exerted forces on the occupant are evaluated based on the geometrical (ellipsoidal, spherical, and cylindrical) shapes of the body segments. From these, the impact between the occupant and the aircraft interior can be predicted.

5.2 Quasi-static Analysis with Finite Element Model of Lumbar Spine

To include a lumbar spine model into the multibody dynamic occupant model, essentials of rigid multibody dynamics and structural analysis must be known. Rigid multibody dynamics treats the physical objects as bodies that undergo motion without any change of shape. Therefore, rigid multibody dynamics is well suited for motion analysis of the occupant segments and the calculation of joint reaction forces. On the other hand, structural analysis is used to determine two main quantities: internal loads and deformation. It is necessary to determine the internal loads to know whether the structure is capable of withstanding the applied loads. The deformations must be determined to assure that excessive displacements do not occur.

One method to treat occupant models that undergo large motions as well as deformations is to assemble the equations of motion in terms of a mixed set of rigid/flexible coordinates. There are still many difficulties in this method corresponding to failure of accurate prediction of responses for systems operating at high speeds, and systems undergoing an impact. Furthermore, numerical integration of large values corresponding to rigid body coordinates and small values corresponding to deformations is usually associated with numerical difficulties, instabilities, and

inefficiencies. The methodology provided here is based on quasi-static analysis of a multibody system. The rigid multibody dynamics is used to predict large motions and some structural deformations at each particular time juncture. A finite element analysis is then performed to determine the corresponding loads on the structure and the unknown deformations. The methodology would result in more highly efficient numerical solutions for systems containing both rigid and flexible bodies.

In the study of occupant biodynamics, it may be necessary to analyze the aggregate motion of segments, the loads as well as deformations of the critical parts of human body and the injury criteria measures. This requires the generation and numerical solution of the rigid body dynamic equations of motion and a highly complex structural analysis, similar to the quasi-static procedure outlined earlier, in conjunction with the numerical solution of the constructed equations. Due to the complexity of the geometry and material properties, the mixed boundary conditions and the nonlinear behaviors of the structures, the finite element method will be used as an important and practical tool for determination of structural responses.

Anatomy of lumbar spine

The human spine is a complex, segmental column of vertebrae that constitutes the major subcranial part of the axial skeleton. The basic functions of the spine are to transmit load, allow motion, and protect the vital spinal cord. The vertebral column consists of twenty-four movable vertebrae. Seven cervical (C1-C7), twelve thoracic (T1-T12), and five lumbar vertebrae (L1-L5). In addition, there are five fused inflexible sacrum and four or five irregular fused coccygeal segments. The vertebrae articulate with each other in a controlled manner through a complex system of vertebrae, ligaments, muscles, facets and discs. Its individual components are united by a series of intervertebral articulations to form a firm but flexible column that supports the trunk and its appendages while providing a protective covering for the spinal cord. When viewed in the frontal plane, the spine generally appears straight and symmetric. When viewed in the sagittal plane, there are four curves. Anteriorly convex in the cervical and lumbar regions and posteriorly convex in the thoracic and sacrococcygeal regions.

The lumbar vertebrae are the lowest five of the spinal column. Compared to other parts of the spine, they are particularly heavy and large. The unique characteristic of the lumbar spine is that it must carry tremendous loads because of the large, super-imposed body weight and vertical impact forces during accidents. The lumbar spine and hips are responsible for the mobility of the trunk. These impose formidable mechanical demands on this region. Kinematically, there is relatively little axial rotation in this region. In flexion-extension, there is usually a cephalocaudal increase in the range of motion in the lumbar spine. The L5-S1 joint offers more sagittal plane motion than the other joints. For the lateral bending, each lever is about the same except for L5-S1, which shows a relatively small amount of motion. The two areas L4-L5 and L5-S1 bear the highest loads and tend to undergo the largest motion.

Review of spine models

Research in the spinal injury mechanism and methods of prevention started during the early 1940's, when the powered pilot extraction systems were being developed to separate pilot from the disabled aircraft. With the development of high speed and large capacity computers and the decrease of computing costs, mathematical modeling of the spine has attracted increasing attention of both biomechanical engineers and scientists. There have been a number of mathematical spine models which can be catalogued into four types: lumped-parameter models, discrete-parameter models, continuum-parameter models, and finite element models.

Lumped-parameter models intend to represent the spine as a simple mass-spring systems. Latham [41] was the first to propose a lumped-parameter model which consisted of a double rigid mass, weightless-spring-coupled system. Based on a single damped spring model of the spine and respective support mass,Payne [42] proposed a Dynamic Response Index (DRI), which is now regulated by FAA and is used to predict probability of a spinal injury in the performance evaluation of airplane ejection seats. It should be recognized that all the single degree-freedom models have the short-coming of predicting only a uniform axial force along the spine, which can not correspond to most of the spinal injuries occurring at the lower thoracic and upper lumbar regions [43].

Discrete-parameter models represent the spine as a collection of segments connected by kinematic joints. The first discrete-parameter model was initiated by Orne and Liu [44]. The model simultaneously accounted for axial, shear and bending deformations of discs, the viscoelastic behavior of the discs, the various size and mass of the vertebrae and discs. Aquino [45] created a lumbar spine model consisting of a series of lumped segments connected by linear springs and dashpots subjected to horizonal deceleration. Experiments were performed with isolated lumbar spinal segments, and agreement between the analytical and the experimental results was good for the range of conditions studied. A few three-dimensional discrete-parameter model of the spine has also been proposed [46-48].

Continuum spinal models have an infinite number of degrees-of-freedom and are capable of studying the simultaneous propagation of the axial, shear, and bending deformations. Among the continuum models, Hell and Lombard [49] represented the spine by a simple straight homogenous elastic rod. Cramer and Liu [50] constructed a more complex continuum spine model, considered as a curved homogeneous beam-column and subjected to a distributed eccentric inertial loading of the human torso. This model can be used for studies on impact at the base of the spine from any direction in the mid-sagittal plane.

Finite element analysis is a powerful and practical alternative to handle structural problems, particularly those with complex geometrical shape, material properties, boundary conditions, and nonlinearity. Liu and Ray [51] constructed a layered media column model with the alternate discs and vertebrae. The model took the geometrical and material properties into account. A +Gz impulsive loading was applied, and simultaneous propagation of the axial, bending, and shear deformations was investigated. Lavaste, et. al [52] designed a three-

dimensional geometrical and mechanical finite element model of the lumbar spine. The geometry of the model is constructed using six parameters per vertebra. Once this model has been fully validated, it will be a useful simulation tool for the mechanical study of the spine behavior in various situations.

In view of the large number of spine models involved, the evaluation of these models is difficult. However, since the studies of spinal models were isolated from the occupant itself and also from crash surroundings, it is very difficult to define some important parameters such as initial conditions, boundary conditions, applied time-varying loads and their locations, as well as the effects of occupant surroundings. In addition, large displacements of lumbar spine generally occur during the crash accidents, and significant errors of computer simulation results are generated by only using linear finite element analysis methods. Therefore, it is necessary to develop a human occupant model which can be used to predict displacements, accelerations, joint loads, and at the same time, the critical loads pertaining to the injuries. Therefore, the primary objective and impetus of these studies have been the development of spinal models that predict the configuration history, loads, stress distribution, and injury mechanisms.

Quasi-static analysis

In finite element analysis, the loads will generally be thought of as being applied, while the displacements are thought of as resulting. However, in analysis of multibody responses, it often happens that we have mixed boundary conditions. An example of a multibody system consisting of three bodies, two rigid bodies connected by a flexible body, is shown in Figure 22. Here, body "i" represents the pelvis, body "j" the thorax, and body "k" the lumbar spine. While performibody are known. The problem is to find the deformed shape of

the entire structure and also the forces and moments acting on the rigid bodies by the deformable body. The quasi-static approach is formulated by rearranging external forces, displacements, and the structural stiffness matrix. To solve the structural equilibrium equations for the unknown forces and displacements, let us partition the known (k) and unknown (u) variables as

$$\begin{bmatrix} \mathbf{F}_u \\ \mathbf{F}_k \end{bmatrix} = \begin{bmatrix} \mathbf{K}_{kk} & \mathbf{K}_{ku} \\ \mathbf{K}_{uk} & \mathbf{K}_{uu} \end{bmatrix} \begin{bmatrix} \delta \mathbf{q}_k \\ \delta \mathbf{q}_u \end{bmatrix} \tag{28}$$

where matrices $\mathbf{K}_{kk}$, $\mathbf{K}_{ku}$, $\mathbf{K}_{uk}$ and $\mathbf{K}_{uu}$ are sub-matrices of rearranged structural stiffness matrix $\mathbf{K}$, $\mathbf{F}_k$ is a vector of known forces acting on the spine, $\mathbf{F}_u$ a vector of unknown forces acting at the ends of lumbar spine, $\delta\mathbf{q}_u$ a vector of unknown displacements of lumbar spine, and $\delta\mathbf{q}_k$ known displacements of nodes 1 and 2 calculated from the rigid body dynamics. The unknown displacements and forces can be determined as

$$\delta \mathbf{q}_u = \mathbf{K}_{uu}^{-1}\left(\mathbf{F}_k - \mathbf{K}_{uk}\, \delta \mathbf{q}_k \right) \tag{29}$$

$$\mathbf{F}_u = \mathbf{K}_{kk}\delta \mathbf{q}_k + \mathbf{K}_{ku}\delta \mathbf{q}_u \ . \tag{30}$$

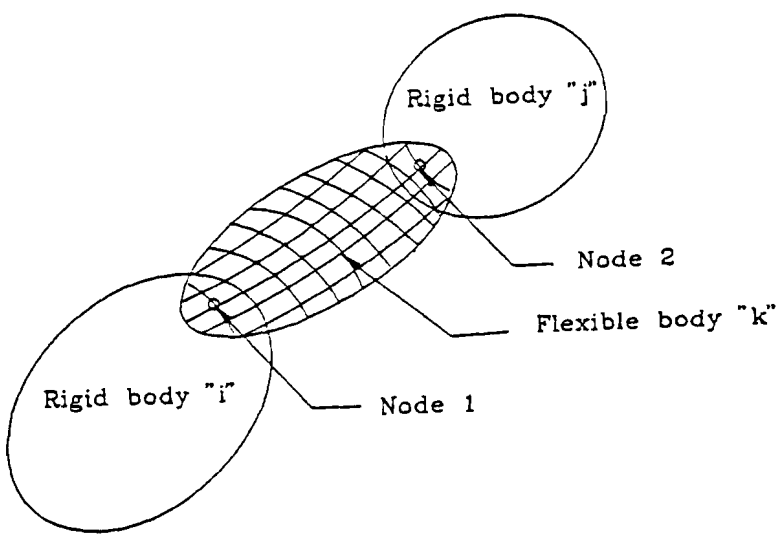

Figure 22. Flexible body between two rigid bodies.

The forces $\mathbf{F}_u$ with some additional damping are included in the rigid body dynamics equations of motion. Using this methodology, a finite element model of the lumbar spine was incorporated in the occupant model, and the loads acting on the spine were calculated. Preliminary results show that the new spinal model can work successfully as compared to experimental data. Further investigations are being conducted in order to construct a layered model with alternate discs and vertebrae.

Finite element model of lumbar spine

For the evaluation of occupant injury during the crash, the forces acting on the spine are critical measurements. In order to predict the configuration history, loads, stress distribution and injury mechanism, detailed information of kinematic, geometric, inertial and material properties of the lumbar spine were collected and evaluated. Based on the information, two kinds of finite element models of lumbar spine were created for both Hybrid II (Part 572) dummy and 50th percentile male human, respectively. The HYBRID II (Part 572) dummy's lumbar spine model consists of ten straight beam elements with rigid bodies at the top and bottom which represent the pelvis and thorax. The beam elements include both axial and bending stiffness, which represent five vertebra and five discs respectively. There are eleven nodes with thirty three degrees-of-freedom. The initially curved configuration of the finite element model is shown in Figure 23. Assume that the curvature of lumbar at seated position is constant, then the curvature radius ρ can be calculated by

$$\rho = \frac{S}{\varphi_e - \varphi_1} \tag{31}$$

where S is the total length of lumbar, φ_1 and φ_e are bottom initial angle and end angle of lumbar spine respect to the global coordinate system. The coordinates of nodes are generated according to the geometric configuration of spine

$$x_i = \rho\ (\cos\varphi_1 - \cos\varphi_i) \qquad z_i = \rho\ (\sin\varphi_i - \sin\varphi_1) \tag{32}$$

where the angles φ_i is determined by

$$\varphi_{i+1} = \varphi_i + \frac{S_i}{\rho} \qquad (i=2,10) \tag{33}$$

where S_i is the length of 'i' th element. To define the mixed boundary conditions of the model, the displacement and force transformations must be determined first. As shown in Figure 24, the displacement relationships of 'i' th element between the global and local coordinate systems are

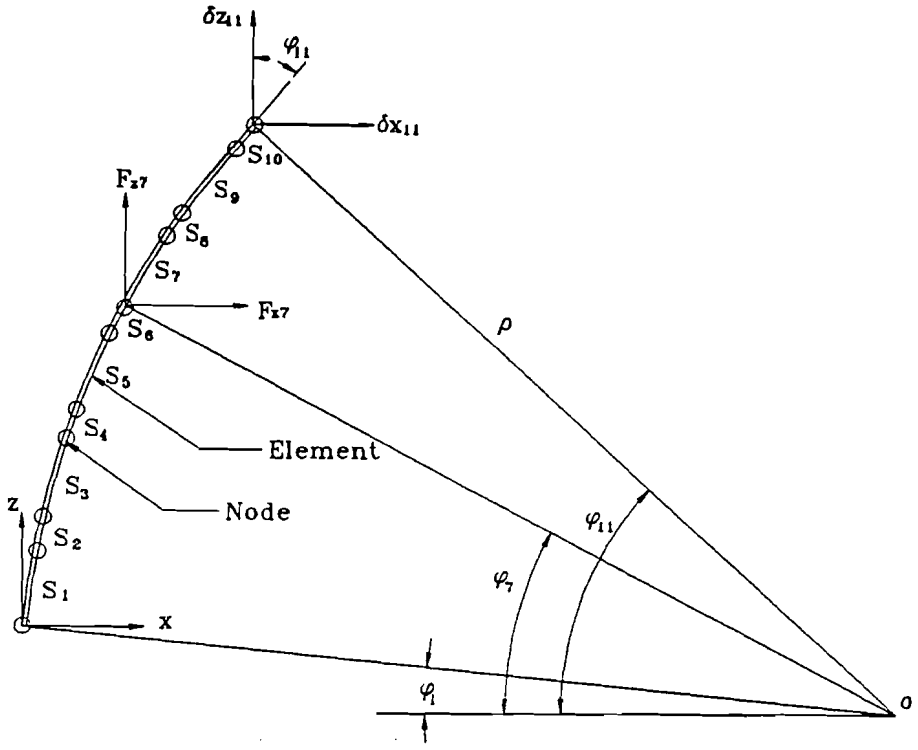

Figure 23. Finite element model of Hybrid II lumbar spine.

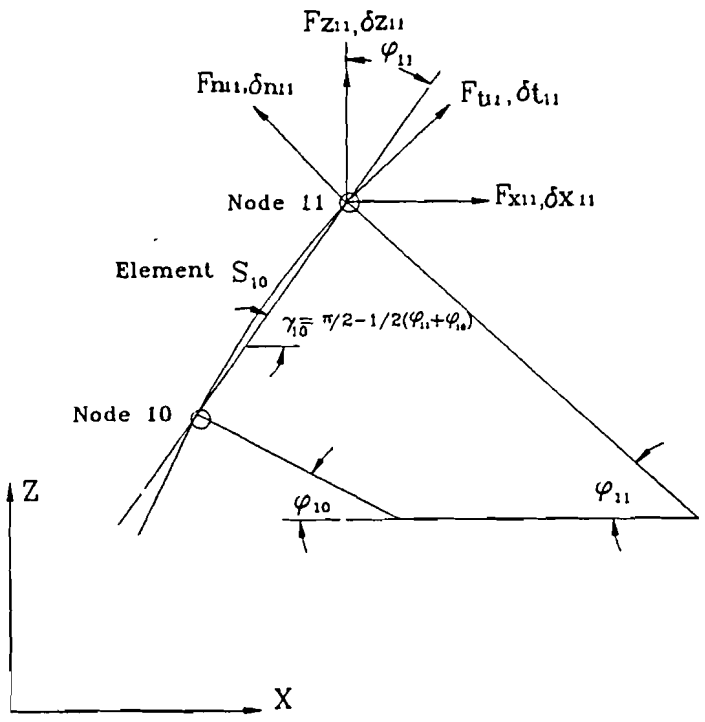

Figure 24. Relationship between global and local coordinate systems.

$$\begin{bmatrix} u_1 \\ v_1 \\ u_2 \\ v_2 \end{bmatrix}_i = \begin{Bmatrix} \sin\gamma & -\cos\gamma & 0 & 0 \\ \cos\gamma & \sin\gamma & 0 & 0 \\ 0 & 0 & \sin\gamma & -\cos\gamma \\ 0 & 0 & \cos\gamma & \sin\gamma \end{Bmatrix}_i \begin{bmatrix} \delta S_1 \\ \delta V_1 \\ \delta S_2 \\ \delta V_2 \end{bmatrix}_i \tag{34}$$

and the force transformations is

$$\begin{bmatrix} F_{x1} \\ F_{z1} \\ F_{x2} \\ F_{z2} \end{bmatrix}_i = \begin{Bmatrix} \sin\gamma & -\cos\gamma & 0 & 0 \\ \cos\gamma & \sin\gamma & 0 & 0 \\ 0 & 0 & \sin\gamma & -\cos\gamma \\ 0 & 0 & \cos\gamma & \sin\gamma \end{Bmatrix}_i \begin{bmatrix} F_{s1} \\ F_{v1} \\ F_{s2} \\ F_{v2} \end{bmatrix}_i \tag{35}$$

Therefore, the displacement boundary conditions at node 1 and node 11 are defined as

$$\begin{aligned} u_1 &= 0.0 \\ v_1 &= 0.0 \\ \varphi_1 &= \varphi_1^0 \end{aligned} \tag{36}$$

and

$$\begin{aligned} u_{11} &= \delta S_{11} \sin\varphi_{11} - \delta V_{11}\cos\varphi_{11} \\ v_{11} &= \delta S_{11} \cos\varphi_{11} + \delta V_{11}\sin\varphi_{11} \\ \varphi_{11} &= \varphi_{11}^0 \end{aligned} \tag{37}$$

where u_i and v_i are nodal displacements, δS_i and δV_i are the axial and shear deformations of lumbar spine. The force boundary conditions are

$$\begin{aligned} F_{xi} &= \sin\varphi_i F_{vi} + \cos\varphi_i F_{vi} \\ F_{zi} &= -\cos\varphi_i F_{vi} + \sin\varphi_i F_{vi} \\ M_i &= M_i^0 \qquad (\ i = 1 \ \textit{and} \ 11\ ) \end{aligned} \tag{38}$$

The external forces and moments acting on the intermediate nodes are those forces and moments such as gravity loads, eccentric loads and moments, etc. Compared to the impact loads during the airplane crash, those loads are relatively small. Therefore, they can be neglected and assumed to be zeros. That is

$$P_{xi} = 0.0 \qquad P_{yi} = 0.0 \qquad T_i = 0.0 \qquad (i=2,10) \tag{39}$$

The geometric data were obtained from the drawings of 50th percentile male test dummy. The spine has 5.375 inches of length, and 2.69 inches of diameter. The area moment of inertia is 2.56 in^4. The material properties of Butyl rubber were initially used for the beam elements, and they were then modified according to the correlations with force-displacement and moment-angular displacement experimental data. Because the non-linear characteristics of the lumbar spine bending moment-angular of rotation [53], the mean value of Young's modules was used in this model which is 7157 lb/in^2, and the Poison' ration is 0.45.

The human lumbar spine model consists of five straight beam elements with rigid bodies at the top and bottom. The beam elements include both axial and bending stiffness, which represent five vertebra and discs respectively. There are six nodes with eighteen degrees-of-freedom. The rigid bodies represent the pelvis and thorax. The initially curved configuration of the finite element model is shown in Figure 25. The original local coordinate system is defined at the bottom end of lumbar spine. These nodal point coordinates were taken from Liu and Ray [51]. The material properties and the geometric data has been prepared by combining the values as given by Orne and Liu [44] and Moffatt et. al [54]. The total length of initially curved lumbar spine is 7.49 inches. The geometrical and physical properties of the lumbar spine are listed in Table 1, and the limits and representative values of ranges of rotation of lumbar spine are listed in Table 2.

Table 3. Geometrical and physical properties of lumbar spine

	Disc		Vertebra				
	Area (in^2)	High (in)	Mass ($lb\text{-}s^2/in$)	High (in)	Inertial (in^4)	E (lb/in^2)	G (lb/in^2)
L1	1.94	.38	.0117	1.04	.135	6000.	2000.
L2	2.22	.41	.0117	1.06	.169	8000.	2600.
L3	2.44	.42	.0117	1.08	.282	8000.	2600.
L4	2.66	.48	.0117	1.16	.220	9000.	3000.
L5	2.72	.36	.0117	1.10	.306	9000.	3000.

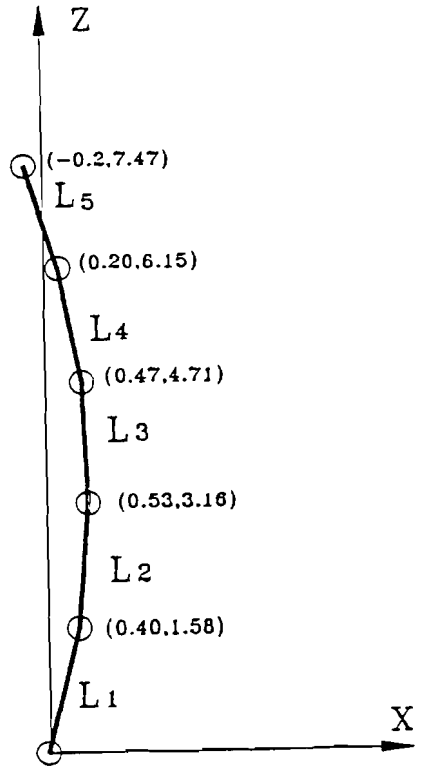

Figure 25. Finite element model of the male human lumbar spine.

Table 4. Limits and representative values of ranges of rotation of lumbar spine

Interspace	Flexion-extension (±deg.)		Lateral Bending (deg.)	
	Limits	Mean Angle	Limits	Mean Angle
L1-L2	5-16	12	3-8	6
L2-L3	8-18	14	3-10	6
L3-L4	6-17	15	4-12	8
L4-L5	9-21	16	3-9	6
L5-S1	10-24	17	2-6	3

5.3 Programming of Nonlinear Finite Element Model of Lumbar Spine

Due to the large deformation of lumbar spine, the mixed force and displacement boundary conditions, as well as the connections with the multibody dynamic occupant model, there are no codes available to deal with quasi-static analysis for the nonlinear finite element model of lumbar spine. Therefore, the lumbar spine model was programmed by author using nonlinear finite element analysis techniques. The input requirements for this code include geometric and material properties of lumbar spine, definitions of the finite element model, gravity loads acting on the lumbar spine, and deformation and force boundary conditions. The outputs of each time step include nodal axial forces, shear forces, element internal forces, bending moments, nodal displacements, and stress distributions. The program consists of seven subroutines and then incorporated into program SOM-LA/TA. It is called by subroutine program RMATX2 of SOM-LA/TA as a part of the efforts to evaluate the elements of joint resistance vector $\mathbf{F}_R(\dot{\mathbf{q}},\mathbf{q})$. The detailed program flow chart is illustrated in Figure 26. For the quasi-static nonlinear finite element analysis, the structural stiffness matrix is constructed according to the latest geometry and material properties at each time step. The mixed boundary conditions are then imposed on the system. In order to solve the unknown forces, the stiffness matrix, the displacement and force vector of the equilibrium equations of the system are re-arranged to separate the known and unknown displacements and forces. The Guasian elimination method is used to solve the unknown displacements from the sub-equilibrium equation. The solved displacements are then substituted into the system equilibrium equation to evaluate the unknown forces acting on the ends of the lumbar spine. Once the nodal displacements are known, the nodal forces and internal forces of elements are evaluated. At this stage, the equilibrium of the system is checked, and the unbalance forces between external and internal forces are calculated. If the out-of-balance forces are smaller than the pre-described limits, the program will continue to the next time step. Otherwise, the updated equilibrium equation will be solved. This procedure will repeat until the satisfactory results are obtained. For the next time step, the nodal coordinates are updated according to the latest configuration of the model and the material properties. The structural stiffness is then calculated. The stiffness will be little different when the spine deformations are small (less than 4%) and the material properties are constants. Once the nodal displacements are known, the internal forces acting at the ends of the elements are calculated by using the frame

element stiffness equation given in chapter II equation (26). The nodal forces are then evaluated by summarizing all the forces acting at each node in a vector manner.

Program validation and verification are very important steps to computer programming. Before incorporating this program into SOM-LA/TA, a series of verifications were performed. Those examples illustrate that the finite element analysis program is able to handle the large displacement non-linear frame problems with mixed boundary conditions.

5.4 Numerical Simulation and Comparison to Experimental Results

For the purpose of evaluation of the occupant model together with a non-linear finite element model of lumbar spine, a general-purpose finite element code, capable of partitioning matrix and handling plane frame problems with mixed boundary conditions, has been programmed. The validation of the code was performed by comparing the numerical results with the classical results. The program was then incorporated into the modified SOM-LA/TA code, and the quasi-static analysis approach has been implemented. As in study, a number of simulations were performed. The work was divided into a number of separate cases which are listed below:

Case 1. Hybrid II dummy seated on an energy absorbing seat with tilted pitch angle.
Case 2. Standard male-human seated on an energy absorbing seat with tilted pitch angle.
Case 3. Hybrid II dummy with Part 23_test_1 (crew) test conditions.

<u>Hybrid II dummy seated on an energy absorbing seat with tilted pitch angle</u>

In this case, analytical study of an energy absorbing seat for the Sikorsky UH-60A Black Hawk helicopter was performed. The setup of the test is shown in Figure 27. The seat consists of a bucket which supports the occupant. Principal functional members of the frame are two vertical guide tubes along which the bucket can move, controlled by energy devices. Vertical inertial crash loads force the seat bucket down the guide tubes against the resistance of energy absorbers. In order to simulate an emergency landing dynamic condition on the horizontal sled, the seat Z-axis was pitched forward 17^0 from the plane of the sled. The occupant selected was a 50th-percentile (part 572) male dummy. The pelvic structure of the dummy used in the test had been modified to include a six-axis load cell at the base of the lumbar spine. Force was thus measured in the dummy spine.

The computer simulation input file was prepared using information both from the SOM-LA/TA User's Menu and biomechanical data measured from blue drawings of Hybrid II dummy and thus allows comparison with previous analytical results from SOM-LA/TA and experimental results from Civic AeroMedical Institute of Federal Aviation Administration. The two-degree-of freedom seat model was used in this simulation. The energy absorber force-deflection characteristics were based on the data from static and dynamic tests of the components. The rotational stiffness of the seat was based on a static test of the system. The input pulse was of

a triangular shape with a maximum value of 41.5 G and a span of 60 millisecond (ms), as shown in Figure 28. The impact velocity was 43.5 ft/sec.

The simulations were implemented on the IBM ES9000-440 mainframe. Some fundamental responses were investigated by comparing results both from the sled impact experiments and simulations. As mentioned earlier, an important measure of safety, and a requirement for aircraft seat certification, is the amount of load transferred to the occupant spine. It was observed in Figure 29 that the lumbar spine loads obtained from experimental test results, the simulation results of SOMLA-FEA (or SOM-LA/TA with a FEA lumbar spine model) and simulation results of SOM-LA/TA had primarily the same patterns. However, the SOMLA-FEA simulation results are more closer to that of experimental results, especially the peak value of lumbar load, which is critically important to assess the occupant injury. The deformation configuration of lumbar spine as a function of time is illustrated in Figure 30. The maximal axial deformation is 0.52 inches corresponding to the maximal axial lumbar load at time 50 ms during the impact simulation. As to the lumbar bending moments presented in Figure 31, the simulation results both from SOMLA-FEA, and SOM-LA/TA have the same pattern and initial frequency, but have higher moment levels compared to that of impact sled test. The possible reasons for these include selection of occupant parameters such as the occupant mass distributions and centers of mass locations for body segments, as well as selections of force-deflection characteristics of restraint system and seat cushions, etc. As compared to the results from diverse types of simulations performed by the author, the bending moments of lumbar spine are very sensitive to those parameter selections.

Figure 32 illustrates the DRI values calculated by both SOMLA-FEA and SOM-LA/TA. It was observed that they had similar patterns, and the maximal DRI value (20.2) obtained from SOM-LA/TA is littler higher than that of SOMLA-FEA (18.9). Figure 33 shows the comparison of Severity Index obtained from SOMLA-FEA and from SOM-LA/TA, which the latter has higher level SI values after time 100 ms. The HIC values from the SOMLA-FEA is 148 and is 172 from the SOM-LA/TA, both are much less than the tolerable value 1000. However, the maximal lumbar spine load exceeds 1500 pounds. Therefore, when evaluating the possible injuries of the occupant, both the critical values must be checked in order to obtain the correct conclusion.

Standard male-human seated on an energy absorbing seat with tilted pitch angle

In this study, the exact impact conditions were used except that a standard 50th percentile male-human was used as the occupant instead of a 50th-percentile (part 572) male dummy. The database of male-human occupant was excerpted from SOM-LA/TA program and then the spine related data was modified in order to incorporated the finite element spine model into the SOMLA-FEA program. As to the lumbar spine loads and bending moments, it was observed that both the simulation results have the same patterns and same order of values. However, these axial loads and bending moments acting on the male human occupant are much larger than those acting on the Hybrid II dummy, even the simulation conditions are exactly same. The main reason for those differences is because the male human and Hybrid II dummy are described in

different databases as shown in Tables 5 and 6. For example, the weight and Y-axis moment of inertia of human's upper torso are 55 pounds and 3.29 lb-in-sec^2, respectively, while that of Hybrid II dummy is only 36 pounds and 0.926 lb-in-sec^2 respectively. The larger upper torso weight and moment of inertia will increase both the lumbar loads and bending moments during the crash. Hence, it is obvious that when the dummy is used to evaluate the dynamic performances of seats and possible injuries of occupant, attention must be paid to that there are still a great difference between the test results with a dummy and actual results with the human passengers. Some seats may pass the impact test successfully, but may not be safe to the passengers. Therefore, the correlations between test dummy and human occupant should be further investigated.

The deformation configuration of lumbar spine in the time history is illustrated in Figure 34. As contrast to the concave curve of Hybrid II dummy's lumbar spine, the human body has lumbar spine with the convex curve. Since the human lumbar spine has less cross-sectional area and longer length than those of Hybrid dummy, the axial deformation of the human lumbar spine is larger than those of dummy as presented in Figure 35. The maximal axial deformation is about 1.0 inches corresponding to the maximal axial lumbar load at time 55 ms during the impact simulation.

Hybrid II dummy with Part 23_test_1 (crew) test conditions

In order to provide further validations, a series of sled dynamic tests were performed at Impact Dynamics Laboratory at National Institute for Aviation Research (NIAR). The experimental tests were set up in comply with Federal Aviation Regulation (Part 23_Test_1 Crew). The GA iron crew seat was used with 60^0 pitch from the plane of the sled as shown in Figure 36. The occupant selected was a 50th-percentile (part 572) male dummy. The deceleration pulse was of a triangular shape with a maximum value of 19 G and a span of 100 ms, as shown in Figure 37. The impact velocity was 42 ft/sec.

The lumbar spine loads acting on the dummy were digitized and compared with the simulation results as illustrated in Figure 38. It is observed that the peak values are 1500 lb from test, 2760 lb from simulation of SOM-LA/TA, and 1930 lb from the simulation of SOMLA-FEA. As to Head Injury Criteria (HIC), the SOMLA-FEA obtained a value of 101.1, which is close enough to the test HIC value 97.7, while the SOM-LA/TA obtained a HIC value of 219.1. The comparison of head resultant accelerations is shown in Figure 39. The peak values both from test and simulation of SOMLA-FEA are almost same, while the patterns have some differences. The test result shows that the head resultant has a high acceleration frequency during the period time 60-90 ms. This is probably because that a high frequency filter 1000 Hz was used for data acquisition in the impact sled test and a lower filter 300 Hz in the simulation. The relationship of resultant accelerations among dummy's head, chest and pelvis is shown in Figure 40. The other important fact is that the lumbar spine is not only subjected to the axial loads and bending moments, but also the shear forces. Figure 41 shows the shear forces as a function of time. It has a similar patten to that of deceleration pulse, and has a peak value of 1500 pounds, which is the same order as the axial forces.

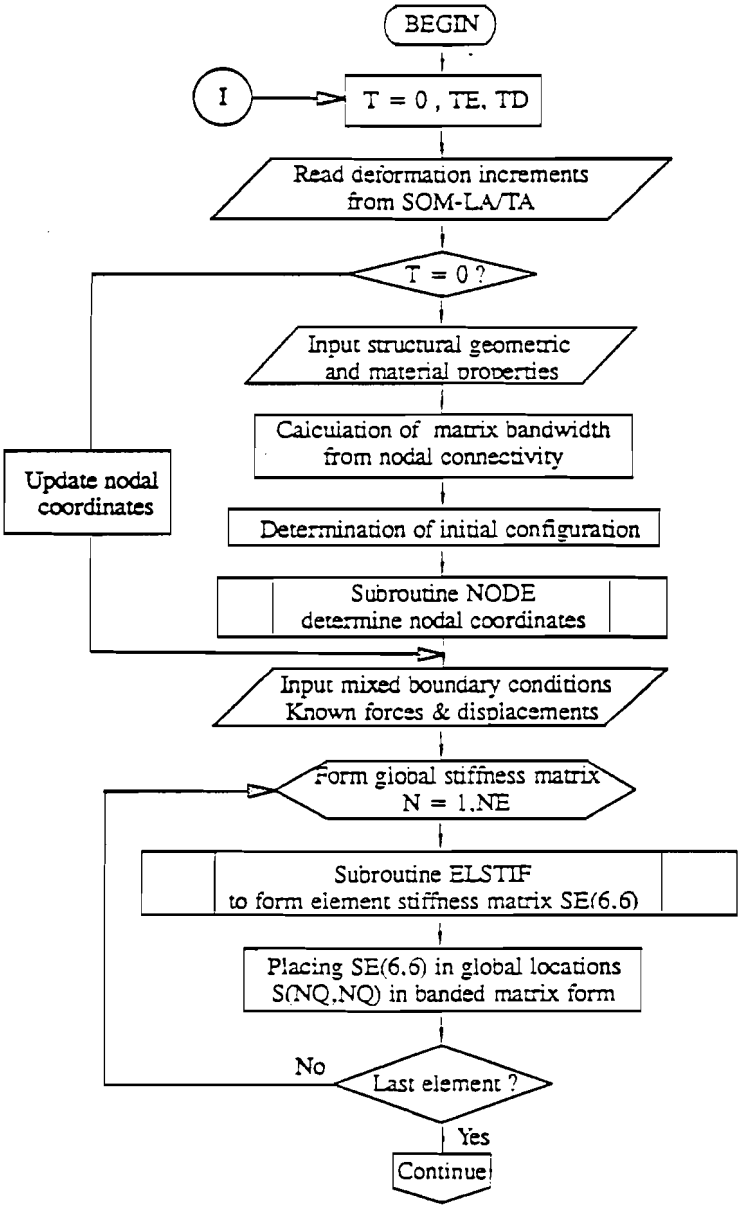

Figure 26. Detailed flowchart of non-linear spine model (part 1).

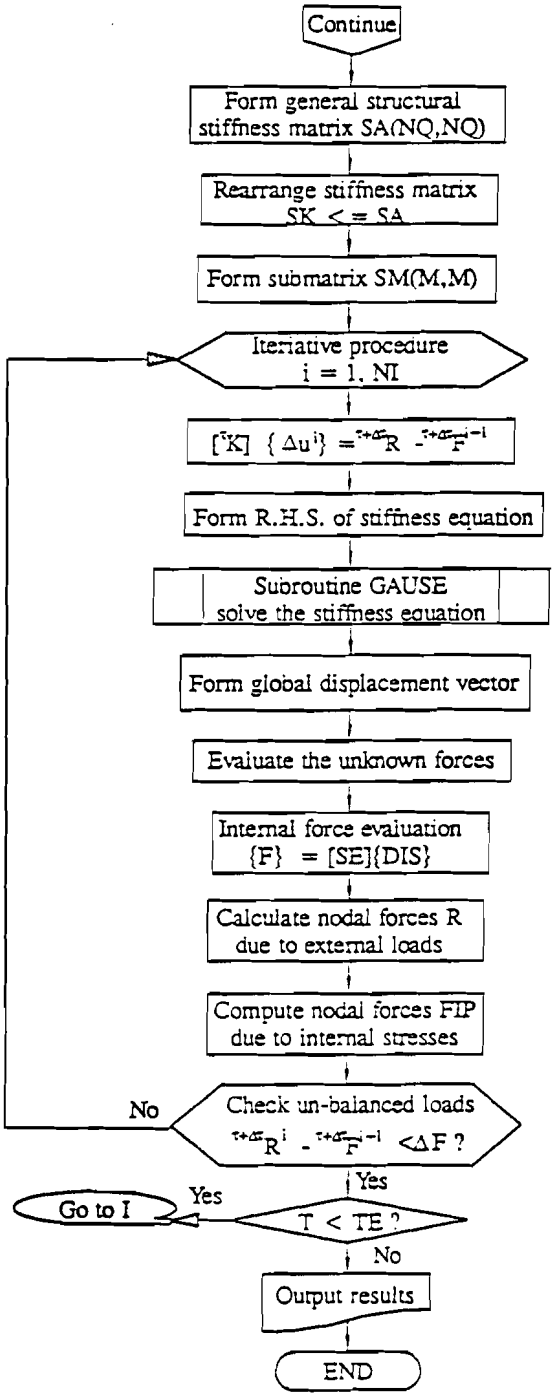

Figure 26. Detailed flowchart of non-linear spine model (part 2).

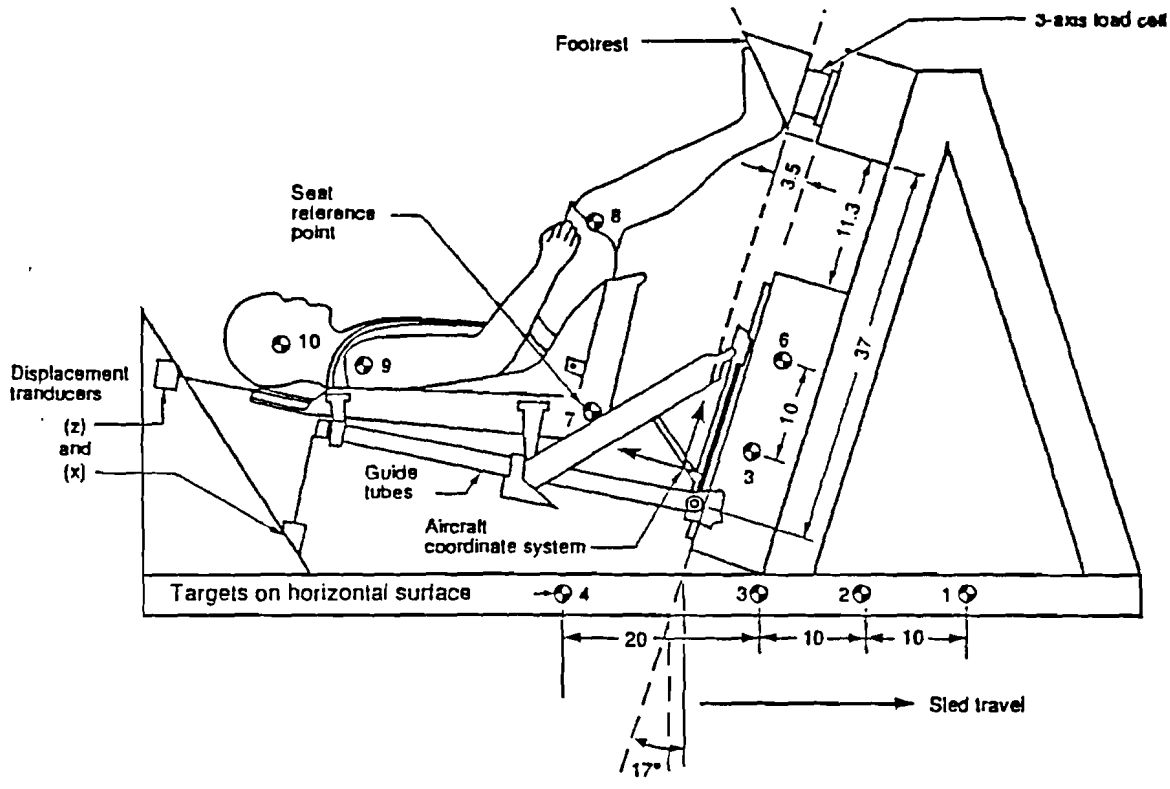

Figure 27. Configuration of testing setup with energy absorbing seat.

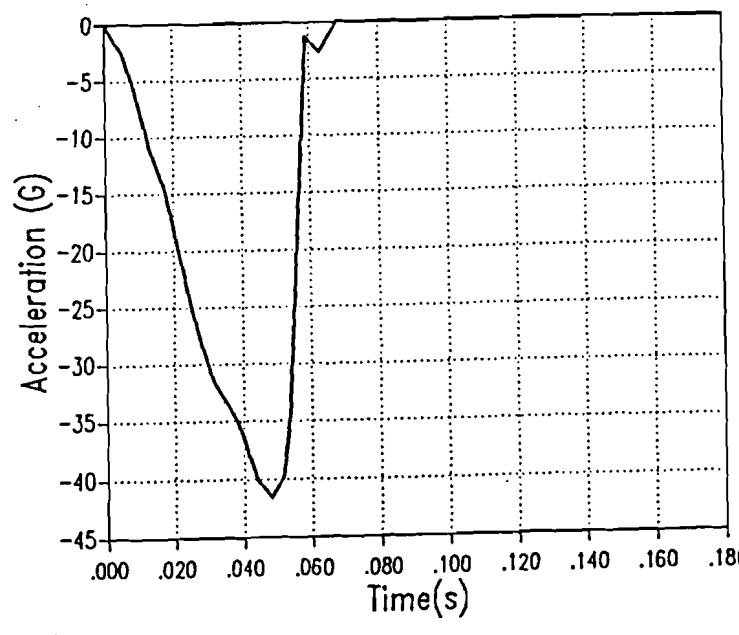

Figure 28. Input pulse for energy-absorbing seat test.

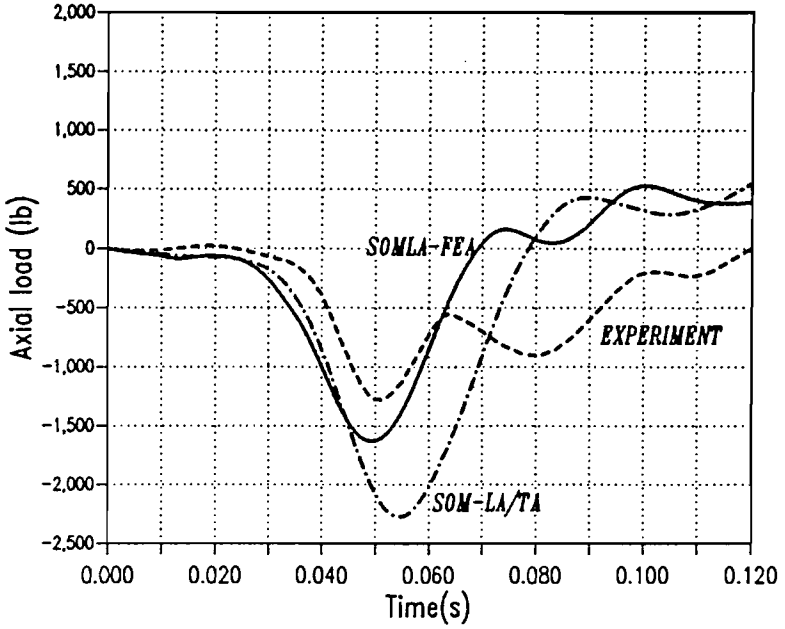

Figure 29. Lumbar spine axial loads in case 1.

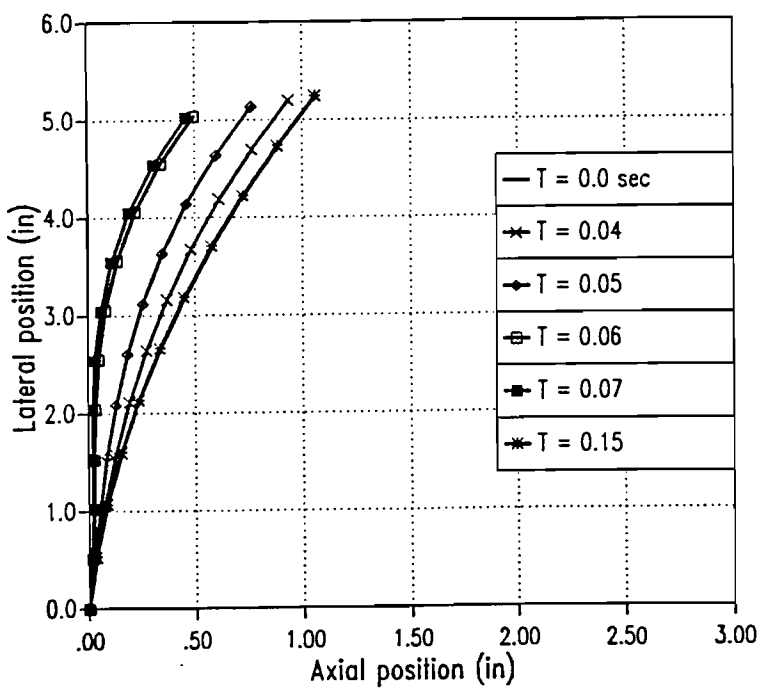

Figure 30. Deformation configuration of lumbar spine in case 1.

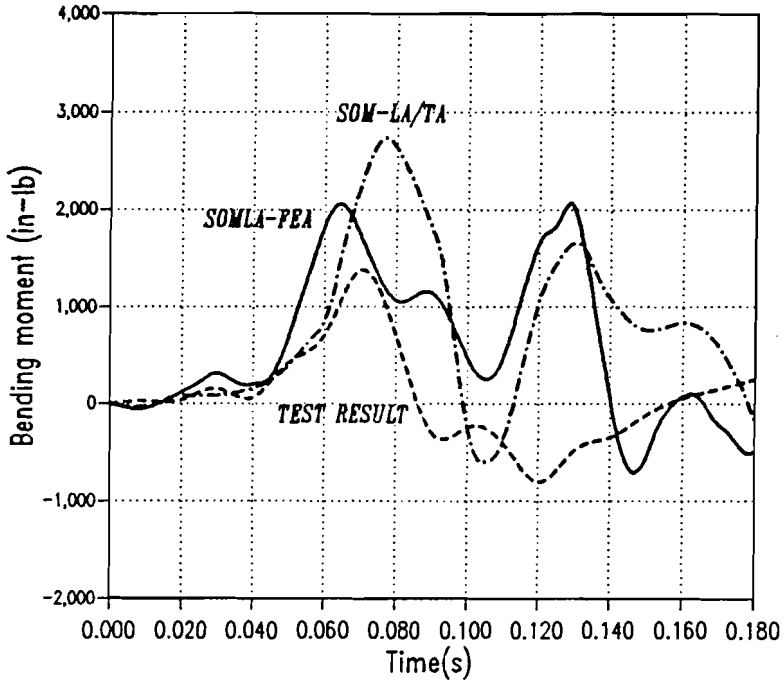

Figure 31. Lumbar spine bending moment in case 1.

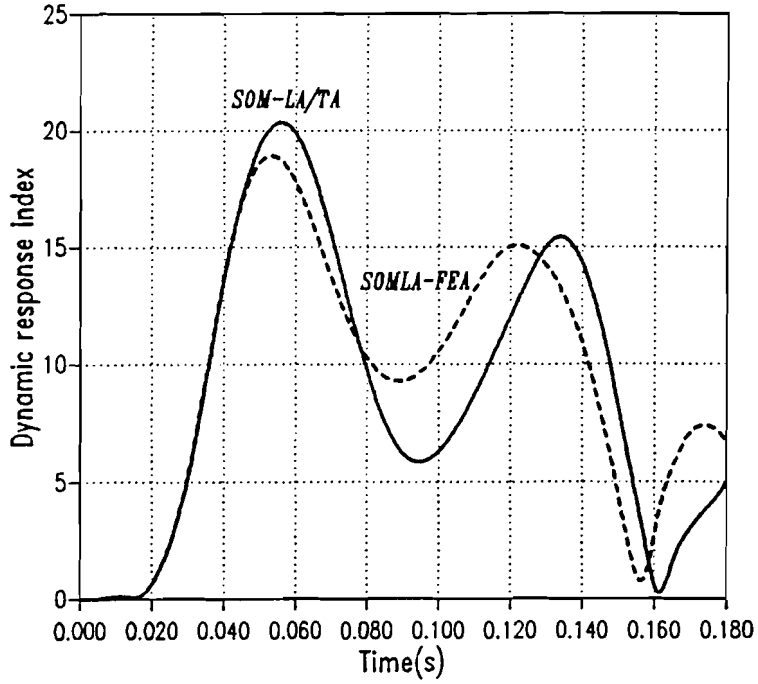

Figure 32. Comparison of Dynamic Response Index in case 1.

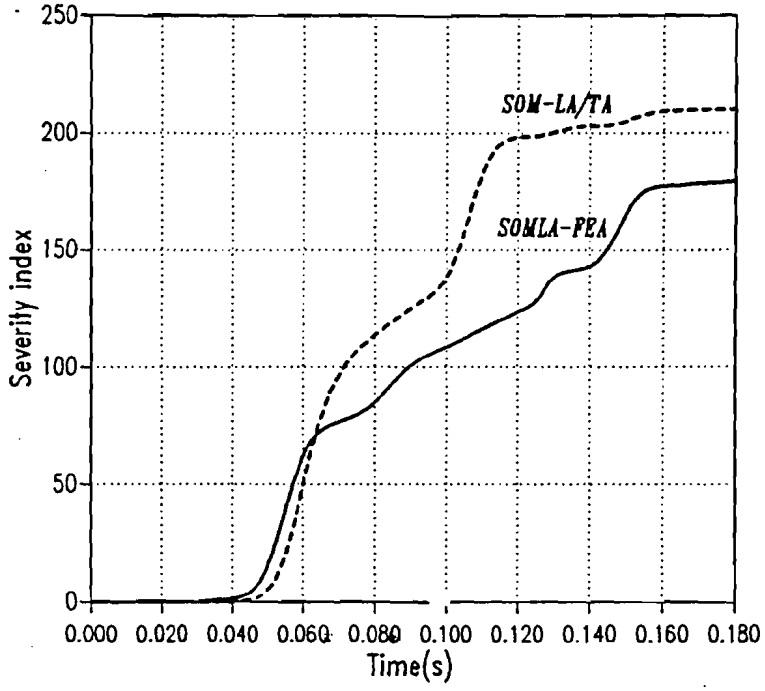

Figure 33. Comparison of Severity Index in case 1.

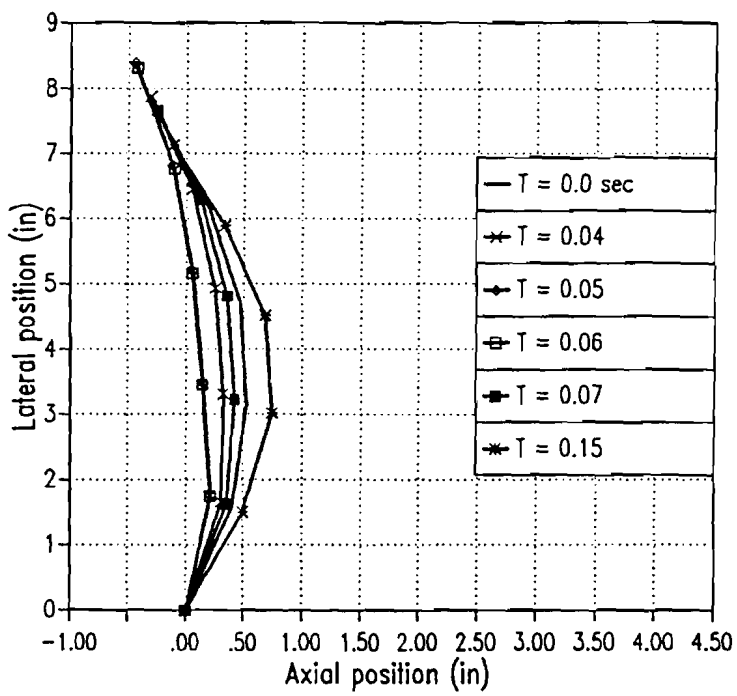

Figure 34. Deformation configuration of lumbar spine in case 2.

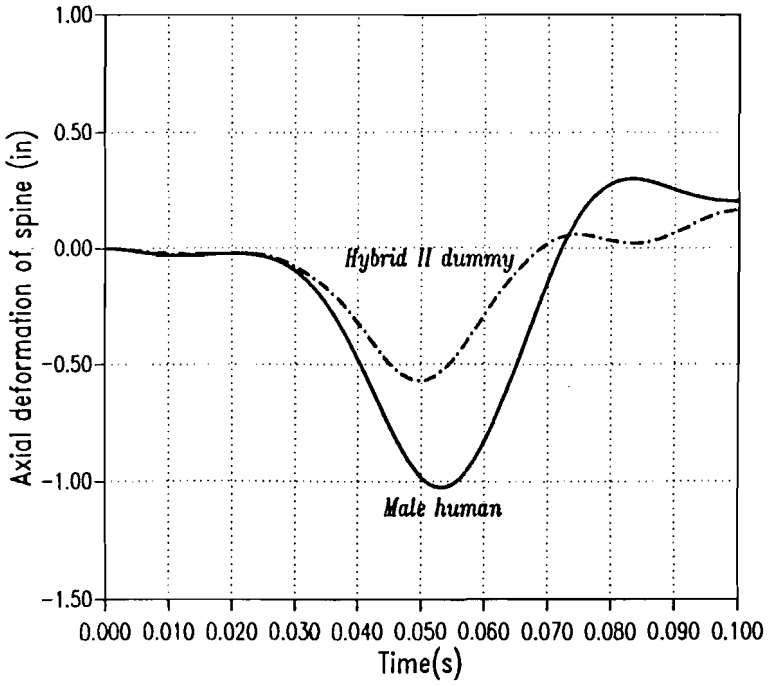

Figure 35. Comparison of lumbar axial deformation between male human and Hybrid II dummy.

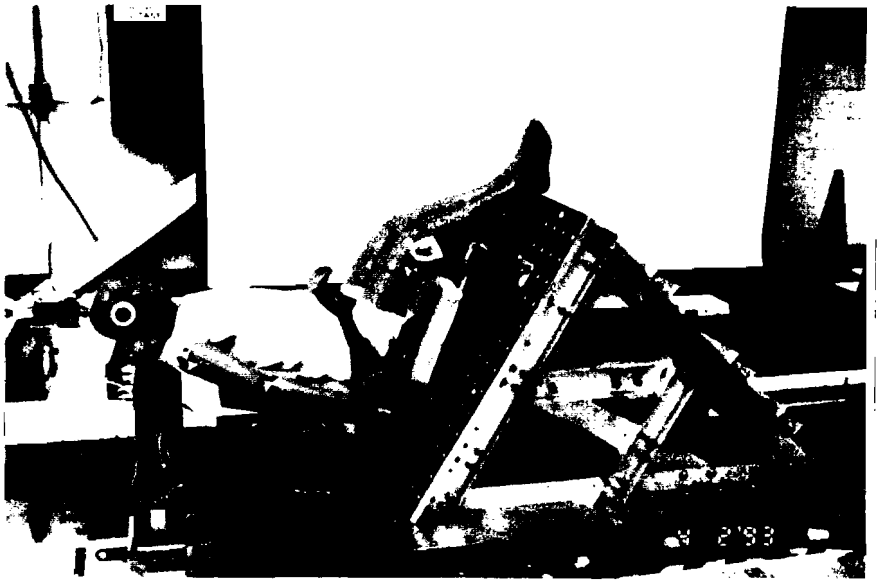

Figure 36. Carriage setup with 60^0 pitch.

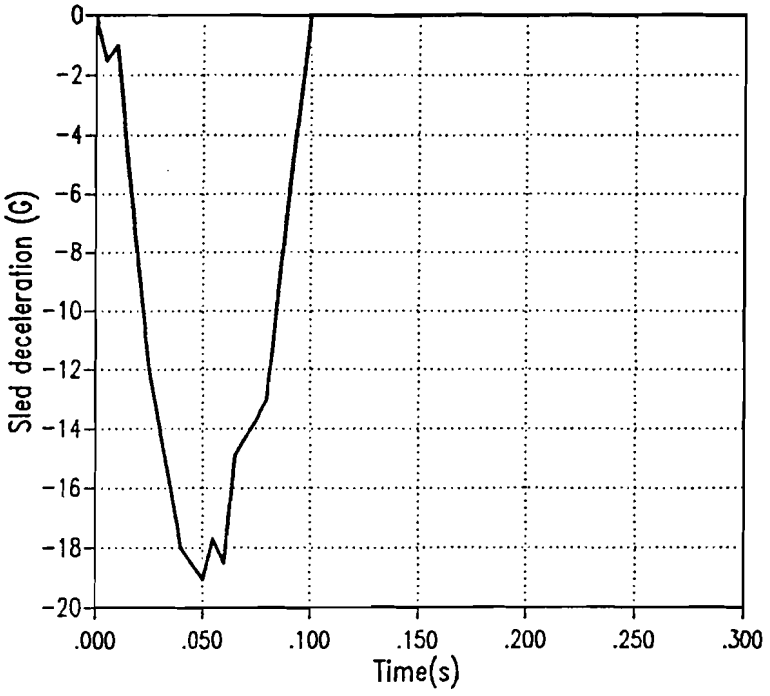

Figure 37. Deceleration pulse of dynamic sled test in case 3.

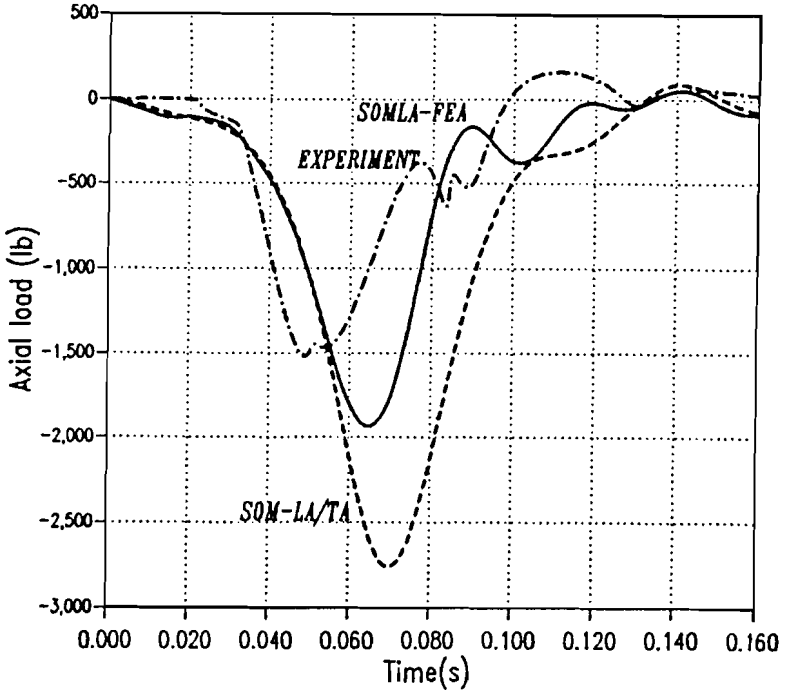

Figure 38. Lumbar spine axial loads in case 3.

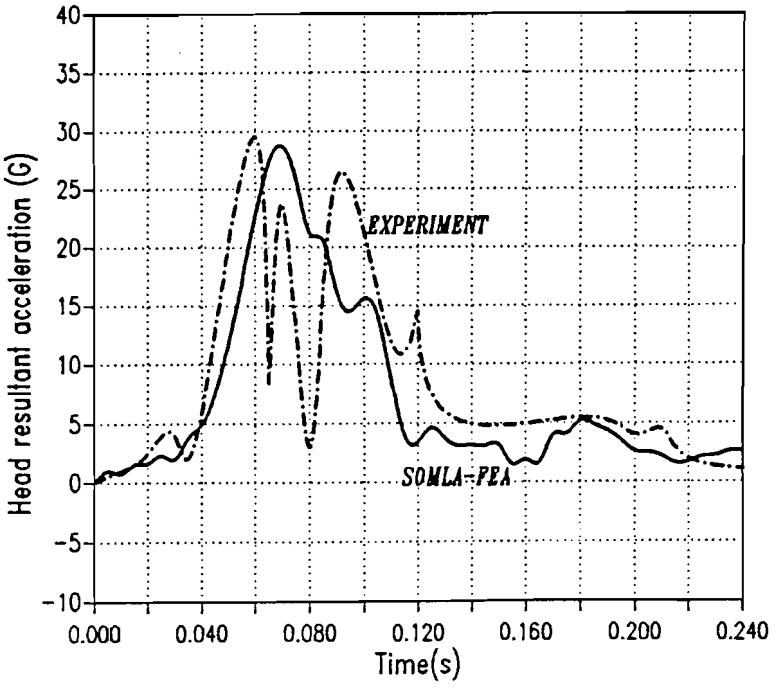

Figure 39. Comparison of head resultant acceleration in case 3.

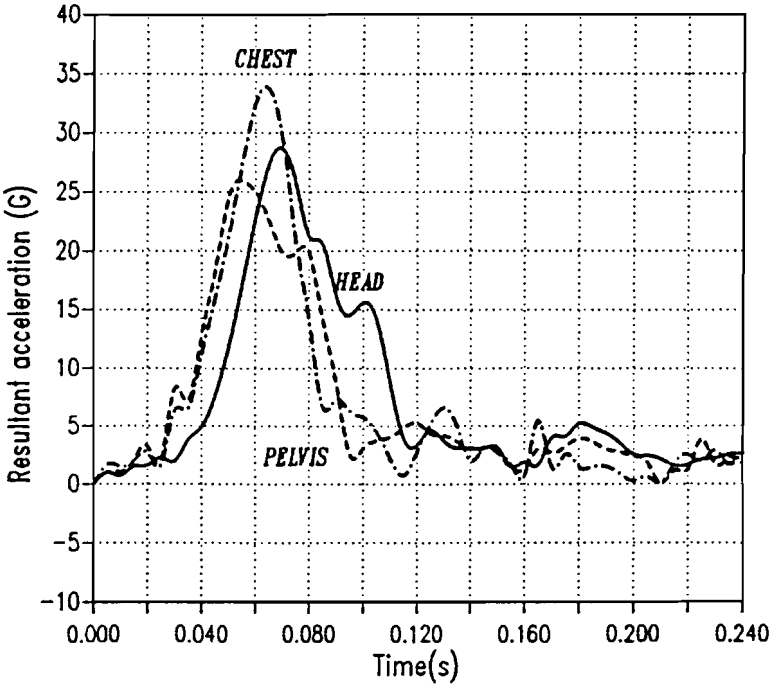

Figure 40. Comparison of chest pelvis and head resultant acceleration in case 3.

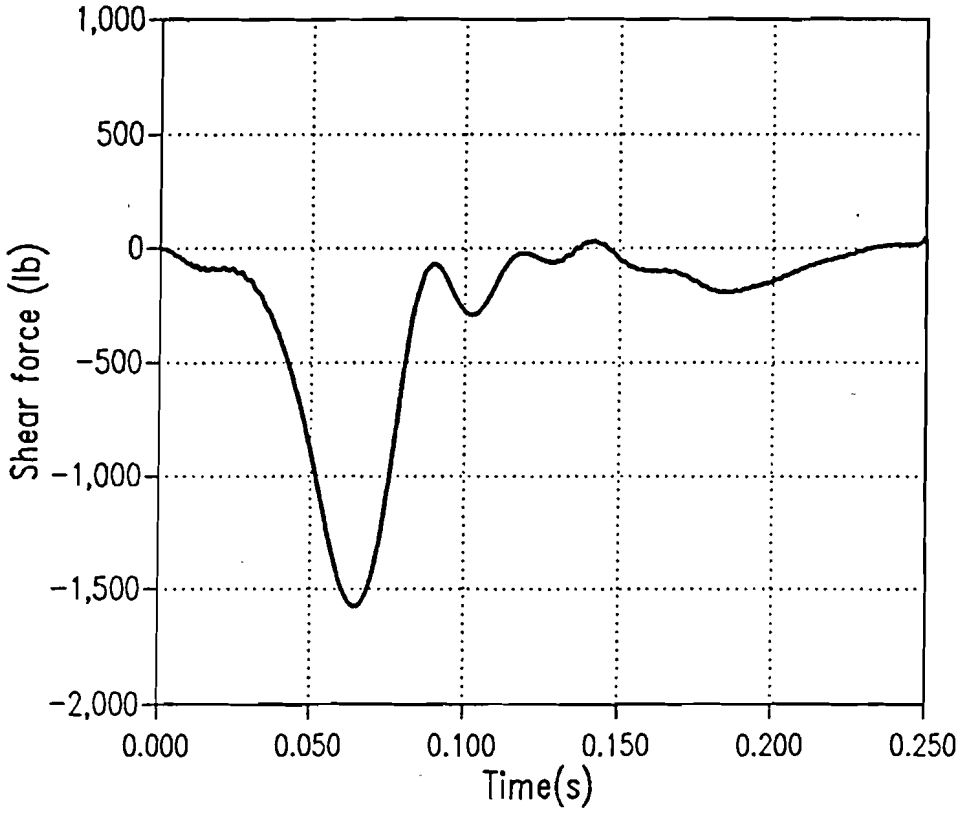

Figure 41. Shear force acting on the lumbar spine in case 3.

6. COMPUTER ANIMATION AND VISUALIZATION

Computer animation and visualization are important tools to interperate the numerical results from the simulation code SOM-LA/TA. Efforts were made to develop the computer animation program at both micro-computer and IBM RISC 6000 workstation.

6.1 PC Version Graphics Post-processing Software

In order to add a graphical output capability for code SOM-LA/TA, a micro-computer based post-processor was developed, which is based on the CAD software -- AutoCAD. Figure 42 represents the system flowchart. The procedure for the development and use of this system is described as follows:

a) Geometric modelling using graphics editor (AutoCAD).

Due to its powerful interactive function, AutoCAD is suitable as a graphics editor for the geometric modelling, especially for 3D objects. It provides some primary 3D objects, such as box, cone, wedge, ball, etc., which are often used in 3D geometric modelling. The flexible user- coordinate-system in AutoCAD ensure easy 3D geometric modelling.

b) Converting AutoCAD graphics database into "DXF" file.

AutoCAD internal graphics database format is difficult to be read by other programs since its format is associated with the computer hardware. AutoCAD "DXFOUT" function allows conversion of its internal graphics data format into DXF (Data Interchange Format) file. DXF file is simply an ASCII text file with a file type of ".DXF" and specially-formatted text.

c) Reading DXF file and dynamic analysis results.

DXF file, as discussed above, contains all geometric information for the model which is created by AutoCAD. The simulation results include the global Cartesian coordinates and orientation of local coordinate system attached on each object in the system. The coordinate data can be from any occupant dynamic analysis software such as SOM-LA/TA, MADYMO, ATB, or directly from experiments.

d) Retrieving body geometry.

In order to retrieve useful geometric information, a filter is used to filter out useless information in DXF file. Except position coordinates X, Y, Z in DXF file, all other information, such as velocities and accelerations are filtered out.

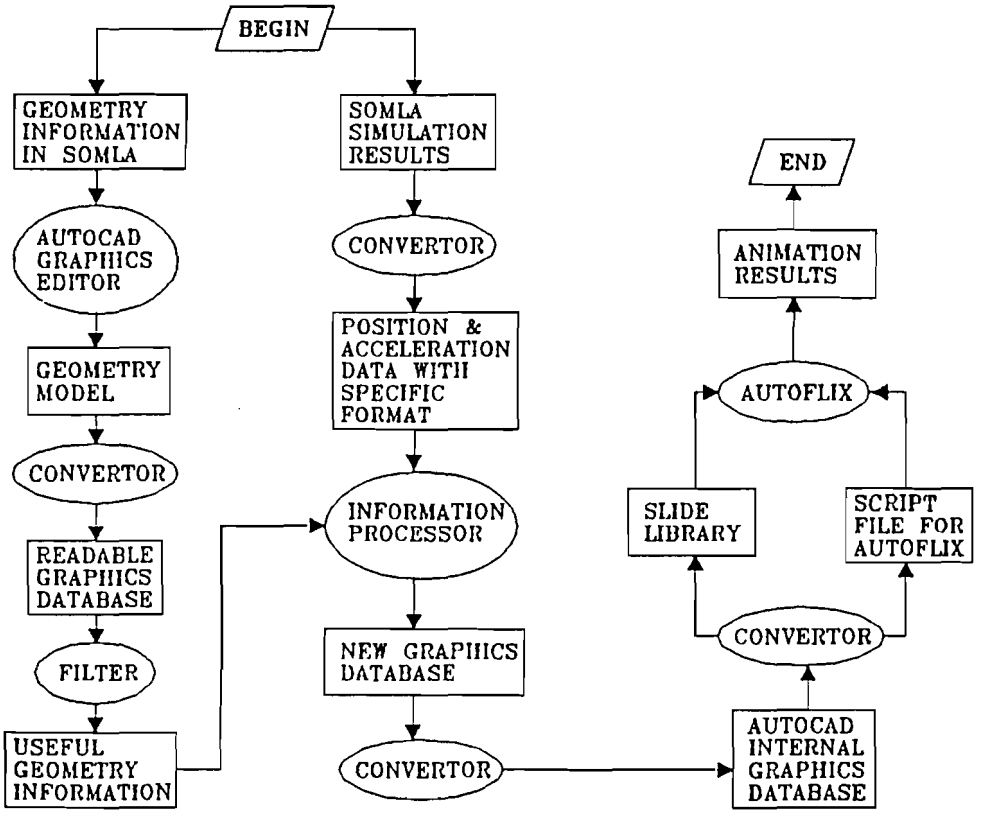

Figure 42. Flowchart of PC version animation system.

e) Assembling local coordinates in the global coordinate system.

The data in DXF file are local coordinates which are measured from the local coordinate system attached to each object's center of mass. Transformation matrix is used to transform local coordinates into the global coordinate system as:

$$\begin{bmatrix} x \\ y \\ z \end{bmatrix} = [\,A\,] \begin{bmatrix} x' \\ y' \\ z' \end{bmatrix} + \begin{bmatrix} x_0 \\ y_0 \\ z_0 \end{bmatrix} ; \tag{41}$$

where [A] is transformation matrix.

$$[A] = \begin{bmatrix} c\phi_2 c\phi_3 & -c\phi_2 s\phi_3 & s\phi_2 \\ c\phi_1 s\phi_3 + s\phi_1 s\phi_2 c\phi_3 & c\phi_1 c\phi_3 - s\phi_1 s\phi_2 s\phi_3 & -s\phi_1 c\phi_2 \\ s\phi_1 s\phi_3 - c\phi_1 s\phi_2 c\phi_3 & s\phi_1 c\phi_3 + c\phi_1 s\phi_2 s\phi_3 & c\phi_1 c\phi_2 \end{bmatrix} \tag{42}$$

c and s -- cosine and sine of any angles;
$\phi 1, \phi 2, \phi 3$ -- Bryant angles for the object;
x ,y, z -- Global coordinates of a point on the object;
x',y',z' -- Local coordinates of a point on the object;
x_0, y_0, z_0 -- Global coordinates of origin of local coordinate system;

f) Generating new DXF files.

New DXF files corresponding to each given time instant are created. The number of DXF files is determined by the simulation results.

g) Updating graphics database and generating each animation frame.

"DXFIN" function is used to convert DXF file into AutoCAD internal graphics data format. All the generated DXF files are converted into graphics database in sequence. For each frame, corresponding slide files are produced for final animation. At the same time, a script file is created for compiling each animation frame automatically.

h) Generating animation.

AUTOFLIX program is used to compile each animation frame to get smooth motion. In order to generate realistic animations, a shading technique is also employed.

i) C programming and AutoLisp controlling.

The AutoCAD graphics database is processed by a C program. The entire system is controlled by an AutoLISP program. Menu driven user interface makes it easy to use. Due to its flexibility and friendly user interface, other mechanical systems can also be graphically verified. Figure 43 illustrates the simulation results of the low-deceleration, forward-facing test with a simple seat structure. A diskette version of the animation program and its related data files will be provided to the FAA at the end of this phase of the project.

6.2 Workstation Version of Graphics Post-processing Software

Program structure

The animation program *dummy.c* features besides the main program, from which most subroutines are called, sixteen subroutines which perform various tasks to comply to the given requirements. Two of these subroutines are written as separate programs, and they are then bound to the structure of the main program. The Figure 44 shows the program flow of the main program. The following table lists all subroutines used in the program:

Start
: display start-up screen and inquire input data for path-data and choice of the dummy model.

wholescreen
: Display graphics on the entire screen.

Menu
: Display menu and invoke menu functions.

Mendial
: Display dial functions.

Disptime
: Provide display for elapsed time.

Move
: Read the input data for the path, and calculate the model transformation matrix for each time step.

Sub
: Read the data from the dummy input data file and create the graphical structures for each segment.

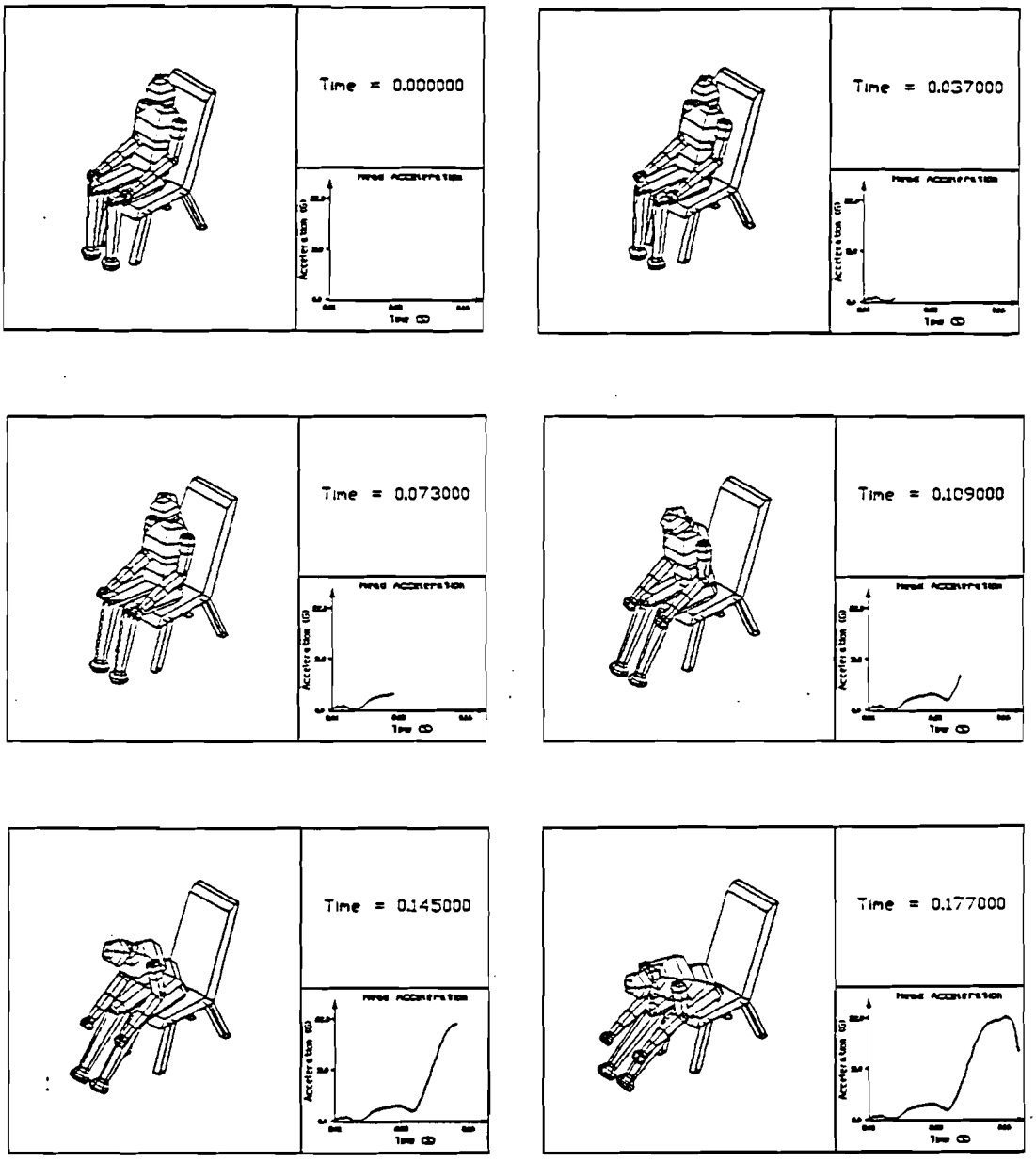

Figure 43. Simulation results of dummy

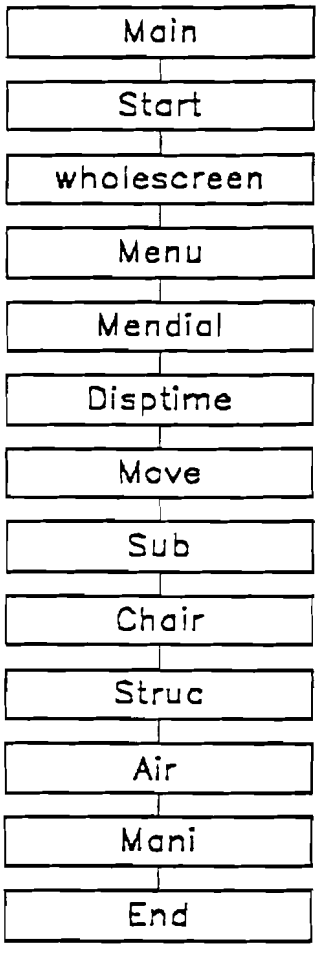

Figure 44. Flowchart of workstation version animation program.

Chair

Display the seat.

Struc

Assemble individual segments of occupant together and form the complete dummy model.

Air

Read the data for the moving reference frame.

Mani

Perform the interactions with the dummy model and the graphics display.

Valuator

Sample the input data from the dials, and calculate the transformation matrix used to change the view representation.

Shade

Perform shading operations.

Chair2

Display second seat.

Back

Generate background grid for shaded dummy.

Timer

Delay the display of two succeeding images for a certain, eligible period of time.

End

Exit program.

Functions of graphical interaction

The animation program offers several functions to interact with its graphics and to perform diverse tasks. To change the view representation and to observe the dummy in different positions, the dials were programmed (Figure 45) to perform the following assignments.

Dial 1 - Zoom the view in and out.
Dial 2 - Rotate the view about the Z-axis.
Dial 3 - Translate the view in X-direction.
Dial 4 - Translate the view in Y-direction.
Dial 5 - Change the speed of animation.

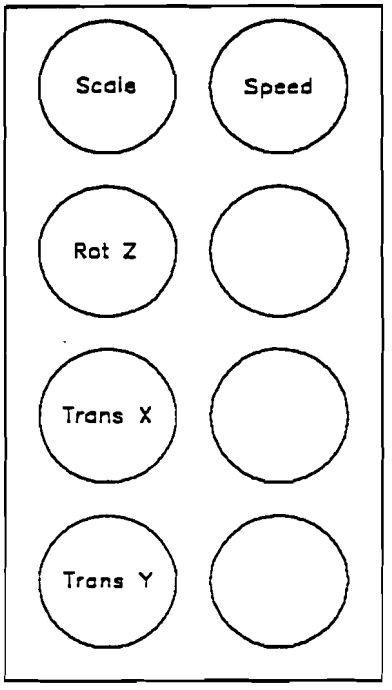

Figure 45. Configuration of dials.

Moving Frame
Seat 2
Start
Stop
Continue
<==
==>
Shade
Exit

Figure 46. Interaction menu on the screen.

Dial number five, the first one on the second column, is used to determine the amount of time elapsed between the display of two succeeding pictures of the animation. Changing the setting of dial five alters this time period in terms of hundreds of a second from 0 to 100 hundreds of a second. The actual valuator, and therefore the time of delay in hundreds of a second, is displayed in the lower left corner of the display screen.

A menu was also developed for ease of interaction of the program and the users. The menu is located on the left side of the screen and the menu items can be picked with the mouse pointer and be invoked with the first mouse button (Figure 46). The following functions are performed by the menu items:

Moving Frame
: Offer possibility of performing animation either in a fixed or a moving reference frame.

Seat 2
: Display a second seat in front of the one where the dummy is seated (in shade mode only).

Start
: Start animation of dummy.

Stop
: Interrupt animation.

Continue
: Continue animation after interrupt.

<==
: Move one picture back.

==>
: Move one picture forward.

Shade
: Shade and unshade the display.

Exit
: Exit program.

The function *Moving frame* allows the user to observe the crash test results either in a moving or a fixed reference frame. This option allows either to concentrate on the motion of the dummy relative to the sled (aircraft), or to observe the crash test inclusive the motion of the crash sled (aircraft). The *Moving frame* option is available either for the shaded or the wire

frame dummy model, and can only be chosen before activating the animation. It is also not possible to use this menu item, if the option *Seat 2* has been chosen to display a second seat. To reset the function, a second mouse-click is necessary.

The function *Seat 2* displays a second seat in front of the one the dummy is seated. This can be achieved by invoking this menu item with a mouse-click. This option is only available for the shaded dummy model in the fixed reference frame and has to be reset with a second mouse-click in order to use the moving reference frame option.

The next four menu items build a unit to control the animation. After invoking the *Start* option with a mouse-click, the animation of the crash test results begins. It is now possible to interrupt the animation at any time, before the end of the sequence is reached, with the *Stop* option. Invoking the *Stop* function lets the program enter an infinite loop which can only be exited using either the *Exit*, *Continue*, '==>' or '<==' function. The *Continue* function continues with the animation, while the *Exit* function exits the program at any time. With '==>' and '<==', it is possible, after interrupting the animation with *Stop*, to move picture by picture forward or backward in the animation sequence. These functions can only be exited using the *Continue* or *Exit* option.

The *Shade* changes the display of the dummy model from a wire-frame representation (Figure 47) to a solid model representation (Figure 48). Since the program automatically starts with the wire-frame option, a first mouse-click on the *Shade* option changes the display from the wire-frame model to a solid model. The solid model representation features also the display of a grid pattern as background. The *Shade* function can be used at any time before or while performing the animation. To reset the function and switch back to the wire-frame model representation, a second mouse-click on this menu-item is necessary.

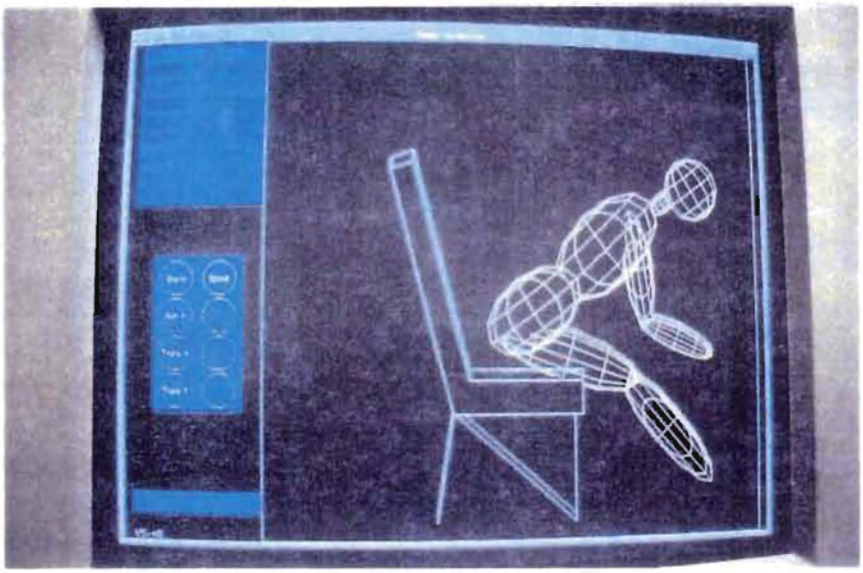

Figure 47. Wire-frame representation of dummy model.

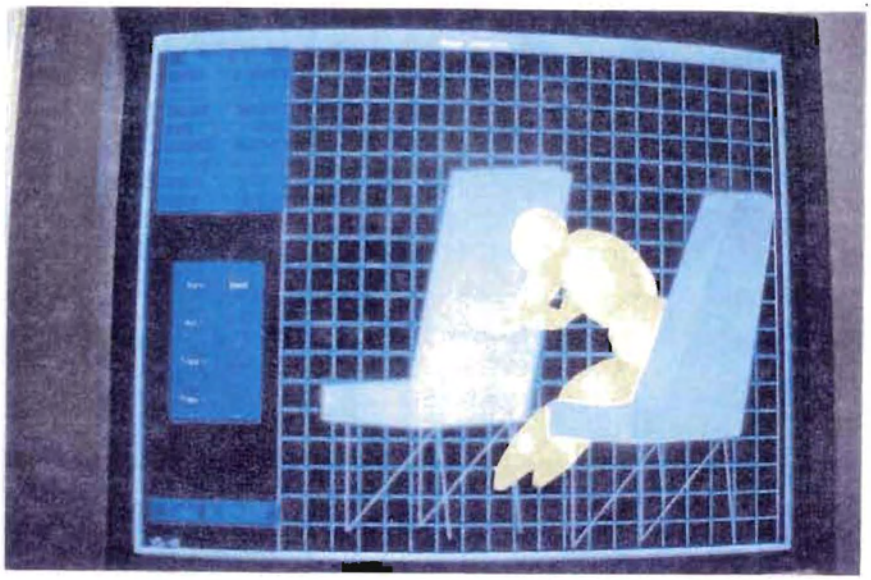

Figure 48. Animation of solid dummy model.

7. EXPERIMENTAL TESTING AND PHOTOMETRIC PROCEDURES

7.1 Impact Dynamics Sled Testing Facilities

Impact Sled-Track Systems

In order to evaluate the dynamic performances of the occupants and validate the simulation results, crash dynamic testing is being performed with impact sled facilities at National Institute for Aviation Research (NIAR). The horizontal impact test sled accelerates and decelerates for either the purpose of dynamic testing of the aircraft structure or for the biodynamic study of a dummy occupant or both. The essence of the impact sled is to generate experimental data that is used to study the dynamic behavior of the crash victims, and injury potentials, to obtain safe designs of the seats and restraint systems. A brief descriptions of the testing procedure, the sled characteristics, the types of dummies used at NIAR, the high speed video as well as the data acquisition system are discussed next.

The horizontal impact test sled, shown in Figure 49, consists of a movable carriage mounted on tracks with a length of 78 feet and driven into a decelerator by a pneumatic propulsion system with a maximum speed of 55 mph. The carriage is designed to carry a maximum payload of 3000 lbs centered horizontally on the bed and at a distance of 3 ft above the upper surface. This load can be accomplished either with the use of anthropomorphic test dummies or with 500 lb weights in order to achieve the desired mass. The sled is also capable of testing sections of the aircraft fuselage.

The impact sled is accelerated down the track by the propulsion system. This is accomplished by two pneumatic motors consisting of a cylinder and piston located between the rails. The piston is connected to the sled by a pair of wire ropes routed over shelves. Propulsion is accomplished by compressed air with a maximum pressure of 200 psi. When the system is pressurized, the piston is pushed through the cylinder by the air thus pulling the sled down the track toward the decelerator. The deceleration system is simple a mechanical device that absorbs energy by various steel straps that undergo continuous plastic deformation as they are impacted by the carriage. The system is able to decelerate the sled from a maximum velocity of 55 mph. The primary deceleration system has a maximum stroke of approximately 48 inches. Larger strokes of up to 108 inches are possible with the use of a hot rolled mild steel. The reason for the varying of stroke and types of steel straps that are used is primarily to achieve the desired deceleration pulse shapes.

Anthromorphic Testing Dummy

Anthropomorphic testing dummies are used as occupants in the sled test experiments. There are standard 50th percentile (Hybrid II) dummies as shown in Figure 50, which represent an average male of weight 175 pounds and height 5 feet 9 inches. This dummy was originally designed by Anderson Research Laboratories, and then modified by General Motors and the

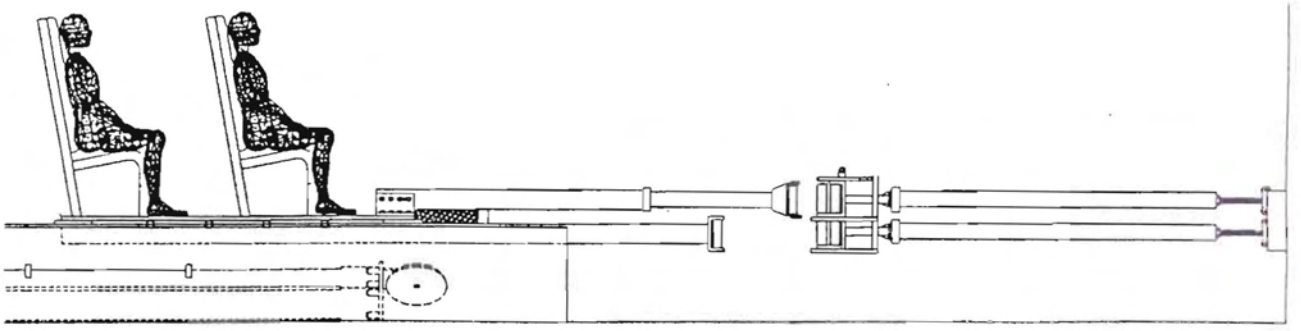

Figure 49. Impact test sled at NIAR.

Figure 50. Standard 50th percentile (Hybrid II) dummy.

National Highway Traffic Safety Administration. This dummy was capable of generating test data with sufficient biofilelity to be used for both automotive and aircraft crahworthiness testing.

A 95th percentile dummy is also available, which represents an average male who weighs 200 pounds and has a height of 6 feet 2 inches. They are fully instrumented and in accordance with 49 CFR part 572, Subpart B. These dummies have openings at the rear part of their head, vertebral column (lumbar) and femur. By fixing accelerometers and transducers inside these openings, the acceleration responses of head, lumbar spine forces, and femur loads, during an impact test, can be determined. To conduct an impact sled test, the dummy is first restrained to a seat with a suitable restraint system and the seat is mounted on the sled. The sled is allowed to accelerate to the required value and then it coasts. The impact then occurs in form of a deceleration pulse caused by the sled probe colliding with a number of steel straps. The experimental data are collected by both the data acquisition system as well as the high speed video system.

Data Acquisition System and High Speed Video

The data acquisition system used with impact sled tests is a microcomputer based DSP technology system. It conforms with the IEEE CAMCA instrumentation hardware standard. The system is capable of 48 channels of data acquisition and is expandable. Each channel provides 12-bit accuracy with a maximum per channel rate of 100 kilo sample per second. This sample rate is independent of the number of channels in operation. Of the 48 channels, 32 are transducer conditioning amplifiers with programmable gain from 1 to 10,000 and 8-pole butterworth filters with a programmable cutoff frequency from 10 Hz to 100 kHz with a resolution of at least 200 steps per decade. The remaining 16 channels provide differential amplifier inputs with a programmable gain from 1 to 50,000. The system also provides enough memory to store a 1.2 second trace when all 48 channels are operating simultaneously at the 100 kilo sample per second trace.

7.2 Automatic Target Tracking Photometric Procedures

In addition to the data from the accelerometers, the displacement, velocity and acceleration of the dummy are recorded and evaluated using a high speed video system and optical target tracking techniques. Visible targets are made on different parts of the dummy, seat and sled. During the motion of the sled, the targets are tracked by a video camera. EktaPro 1000 can record at six different frame rates. That is, 30, 60, 125, 250, 500, and 1000 frames/second, respectively. Setting up the frame properly is one of the most important consideration in data acquisition. Generally, higher the frame rate the better precision. During the impact test, the cameras are set at the position for recording the event. Once a crash test has been recorded according to the requirements, a software called Motion Pro is used for data collection, such as displacements, velocities and accelerations. It can also be used to issue commands to the analyzer to control the video system from a personal computer.

Although the Motion Pro software is very capable, there are still a lot of difficulties associated with the data analysis by the optical method. First, the data collected by this method is only considered accurate if it is collected using well defined and verifiable procedures. These include proper lighting, imager locations, angles and frame rate, etc. Second, manual collection of the data frame by frame is tedious and time consuming, and causes a problem of accuracy because of the difficulties of following the pixel in each frame. Finally, the data collected manually is usually noisy and distorted. To solve the mentioned problems, an automatic target tracking photometric procedures were developed so that the accuracy is enhanced and a great deal of time is saved.

Data collection process

In dynamic testing, high speed photographs are taken to provide a visual record of the test kinematics. This is of great help for the evaluation and explanation of any problem that may occur during the test. These recordings are also used to determine head accelerations, displacements and velocities. Targets defined on the subjects (such as dummy head) are to be tracked after the test. For the purpose of analysis, attention should be taken that the camera's angle produces an accurate representation of the motion. An Ektapro 1000 motion analyzer is used to tape the crash test. Some of the essential features of the motion analyzer are discussed below.

Ektapro 1000 motion analyzer is designed to provide visual records of the test setup. It is menu driven and has an interactive display which makes evaluating motion related problems very simple. The system has a "LIVE" setup feature which helps the user to make sure that the image is exactly what is required to solve the problem. Whatever is displayed on the monitor of the analyzer is exactly what will be captured on the tape when record button is pressed. Images recorded are instantaneously available for analysis. The system is divided in to different modules:

a) Imager

Imager is used to obtained the live images of the subject on which it is focused. Light that enters the imager through imager lens is converted into an electrical or video signal. Video signal produced is proportional to the intensity of light. Light intensity coming from different directions changes the amplitude of the video signal. This video signal is amplified and sent to the main processor through imager cable.

b) Sensor

The sensor consists of a solid state image array. This array has thousands of photo capacitative cells, which converts the focused light of the lens to a corresponding electrical signal. The amount of charge stored in each cell varies with the intensity of light. Charge stored in each picture element (pixel) is scanned through a scanning process and picked up as the pixel releases its charge and new charge begins to accumulate for the next screen, thus

generating a video signal. Video signal is a linear sequence of varying amount of charge from each scanned pixel.

c) Analog sampling

Electrical signal is generated in analog form for the amount of light received, thus the video signal resulting from scanning process of the sensor output is not immediately usable. The video signal received is sampled by two analog sampler boards. These boards are used to sample the video information.

The motion analyzer has three operating modes:

a) LIVE

During the LIVE mode operation the monitor displays the exact picture that will be recorded at the selected frame rate. Imager is focused on the subject to be recorded. Light entered through the lens is converted into an analog video signal which is then converted into a digital signal by an analog to digital convertor (A/D convertor). These digitized video signals are stored in a Frame Buffer in the same way as the data is stored in the computer memory.

b) RECORD

In record mode, the processor puts the image on the monitor in exactly the same way as in live mode. However the tape is moved at the user selected speed (frame rate) by the help of modulator and record boards. The modulator converts the imager video signal into a frequency modulated signal and the record board provides the energy required to drive the record head.

c) PLAY

PLAY mode is used to review a recorded event. The processor enters the play mode when the tape transports signals which move the tape forward at the current speed. Play mode uses a demodulation board to convert the frequency modulated signal back to a video signal. A/D convertor processes the output of the demodulated signal instead of using a signal from the imager.

<u>Lighting system</u>

Lighting is one of the most important requirement for motion analysis. Three considerations are very essential for lighting of the motion analysis video-graph. First, sufficient lighting should be provide for extremely high frame rates. Secondly, reflections from the subject which tend to obscure the image should be eliminated. Thirdly, there should have sufficient depth of field so that the subjects in motion remain in focus throughout the recording. In order to highlight the subject to be analyzed, it is suggested by the manufacturers to use white medical tape, black photographers tape or white and black paints. White tape could be applied to the

subject that is to be analyzed so that the area stands out. Black tape or paint can be used to cover the area that produces undesirable reflections. Undesirable reflections may be reduced by using polarizing filters or by diffusing filters on the light.

Communication interface device

The cameras are set at the position for recording of the event. By using LIVE Command to the analyzer we start displaying live images from the currently selected camera position. By focusing the cameras to the required position, the REC command is issued to start recording. Setting up the frame rate is one of the most important consideration in data acquisition. Higher the frame rate the better the precision. The FRT command is used to select the frame rate. As soon as the FRT (frame rate) command is issued the motion analyzer is set to LIVE state. One of the important consideration while using this command is that the analyzer must be in STOP or LIVE state. Other added features of motion analyzer is customizing the video screen by drawing lines, boxes, and text along with the other support functions.

The graphic commands consist of two main categories, video ram and bit map ram.

a) Video Ram

Video ram contains the image displayed on the screen. This can originate either from the imager or tape. Each pixel in this region can take 0 to 255 values, where 0 represents black and 255 represents white and between 0 - 255 are different shades of grey. Except for STOP state this is updated with new image, any command given will be automatically erased with the frame update.

b) Bit Map Ram

The bit map ram contains the image of the data frame border and the reticle. Unlike the video ram the bit map ram is not effected by the frame update. The graphic related commands could be helpful in locating points. The pixel values obtained by the help of these commands are used to process the image and it is also used to automate the data collection process.

Software of high speed video system

Once a crash test has been recorded according to the requirements, it is used for the data analysis to determine the parameters such as displacement, velocity, and acceleration of the target points. The software Motion Pro is used for data collection. It is a menu driven software designed to facilitate the task of digitizing object motion recorded with high speed video system. It can be used to collect coordinates of points, centroids, angles, and line segments. It can also be used to issue commands to the analyzer to control the video system from a personal computer. The program has several integrated program modules that can be activated by the user.

In order to collect data the tape is scanned and cataloged first. The image will be scaled with respect to the object so that the measurements can be converted to world coordinates. This is done by measuring the actual distance between two land marks in the object space. The data are then collected frame by frame procedure in which the operator has to identify points in sequential images. The target placed on dummy's head during the crash test was measured. Equations were developed to calculate velocity of the head during the crash.

As mentioned earlier, many difficulties are associated with data analysis by optical method. One of the major problems faced in data collection is tracking the target points frame by frame. Tracking a particular pixel in each frame is not only a difficult and tedious process, but also it could produce noisy and distorted data, as shown in the Figure 51.

Data analysis

To smooth out the data a filtering technique was used. This technique is called twenty five point averaging technique which smooths out the data. Figure 52 shows the smoothed curve associated with the data collected of Figure 51. For example, to find out X(1) we average the first twenty five points

$$X(1) = [X(1) + X(2) + \ldots X(25)]/25$$

Once the head strike path is filtered the data points obtained are used to calculate the velocity, as the first derivative of displacement. To differentiate discrete set of points forward difference technique was used. Let X(t) be a displacement of point in x-direction at time t, X(t+1) be displacement of point in x direction at time t + 1 and Δt be 0.001 second (since the recording is 1000 frames/sec). Using the forward difference operation the velocity will be

$$V(t) = (X(t+1) - X(t))/t$$

The velocity obtained by this procedure is also distorted, this is again filtered using the same 25 points average technique. The velocity plots are shown in Figure 53 by using filtered data, achieved by using 25 point average technique. The same procedure is also used to obtain the acceleration.

Again the acceleration data is jaggered and needs to be filtered. The same averaging process as well as velocity is used to smooth the data (Figure 54). Velocity and acceleration in y-direction are calculated similarly. The acceleration data obtained from the above procedure is used to calculate HIC.

Automated target tracking

The solution to the mentioned problems is automating the target tracking so that accuracy is enhanced and a great deal of time is saved. One major help to the process of automation is the built-in library. These commands can be typed on the computer screen, to perform the

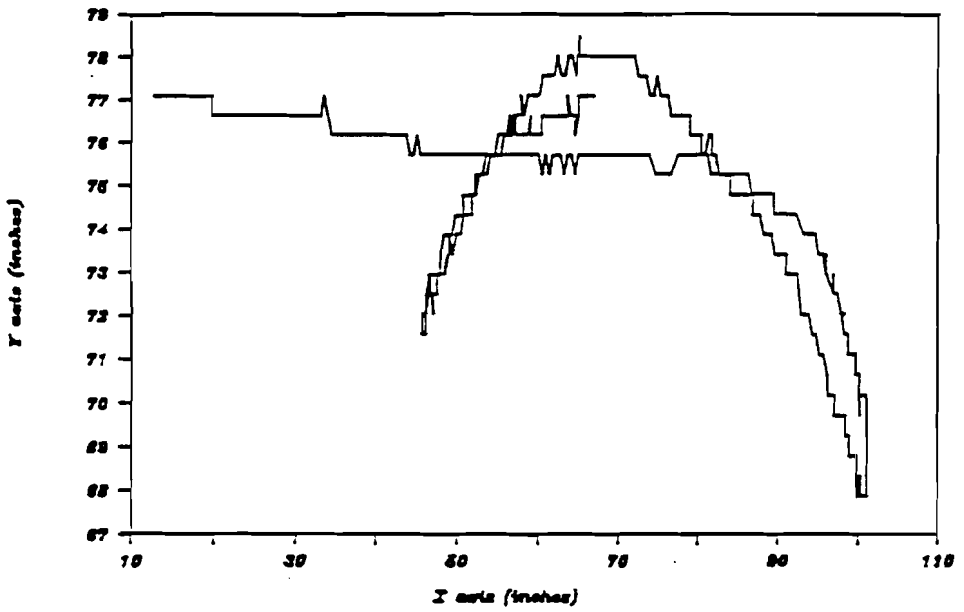

Figure 51. Un-filtered head strike path.

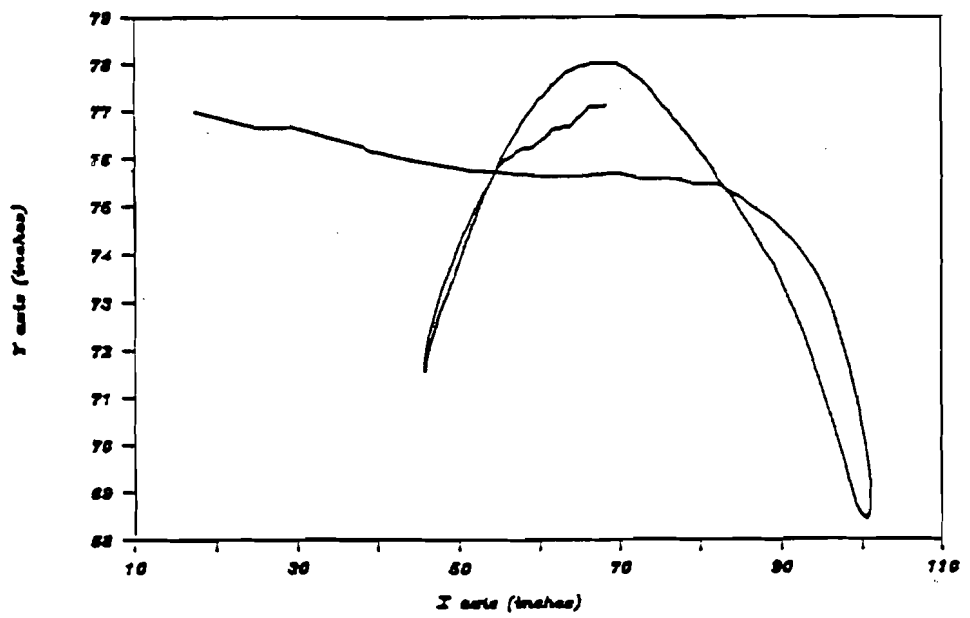

Figure 52. Head strike path smoothed by filtering technique.

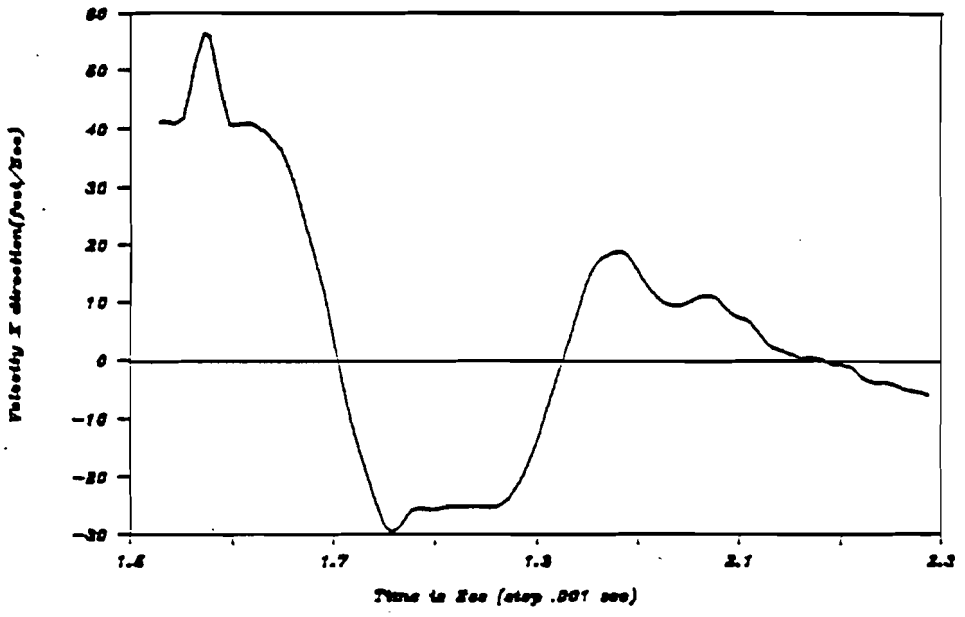

Figure 53. Smoothed head velocity in X direction.

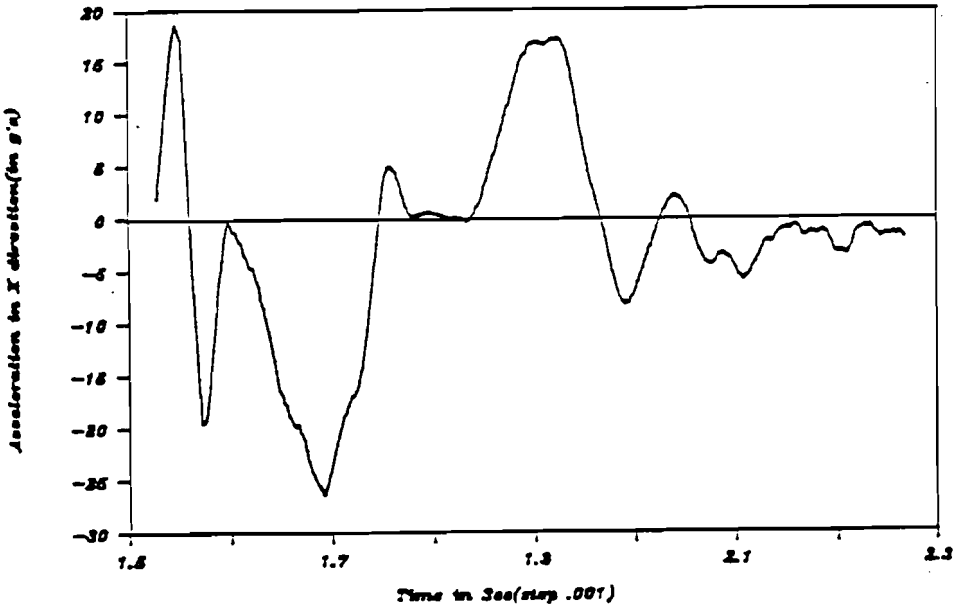

'Figure 54. Smoothed head acceleration in X direction.

required tasks. All these commands use a three letter abbreviation to identify the task performed. Some commands and automation process are discussed below.

a) PLY

This command will start playing the tape from the current tape position. To automate the process the reticle is positioned at the target point.

b) SAR x1,y1,x2,y2

The SAR command is abbreviated for select area, where (x1,y1) are the first coordinates and (x2,y2) the second coordinates. After positioning the reticle at the target, SAR command is used to define the target area to be searched. All the pixels that are inside this area will respond to any command issued after SAR.

c) SVD

Once the area selected, SVD command is used to send the information to the analyzer. That is, SVD sends the pixel values to the computer where target tracking is in progress.

d) JOG

After retrieving the position we assign this value to one of our variables and update our screen. The command is used for updating the screen is JOG.

e) STP

After updating the frame, STP command is issued which stands for stop. There are two reasons for stopping. The first one is that SAR and SVD commands cannot be issued in any other states, and secondly we need to check our target position in the updated frame using a search technique.

The communication interface accessory, which is used to communicate with computers, supports both serial and parallel communications. Serial communication is supported through and RS-232-C interface and parallel communication through and IEEE-488 interface. Here we use RS 232 C serial port. The serial port was connected to the computer. To communicate through the serial port the conditions of the computer and motion analyzer must match. These include "Baud rate", "Word length", "Stop bits", "Parity" and "Echo".

To track the target automatically, the pixel values obtained by SAR and SVD commands are used to search the target. These pixel values are then analyzed. Each pixel can have a value from 0 to 255, where 0 represents a black pixel, 255 represents a white pixel and in between are shades of gray. The target is a black circle enclosed by a white box which is bordered by a black box, placed on the dummy's head (see Figure 55). The frame is continuously updated,

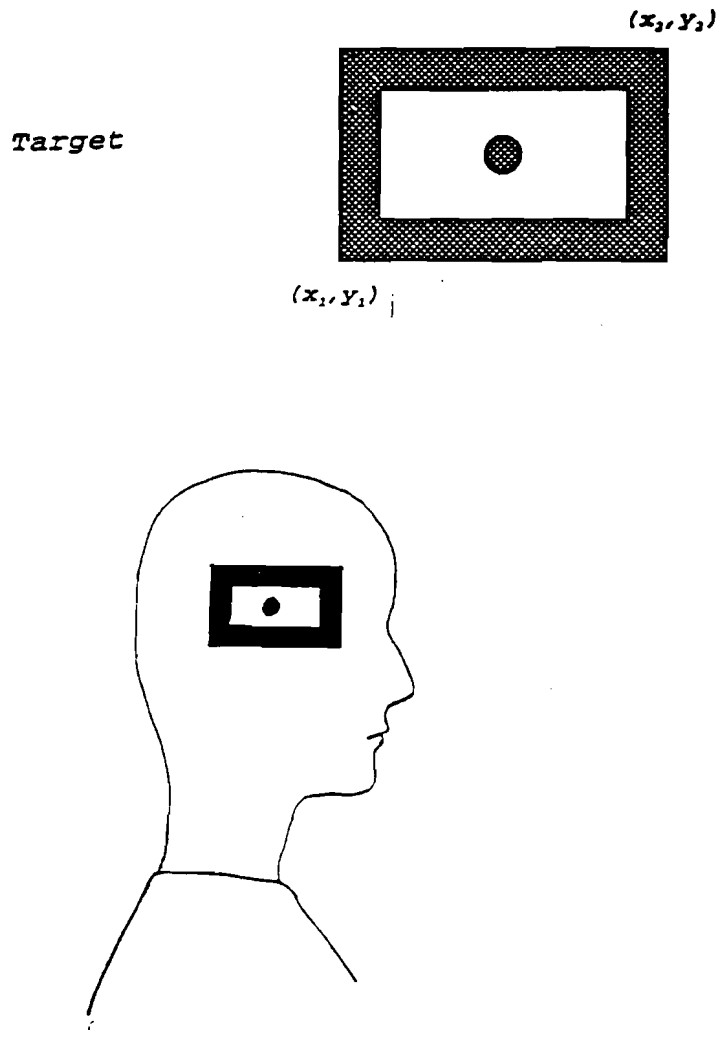

Figure 55. Target configuration on the dummy head.

and each time pixel values are analyzed to determine the new target location. The technique for searching the target is based on the detection of this particular configuration, i.e. black, white, and black. The reticle is placed at x1, y1 coordinates. The search area is defined from x1, y1 to x2, y2 coordinates, which will enclose the whole target area. The pixel values sent by the SVD command to the computer from the motion analyzer are stored in an array.

The search for the target is conducted in three steps. In the first step the search is started simultaneously from x1, y1 coordinates at the bottom left corner and x2, y2 coordinates at the top right corner of the search area. The search is continued until four white pixels are consecutively located on either side. This indicates that the search has now entered the white area near its border. Now the second step of the search begins. In the second step, after the detection of four white pixels, the search is again started by jumping up one pixel value at the lower white corner and jumping down another pixel value at the upper right corner. The search is now continued in the white area only, for the detection of black pixels. As soon as black pixels are detected, the area around it is searched for more black pixels. In the third step, the black pixel having the least value is taken as the target. This pixel will be the new target location. The pixel coordinates are stored to provide the head strike envelope. The black border around the target helps to differentiate the target from the background wall. At the time of impact, the dummies head moves further than the area selected by the SAR command. This causes the search algorithm to look for the target on the background wall which is white, and we loose the target on the dummy's head. The black border helps to relocate the target position once it has moved out of the range of the specified area. Once the new target position is located, the frame is updated and the process is repeated until the last frame has been reached.

The problem in using this technique is that we might encounter situation where the target is covered by dummy parts. One solution to this problem could be the prediction of the target position at the frame using spline curves by updating the frame until the target appears again. Then join all the points to fit the curve. For the changing intensity we use the averaging technique.

Comparison of results

For the verification, the data collected by the optical method was compared to the data obtained manually. Figure 56 and 57 shows the head strike envelope obtained manually and with the automated target tracking technique respectively. By comparing the two curves it is noted that the curve obtained by the automated technique is much smoother. This curve could have been much more smooth if proper lighting system had been used during the recording. Poor lighting system obscures the target and reduces the distinction between the target and the surrounding area by creating a large number of grey pixels of different values not sufficiently different from white and black pixels. Figures 58 and 59 shows the comparison between the acceleration obtained by the manual and automated tracking techniques, respectively. The difference between the two curves is not much because the head strike paths after being filtered are basically the same, for the two techniques.

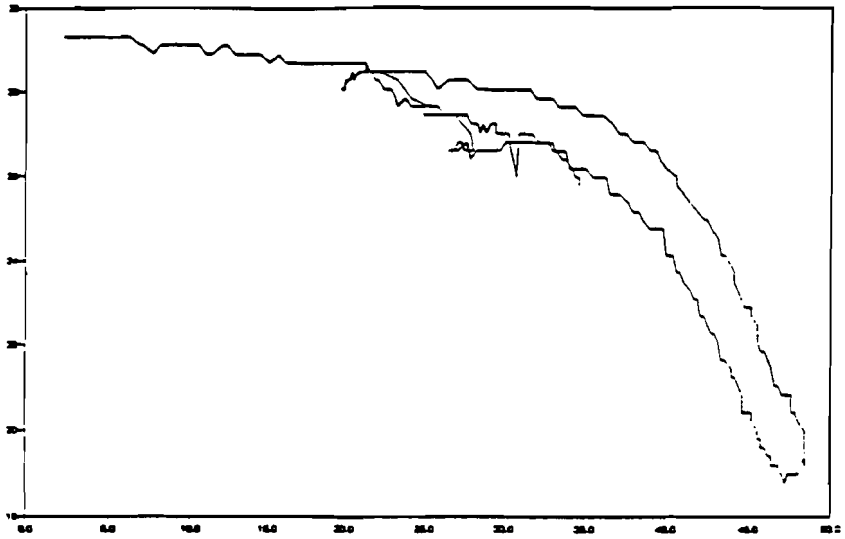

Figure 56. Head stike path obtained manually.

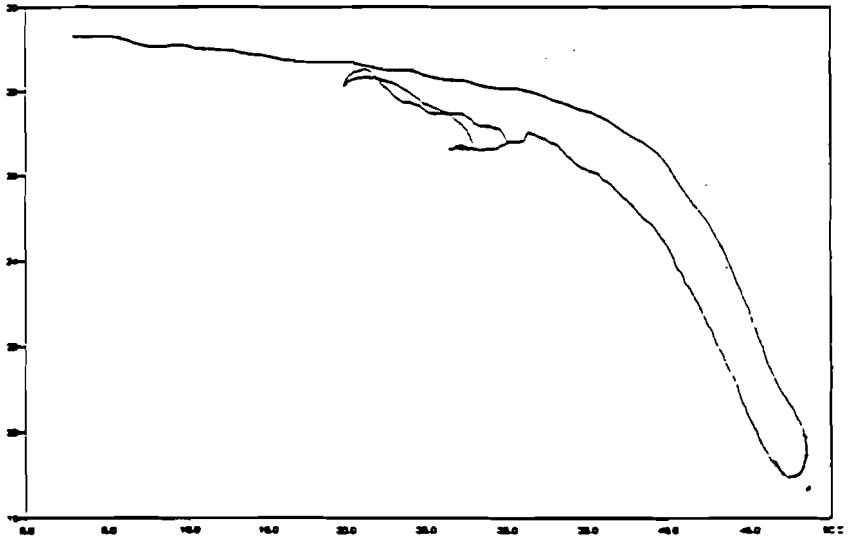

Figure 57. Head strike path obtained automatically.

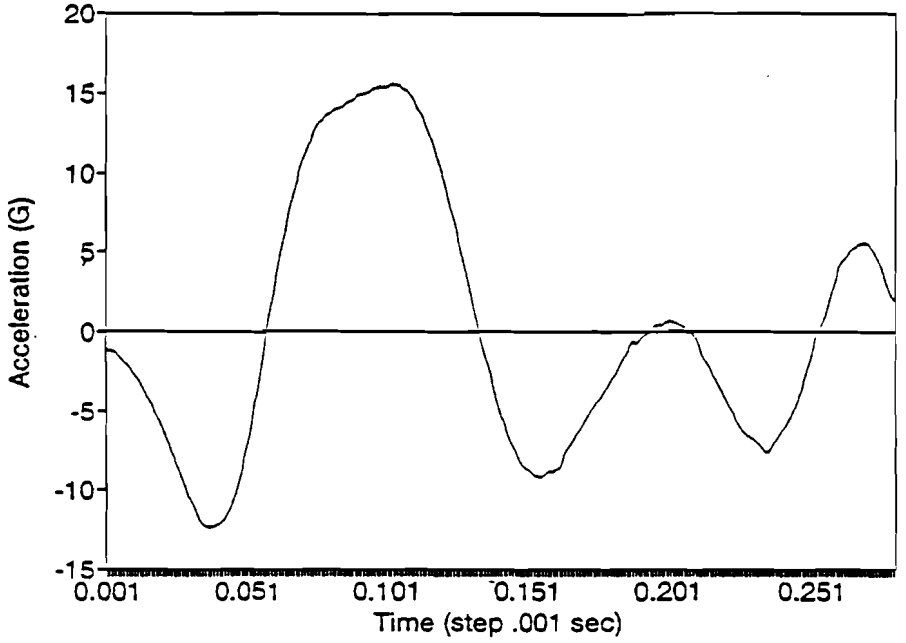

Figure 58. Head acceleration in X direction obtained by manual tracking.

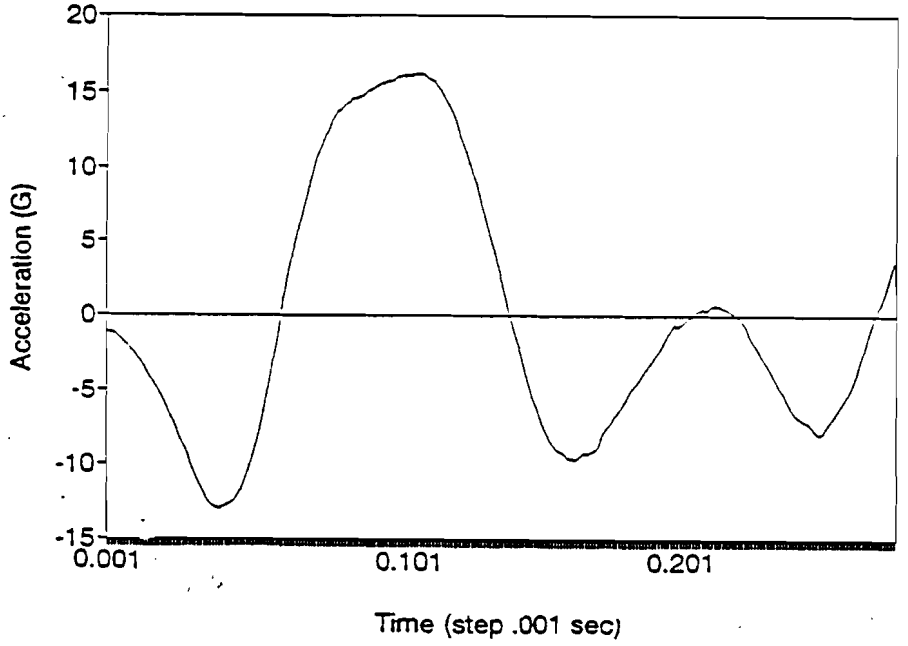

Figure 59. Head acceleration in X direction obtained by automatic tracking.

8. CONCLUSIONS AND RECOMMENDATIONS

8.1 Conclusions

The knowledge of occupant responses in a crash will help in understanding and determining the type and probable causes of injuries that may be sustained by the pilot or passengers during a crash. This knowledge may in turn be used in the design and development of safer seats, restraint systems, and occupant surroundings. SOM-LA/TA Mathematical models based on principles of the multibody dynamics and finite element methods along with numerical techniques, are powerful tools that can be used to gain insight into the gross motion of occupant segments and to evaluate the loads and deformations of some critical parts of human body. These critical parts repeatedly bear serious injuries or significantly affect the overall dynamic behavior of the body as a result of a crash. The following lists the general tasks conducted in this investigation and the conclusions made.

1. A comprehensive study of the capabilities of the program SOM-LA/TA has been performed and deficiencies in its occupant models have been identified. Some improvements of code SOM-LA/TA and occupant model were achieved. The improved code SOM-LA/TA will be a powerful tool to study the post-crash dynamic behavior of the aircraft occupants and to assess the occupant survivability and performances of seat/occupant protection systems under various crash environments.

2. Occupant models in code SOM-LA/TA have been assessed and validated by comparing with the results obtained from tests performed at FAA, CAMI and NIAR, as well as from the dynamics code MADYMO. Generally, the results from the computer simulation match the experimental results well in terms of segment positions. However some differences were observed, especially in the segment accelerations, which could be most likely due to the value of some parameters within the programs such as stiffness characteristics and damping coefficients of occupant lumbar spine and neck.

3. A quasi-static methodology for the dynamic analysis of multi-body systems with flexible structures undergoing large motion and complicated structural deformations has been developed. Detailed information of kinematic, geometric, inertial and material properties of the lumbar spine was collected and evaluated. Based on the developed method and collected information, two types of finite element models of lumbar spine were created and incorporated into SOM-LA/TA for both Hybrid II (part 572) dummy and 50th percentile male human, respectively. Comparison of the two isolated models showed that the relationship between lumbar load and displacement is linear for both lumbar spine models. More importantly, the lumbar spine model for Hybrid II dummy is much stiffer than that of male human. The spinal axial loads, bending moments, shear forces, internal forces, nodal forces and deformations time history can be predicted with these new additions. These detailed information will help in studying the spinal injury level and injury mechanisms, injury prevention and design of the occupant safety devices.

4. A crash dynamic program SOMLA-FEA, which is based on the newly developed nonlinear finite element spine model and modified software SOM-LA/TA, was developed and the numerical simulations for diverse cases were performed. These analytical results have been compared with the experimental results from CAMI and from NIAR. The analytical results of SOM-LA/FEA provide a closer similarity to the experimental ones than the ones provided by the original SOM-LA/TA. It was further shown that the occupant model containing the spine model is again stiffer for the Hybrid II dummy than for the average size male human.

5. For the prediction of occupant head injuries, formulations and mechanisms of head injury have been evaluated. This study has also revealed the review of literature on background of HIC and computational methods to evaluate the HIC. A program code called HIC has been developed using direct computational approach, and the HIC value obtained from this program has been shown to match the HIC values obtained from other programs.

6. For the average size male occupant, a dynamic multibody model of head-neck has been created. The multibody model consists of the head and the seven vertebrae (C1 through C7) attached to an upper thoracic region (T1) combined with the torso as a rigid base. This detailed head-neck model will be incorporated into SOM-LA/TA in future investigations.

7. The deficiencies of HIC in prediction of injuries as a result of rotation of the head was discussed. It was also mentioned that for a particular crash scenario, the HIC may fall below 1000, but the person's neck may break. Therefore, it is important to use the tolerable neck moments in prediction of neck injuries. The tolerance for the neck moment before injury occurs are 42 lb-ft in extension and 144 lb-ft in flexion respectively.

8. A nonlinear contact force model of an occupant seated behind the interior walls was developed and parametric analysis was performed. For the given impact conditions, the occupant injury will be minimized if the proper materials of bulkheads are chosen. A simple procedure was developed for the selection of proper padding material for aircraft bulkheads.

9. In order to add graphical output capability to SOM-LA/TA, the post-processor was developed both on micro-computer and on IBM RISC/6000 workstation. These will be greatly helpful in visualizing and interpreting the numerical results and better understanding the simulation process.

10. Impact sled testing is the most important experimental approach to evaluate the performances of safety devices and occupant injuries. However, this method is found to be more complex, time consuming and expensive. Hence feasibility analysis of a non-sled method has been performed to evaluate the HIC. The idea is first to isolate the motion of the occupant head to see whether similar response can be obtained with only

the head or similar head forms. Secondly, the procedure can be used to test bulkhead materials.

11. In addition to the data from the accelerometers, the displacement, velocity and acceleration of the dummy are recorded and evaluated using a high speed video system and optical target tracking techniques. The collected data from the photometric analysis is considered accurate only if it is obtained using well defined and verifiable procedures. These include proper lighting, image locations, angles and frame rate, etc. Also, manual collection of the data, frame by frame is tedious and time consuming, and may cause much noise in the data. To solve the mentioned problems, an automated target tracking photometric procedures were developed so that the accuracy is enhanced and a great deal of time is saved.

8.2 Recommendations

Much progress has been made in this research. However further improvements are still needed as cited below.

1. More model validations need to be performed such as determination of spine deformations time history, bending moments on the spine, and stress distributions. One more important issue is shear force acting on the spine and related injuries, especially for those horizonal impact tests, which the shear force might be more important than the axial loads acting on the lumbar spine.

2. Further improvements of the 2-D occupant model in prediction of the bending moment are needed. A finite element model of the head-neck as well as detailed stress distributions on the vertebrae and discs are also of use.

3. A nonlinear lumbar spine model for 3-D occupant model needs to be created. The spine model must include the torsional stiffness.

4. Correlation of the Hybrid II dummy and wider range of occupant sizes to the injury evaluation and criteria are needed to be performed.

5. A measure of head-neck injury is needed such that it takes the rotational acceleration of the head into consideration. There is obviously a need to do more research for a fuller understanding of the mechanisms of injury to the head and to determine the parameters which best describe the tolerance of the head.

6. Studies on improvement of commuter aircraft safety are needed to re-construct variety of commuter aircraft crash scenarios using the computer capabilities of NIAR. In an effort to evaluate and improve occupant survival, information on different size occupants need to be collected, and their corresponding biodynamic responses need to be predicted. This information will be used to define a dynamic test program.

9. REFERENCES

[1] Laananen, D.H., Bolukbasi, A.O., and Coltman, J.W., "Computer Simulation of an Aircraft Seat and Occupant in a Crash Environment, Volume I - Technical report, TR-82401," Simula, Inc., Tempe, Arizona; DOT/FAA/CT-82/33-I, U.S. Department of Transportation, Federal Aviation Administration Technical Center, Atlantic City Airport, New Jersey, September 1982.

[2] Laananen, D.H., Bolukbasi, A.O., and Coltman, J.W., "Computer Simulation of an Aircraft Seat and Occupant in a Crash Environment, Volume II - Program SOM-LA User Manual, TR-81415," Simula, Inc., Tempe, Arizona; DOT/FAA/CT-82/33-II, U.S. Department of Transportation, Federal Aviation Administration Technical Center, Atlantic City Airport, New Jersey, March 1983.

[3] Laananen, D.H., "Computer Simulation of an Aircraft Seat and Occupant(s) in a Crash Environment - Program SOM-LA/SOM-TA User Manual," DOT/FAA/CT-90/XX, U.S. Department of Transportation, Federal Aviation Administration Technical Center, Atlantic City Airport, New Jersey, January 1990.

[4] Laananen, D.H., "Computer Simulation of an Aircraft Seat and Occupant(s) in a Crash Environment - Program SOM-LA/SOM-TA User Manual," DOT/FAA/CT-90/4 , U.S. Department of Transportation, Federal Aviation Administration Technical Center, Atlantic City Airport, New Jersey, May 1991.

[5] Denny-Brown, D., and Russell, W.R., "Experimental Cerebral Concussion," *Brain*, Vol. 64, pp. 93-164, 1941.

[6] Unterharnscheidt, F. and Higgins, L.S., Pathomorphology of Experimental Head Injury Due to Rotational Accelerations," *Acta Neuropath*, Vol. 12, pp. 200-204, 1969.

[7] Gennarelli, T.A., and Thibault, L.E., "Biomechanics of Acute Subdural Hematoma," *J. Trauma*, Vol. 22, pp. 680-686, 1982.

[8] Wisemans, J., " Comparison of Human Volunteer and Cadaver Head-Neck Response in Frontal Flexion," Proc. 31st Stapp Car Crash Conference, Paper No. 872194, 1987.

[9] Duhaime, A.C., and Genneralli, T.A., "The Shaken Baby Syndrome: A Clinical, Pathological, and Biomechanical Study," *J. Neurosurg*, Vol. 66, pp. 409-415, 1987.

[10] Guthkelch, A.N., "Infantile Subdural Hematoma and Its Relationship to Whiplash Injuries," *British Medical J.*, Vol. 2, pp. 430-431, 1971.

[11] Gadd, C., "Use of a Weighted Impulse Criteria for Estimating Injury Hazards," Proc. Tenth Stapp Car Crash Conference, Paper No. 660793, 1963.

[12] Lau, I.V., Viano, D.C., "The Viscous Criterion: Bases and Application of Injury Severity Index for Soft Tissues," *SAE Transactions*, Vol. 9, 1986, Paper 189, pp. 123-142. 30th Stapp Car Crash Conference, SAE No. 861882, 1986.

[13] Viano, D.C., and Lau, I.V., "A Viscous Tolerance Criterion for Soft Tissue Injury Assessment," *J. Biomechanics*, Vol. 21, No. 5, pp. 387-399, 1988.

[14] Bloom, A., Cickowski, W., and Roberts, V., "Sophisticated Sam -- A New Concept in Dummies," Proc. SAE Automation Engineering Congress, Paper No. 680031, Detroit, MI, 1961.

[15] EUROSID User's Manual, TNO Road-Vehicle Research Institute, Delft, 1987.

[16] Kelps, J., and Whitestone, J., "HYBRID III Geometrical and Inertial Properties," SAE 880638, International Conference and Exposition, Detroit, 1988.

[17] McHenry, R.R., "Analysis of Dynamics of Automobile Passenger-Restraint System," Proc. 7th Stapp Car Crash Conference, pp. 207-249, 1963.

[18] Segal, D.J., "Revised Computer Simulation of the Automobile Crash Victim," Cornell Aeronautical Laboratory, Rep. No. VJ-2759-V-2, 1971.

[19] Danforth, J.P., and Randall, C.D., "Modified ROS Occupant Dynamics Simulation User Manual," General Motors Corp. Research Labs., Publ. No. GMR-1254, 1972.

[20] Robbins, D.H., Bennett, R.O., and Roberts, V.L., "HSRI Two-dimensional Crash Victim Simulator: Analysis, Verification, and User's Manual - Final Report," University of Michigan, Highway Safety Research Institute, Rep. No. HSRI-Bio-M-70-8, 1970.

[21] Robbins, D.H., Bowman, B.W., and Bennett, R.O., "The MVMA Two-dimensional Crash Victim Simulation," Proc. 18th Stapp Car Crash Conf., pp. 657-678, 1972.

[22] Alem, N. M., Bowman, B. M., Melvin, J. W. and Benson, J. B., "Whole-body human surrogate response to three-point harness restraint," SAE 780895, Proceedings of 22nd Strapp Car Crash Conference, SAE, Warrendale, PA, 1978.

[23] Viano, D. C., Culver, C. C. and Prisk, B., "Influence of initial length of lap-shoulder belt on occupant dynamics - a comparison of sled testing and MVMA-2D modeling," SAE 801309, Proceedings of 24th Strapp Car Crash Conference, SAE, Warrendale, PA, 1980.

[24] Glancy, J.J., and Larson, S.E., "User's Guide for Program SIMULA," Dynamic Science, Rep. TDR No. 72-23, 1971.

[25] Twiggs, D.W., and Karnes, R.N., "PROMETHEUS - A User Oriented Program for Human Crash Dynamics," Boeing Comp. Services, Inc., Rep. No. BCS40038, 1974.

[26] Robbins, D.H., "Three-dimensional Simulation of Advanced Automotive Restraint System," SAE Paper No. 700421, Int. Auto. Safety Conf. Compendium, pp. 30, 1970.

[27] Robbins, D. H., Bennett, Jr., R. O. and Bowman, B. M., "User-oriented mathematic crash victim simulator," 720962

[28] Bartz, J.A., "A Three-dimensional Computer Simulation of a Motor Vehicle Crash Victim," Calspan Rep. No. VJ-2978-V1, 1971.

[29] Fleck, J.T., and Butler, F.E., and Vogel, G.L., "An Improved three-dimensional Computer Simulation of Motor vehicle Crash Victims," Vol. I-IV, Rep. Nos. DOT-HS-81507, -508, -509, -510, 1974.

[30] Fleck, J.T., and Butler F.E., "Validation of Crash Victim Simulator," Vol. 1-4, Rep. No. ZS-5881-v-1, DOT-HS-6-01300, 1981.

[31] Huston, R.L., Hessel, R., and Passerallo, C., "A Three-dimensional Vehicle -Man Model of Collision and High Acceleration Studies," SAE Paper No. 740275, 1974.

[32] Bosio, A.C., and Bowman, B.W., "Analysis of head and Neck Dynamic Response of the US Adult Military Population. UMTRL-86-14, 1986. Articulated Total Body (ATB) Model, Wright-Patterson Air Force Base, Ohio.

[33] Wisemans, J., Maltha, J., Van Wijk, J., and Janssen, E.G., " MADYMO - A Crash Victim Simulation Computer Program for Biomechanical Research and Optimization of Designs for Impact Injury Prevention," AGARD Meeting, Kooln, Germany, 1982.

[34] Van Wijk, J., Wisemans, J., Maltha, J., and Wittebrood, L., "MADYMO pedestrian simulations," SAE 830060, Pedestrian Impact Injury and Assessment, SAE, Warrendale, PA, 1983.

[35] Lankarani, H. M., Ma, D., and Ermer, G., "Dynamic behavior of the human body subjected to impact condition, with and without restraint," Proceedings of AIAA/FAA Joint Symposium of General Aviation Systems, May 1990.

[36] Ma, D. and Lankarani, H. M., "Computer simulation of an aircraft occupant-restraint system," Proceedings of AIAA Techfest XVII, Wichita, November 1990.

[37] McElhaney, J. H., Roberts, V. L., Hilyard, J. F., "Head injury tolerance and criteria," Hand book of human tolerance, chap. 4, published by Japan Automobile Research Institute Inc. (JARI).

[38] "Test devise head contact duration analysis," - J 2052 March, 1990, SAE information report p 34.198.

[39] Gadd, C., "Use of a weighted impulse criteria for estimating injury hazards," *Proceedings Tenth Stapp Car Crash Conference*, Paper No. 660793, 1963.

[40] Lankarani, H. M., Menon, R., Malapati, S., "Response of a Dynamic Model of Head-Neck to Extension Whiplash," Presented at NACOB II: The Second North American Congress on Biomechanics, Chicago, August 24th - 28th, 1992.

[41] Latham, F., "A study in body ballistics: seat ejection," Proceedings of the Royal Society, Series B., Vol. 147, 1957, pp. 121-39.

[42] Payne, P. R., "The dynamics of human restraint systems," Impact Acceleration Stress, Publication No. 977, National Academy of sciences-National Research council, Washington, D. C.,1962, pp. 195-257.

[43] Liu, K. Y., "Dynamic spinal injury: mechanisms, modeling, and systems for minimizing trauma," Human Body Dynamics, Oxford University Press, 1981.

[44] Orne, D., and Liu, Y. K., "A mathematical model of spinal response to impact," Journal of Biomechanics, Vol. 4, 1971, pp. 48-72.

[45] Aquino, C. F., "A dynamic model of the lumbar spine," Journal of Biomechanics, Vol. 3, 1970, pp. 473-86.

[46] Panjabi, M. M., and White, A. A., " A mathematical approach for three-dimensional analysis of the mechanics of the spine," Journal of Biomechanics, Vol. 4, 1971, pp. 203-12.

[47] Schwer, L. E., "A three-dimensional large displacement transient analysis of the human spine and torso," Ph.D. Dissertation, University of Illinois, Chicago, 1976.

[48] Luo, Z. and Goldsmith, W, "Reaction of a human head/neck/torso system to shock," J. Biomechanics, Vol. 24, No. 7, pp.499-510, 1991.

[49] Hell, L. L., and Lombard, C. F.,"Theoretical investigations of dynamic response of man to high vertical accelerations," Aviation Medicine, Vol. 29, 1958, pp. 65-77.

[50] Gramer, H. J., Liu, Y. K., and Von Rosenberg, D. U.,"A distributed parameter model of the inertially loaded human spine," J. Biomechanics Vol.9, pp.115-130, 1976.

[51] Liu, Y. K., and Ray, G., "A finite element analysis of wave propagation in human spine," Final Report AMRL-TR-73-40, Aerospace Medical Research Laboratory, Wright-Patterson Air Force Base, Ohio, 1973.

[52] Lavaste, F., Skalli, W., Robin, S., Roy-Camille, R. and Mazel, C., "Three-dimensional geometrical and mechanical modeling of the lumbar spine," J. Biomechanics, Vol. 25, No. 10, pp.1153-1164, 1992.

[53] D. E. Midoun, E. Abramoski, M.K. Rao, and R. Kalidindi, "Development of a finite element based model of the side impact dummy," ASME paper 930444.

[54] Moffatt, C. A., Howard, R. H., Hegedus, D. M. and Cheng, J. L., "The investigation of vertebral injury sustained during air crew ejection," Technical Report, Contract No. NAS2-5062, Aeronautics and Space Administration, Ames Research Center, Moffett Field, CA., 1969.

[55] Lankarani, H. M. Malapati, S., and Menon, R., "Evaluation of Head Injury Criteria," NIAR Report 93-2, Wichita State University, 1993.

[56] Lankarani, H. M. and Sanjeev, A. "Design of Non-sled Setup to Measure Head Injury Criteria," NIAR Report 92-20, Wichita State University, 1992.

[57] Gowdy, V., and DeWeese, R., "Evaluation of Head Impact Kinematics for Passengers Seated Behind Interior Walls," Proc. Third Annual Conf. on Aircraft Interiors, National Institute for Aviation Research, Wichita State University, October 1991.

[58] Monk, W. M. and sulivan, L. K.,"Energy Absorbing Meterial Selection Methodology for Head/ A-pillar Impact," SEA, Proc. 33rd Stapp Car Crash Conf.

[59] Lankarani, H. M., "Biodynamic Responses for Evaluation of Aircraft Crash Safety-Phase I," Final Report to Federal Aviation Administration, September 1991.